A. COVER PAGE

Project Title: A Study of Protective Clothing to Prevent Nanoparticle Exposure and Surface Contamination	
Grant Number: 1R21OH012361-01	**Project/Grant Period:** 11/07/2020 - 09/14/2021
Reporting Period: 11/07/2020 - 09/14/2021	**Requested Budget Period:** 11/07/2020 - 09/14/2021
Report Term Frequency: Final	**Date Submitted:** 06/13/2023
Program Director/Principal Investigator Information: CANDACESUJUNG TSAI , BS DSC MS MS **Phone Number:** 3102069258 **Email:** candacetsai@ucla.edu	**Recipient Organization:** UNIVERSITY OF CALIFORNIA LOS ANGELES Office of Contract and Grant Administration 10889 Wilshire Boulevard, Suite 700 LOS ANGELES, CA 900952000 **DUNS:** 092530369 **UEI:** RN64EPNH8JC6 **EIN:** 1956006143A1 **RECIPIENT ID:**
Change of Contact PD/PI: NA	
Administrative Official: FRANK FALCONII 10889 Wilshire Boulevard Suite 700 Los Angeles, CA 90095 **Phone number:** 310-206-9898 **Email:** frank.falcon@research.ucla.edu	**Signing Official:** FRANK FALCONII 10889 Wilshire Boulevard Suite 700 Los Angeles, CA 90095 **Phone number:** 310-206-9898 **Email:** frank.falcon@research.ucla.edu
Human Subjects: NA	**Vertebrate Animals:** NA
hESC: No	**Inventions/Patents:** No

B. ACCOMPLISHMENTS

B.1 WHAT ARE THE MAJOR GOALS OF THE PROJECT?

The proliferation of new applications in nanotechnology has highlighted the need to protect researchers in laboratories and workers in production facilities from exposure to engineered nanoparticles (ENPs) through skin contact or inhalation. Workers wearing contaminated clothing are at high risk of inhaling ENPs released from that clothing without any awareness of the potential danger. We have recently documented the significant release of metal oxide ENPs from laboratory clothing and highlighted serious concerns regarding the need to better understand the factors associated with ENP exposure from workplace attire. Importantly, when leaving the laboratory/production line, researchers and workers are unaware of the possible ENP exposure from contaminated clothing that they bring back to the office, home or public places. This contaminated clothing also poses a significant risk to non-workers in these outside of the workplace settings. It is well documented in the past, for example, that exposure to asbestos fibers from contaminated clothing has caused many workers and non-workers to suffer from asbestos-related diseases. It is worrying to note that ENPs are 1/10 to 1/100 the size of asbestos particles. Thus, the number of exposed ENPs could be >1000 more than that of such micron asbestos fibers, yet they are still invisible to the human eye. The goal of this study is to address key knowledge gaps in the understanding of ENP contamination of laboratory protective clothing and identify ways to prevent and minimize the problem.
To achieve this goal, this project studied the propensity for contamination of major protective clothing fabrics by clinically significant ENPs as well as the potential for subsequent exposure to individuals who come into contact with these fabrics. Our study focused on key mechanistic aspects of ENP-fabric interactions such as mechanical force and electrical charge. The quantitative assessment of ENP adhesion and release from contaminated clothing will allow us to identify optimal fabric characteristics for protection against toxic ENPs. Importantly, we will use novel sampling techniques and state of the art technologies, including direct-reading air monitoring instruments, a nanoparticle sampler possessing a proprietary modification that we made to improve performance, designed for nanoparticle collection to determine exposure, and advanced microscopic analysis - including atomic force microscopy (AFM) to investigate the mechanical forces and electrical charges associated with ENP-fabric interactions. Practically, we used plasma surface treatment to functionalize fabric fiber surface to improve surface properties.

B.1.a Have the major goals changed since the initial competing award or previous report?

No

B.2 WHAT WAS ACCOMPLISHED UNDER THESE GOALS?

File Uploaded : NIOSH R21 Final Report_submit_Tsai.pdf

B.3 COMPETITIVE REVISIONS/ADMINISTRATIVE SUPPLEMENTS

For this reporting period, is there one or more Revision/Supplement associated with this award for which reporting is required?

No

B.4 WHAT OPPORTUNITIES FOR TRAINING AND PROFESSIONAL DEVELOPMENT HAS THE PROJECT PROVIDED?

NOTHING TO REPORT

B.5 HOW HAVE THE RESULTS BEEN DISSEMINATED TO COMMUNITIES OF INTEREST?

Our findings and results have been published in two peer-reviewed journal articles and presented in multiple scientific

conferences. The publications are shared with NIOSH Nanotechnology Research Center (NTRC). The PI has discussed with NIOSH NTRC regarding the need for lab coat use guidelines in which our findings can serve important insights of developing the guidelines.

B.6 WHAT DO YOU PLAN TO DO DURING THE NEXT REPORTING PERIOD TO ACCOMPLISH THE GOALS?

Not Applicable

FINAL REPORT

Project Title: A Study of Protective Clothing to Prevent Nanoparticle Exposure and Surface Contamination

NIOSH Awarded Grant Agreement Number: 1 R21OH011507-01-00

Grant Agreement Project Period: 09/15/2019 – 05/14/2023

Final Report Completed: 06/05/2023

Principle Investigator: Dr. Candace Su-Jung Tsai

Awarded Institute:

Department of Environmental & Radiological Health Sciences, College of Veterinary Medicine & Biomedical Sciences, Colorado State University, 80523 CO

Mailing Address: 1681 Campus Delivery, EH Room 153, Fort Collins CO, 80523-1681

And

Department of Environmental Health Sciences, Fielding School of Public Health, University of California Los Angeles, Los Angeles, California 90095-1735

Mailing Address: 650 Charles E. Young Drive S., MC 177220, Los Angeles, California 90095-1735

Email: Candace.Tsai@colostate.edu and candacetsai@ucle.edu

Office: +1 (310) 206-9258

TABLE OF CONTENTS

Project Title: A Study of Protective Clothing to Prevent Nanoparticle Exposure and Surface Contamination....iv
Abstract....iv
SECTION 1 OF THE REPORT 5
Significant or Key Findings....6
Translation of Findings 8
Research Outcomes/Impact 9
SECTION 2 OF THE REPORT 10
CHAPTER 1: Quantitatively document the severity of ENP exposure by both the dermal and inhalation routes from contamination of major fabrics used in laboratory clothing. 11
Introduction....11
Methodology 11
Materials 12
Facilities, Equipment and Procedure 12
Experimental process.... 14
Results And Discussion....16
Resuspension Status of Nanoparticles from Contaminated Clothing.... 16
Mass change analysis 17
Size distributions analysis of released nanoparticles 18
Integrated analysis of released particle sizes, morphology, and concentrations..... 20
Theoretical discussion of particle-fabric adhesion.... 25
Mechanical properties (durability) of lab coat fabrics 27
Conclusion 28
References....29
CHAPTER 2: Quantitatively document the severity of ENP exposure by penetrating fabric from contamination of major fabrics used in laboratory clothing.....31
Introduction....31
Methodology 32
Materials 32
Facilities, Equipment, and Procedure 33
Fabric Preparation.... 34
Aerosolization of ENPs 34
Scanning Electron Microscopy (SEM) Analysis 35
Statistical Analysis 35
Results And Discussion....35
Fabric Characteristics 35
Penetration of Different Fabrics Against the Same ENP 37
Relationships Between ENP Penetration and Fabric Type.... 39
Conclusions....40
References....41
CHAPTER 3: Elucidate the mechanism of differential ENP interactions with major laboratory clothing fabrics.....43
Introduction....43

Methodology 44
Introductory Remarks 44
Atomic Force Microscope Capabilities 45
Summary of Experimental Protocols Developed 46
Results 47
AFM Results 47
Discussion of Important Features in F(z) 48
Central Results 50
Discussion 51
Conclusions 52
Future Work 53
CHAPTER 4: Achieve a significant reduction in ENP contamination/exposure by altering surface key properties of the fabric 54
Introduction 54
Methodology 55
Materials 55
Plasma modification of fabric swatches 56
Fabric contamination with ENPs 56
Materials characterization 57
Results And Discussion 58
Conclusion 69
References 70
Appendix 74
Chapter 1 supplementary materials 74
Chapter 4 supplementary materials 86

Project Title: A Study of Protective Clothing to Prevent Nanoparticle Exposure and Surface Contamination

Abstract

Although nanoparticles have been incorporated in a range of applications, human exposure through surface contamination remains of concern and under investigated. This is especially true in the context of industrial and research labs, where workers may become contaminated with nanoparticles. Development of appropriate personal protective equipment requires a deeper understanding of how nanoparticles interact with fabrics. Here, the contamination and resuspension behavior of Al_2O_3, carbon black (CB), and carbon nanotubes (CNT) with four common lab coat materials (100% cotton, 80/20 polyester/cotton blend, 100% polypropylene, and Tyvek®) is presented in this study.

We investigated engineered nanoparticle (ENP) release associated with the contamination of personal protective clothing during the simulated motion of the human wearing the ENP-contaminated protective clothing and evaluated the relative ENP retention on the fabric. The release of airborne ENPs can contribute to inhalation exposure, which is the route of exposure of most concern to cause adverse health effects in the pulmonary system. The evaluation focuses on four popular fabric materials making the laboratory coats and three types of ENPs (Al_2O_3, carbon black and CNT) as noted above. The magnitudes of particle contamination and resuspension were investigated by measuring the number concentration increase of airborne particles in sizes of 10 nm to 10 μm and the weight changes on fabric pieces. Collected aerosol particles and contaminated fabric surfaces were further characterized for understanding particle morphology, elements, agglomeration and surface contamination status. The particle resuspension from contaminated lab coat fabric was found to vary by the type of fabric material. Cotton fabric showed the highest level of particle resuspension for all three tested ENPs. Data were evaluated to determine the dominant forces responsible for ENP adhesion on the surface of the fabric. Tyvek® fabric was determined as the best fabric for trapping Al_2O_3 and carbon black ENPs indicating less resuspension of particles meaning lower subsequent release, but not durable enough to wear for the long term compared with other fabrics. In addition, the viscoelastic properties shown by all the fabrics except Tyvek suggest alternate routes to a more efficient trapping of ENPs. For example, physically pressing a lab coat exposed to ENP contamination overnight might serve to more firmly embedded ENPs in the contamination layer before the lab coat is used the next day.

To understand the effects of fabric weave pattern and surface chemistry on nanomaterial-fabric interactions, fabrics were treated with a C_3F_8 or $H_2O_{(v)}$ plasma to alter surface wettability while maintaining bulk morphology. Changes in surface chemistry and wettability were measured using X-ray photoelectron spectroscopy (XPS) and water contact angle (WCA) goniometry on untreated and plasma treated materials. Contamination and release of nanomaterials were quantified by monitoring the change in mass after contamination and shaking of the fabrics and using scanning electron microscopy (SEM) image analysis. Overall, the lowest contamination levels arise from exposure to CNT. Plasma treatment results in differential contamination, with the $H_2O_{(v)}$ plasma treated fabrics demonstrating the lowest CB contamination, whereas the lowest Al_2O_3 contamination and resuspension occurs with the C_3F_8 plasma treated cotton. A complex mechanism for nanoparticle interaction with fabrics involving surface chemistry, morphology, and intermolecular forces is discussed in the report.

SECTION 1 OF THE REPORT

Significant or Key Findings

This research results respond to the NIOSH National Occupational Research Agenda (NORA), specifically, Intermediate Goal 9.2 of the National Manufacturing Agenda: "conduct surveillance and develop exposure assessment methods, engineering controls, containment systems, and other interventions for occupational risks, protective factors, and outcomes as a result of exposure to nanoparticles and nanomaterials."

Objective 1: Quantitatively document the severity of engineered nanoparticle (ENP) exposure by both the dermal and inhalation routes from contamination of major fabrics used in laboratory clothing.

This study showed substantial particle release results for all types of tested fabrics. The release inhalable particle concentration for cotton and polyester cotton fabric were determined to be the highest from the aerosolization of Al_2O_3 and carbon black (CB) ENPs, while Tyvek® and polypropylene showed the lowest amount of release concentration. From the exposure of carbon nanotube (CNT) ENPs, the cotton fabric showed the highest release concentration compared with other tested fabrics. The release concentration of cotton and polyester cotton were significantly different from Tyvek® and polypropylene for Al_2O_3 and carbon black ENPs, while for CNT ENPs cotton fabric turned out to be significantly different from all other fabrics. Moreover, for all types of tested fabrics the total number concentrations of resuspended ENPs at the breathing zone are higher than particles released from the back side of the worker wearing the contaminated protective clothing. The total number concentration from one hour contamination and six-hour release processes could represent the exposure of full-shift work presenting risk of human exposure. Regarding exposure to multiple ENPs, it will require further studies to discover the rules of contamination based on chemical composition, particle size and other surface properties of a mixture.

Regarding dermal route of exposure from penetration of contaminated ENPs, several findings are concluded here. First, Tyvek fabric was shown to be the most protective. Tyvek consistently showed the lowest penetration percentages when challenged with all three different types of ENPs, and some results showed that Tyvek had statistically significantly lower penetration than all three other fabrics. Most of the other data when comparing Tyvek fabric to the other four types of fabric was suggestive that Tyvek was more protective, however, the data was not significant at the 0.05 significance level. Second, polypropylene had the highest penetration percentages when challenged with Al_2O_3 and CB nanoparticles in the 100 nm-1 μm size range, and when averaged over the entire time period over all the size ranges measured. This may be explained by the fact that polypropylene has the highest calculated porosity when compared to the other three fabrics, and the governing mode of deposition for particles of this size is interception.

Objective 2: Elucidate the mechanism of differential ENP interactions with major laboratory clothing fabrics.

Based on results of mass change measured before contamination and after the release processes, Tyvek® fabric indicated the statistically highest value of mass change per unit mass from the exposure of Al_2O_3 and CB; for CNT ENPs all fabrics showed a statistically similar level of mass change per unit mass. Some of the ENPs stay on the surface of the fabric due to the ENP adhesive forces. Two fundamental forces might be responsible for Al_2O_3 and CB ENP adhesion are van der Waals force and capillary force, but it was difficult to determine for CNT ENPs due to their non-circular shape. Our analysis presented that the dominant force for adhesion of ENPs with

fabric fiber varies by the environmental condition (such as humidity). Capillary force can differ greatly with fabric absorbing moisture.

The primary technical tool employed in this study to elucidate ENP interacting force with fabric fiber is the Atomic Force Microscope (AFM). The AFM measures the interaction of a sharp tip integrally attached to a flexible microcantilever as the tip is made to approach, contact, indent and then withdraw from the surface of a fabric of interest. Thus, with this context in mind, it seems natural to investigate what can be quantitatively learned about ENP/fabric interactions using an AFM. Data acquired during an AFM experiment are often referred to as an F(z) curve because the force F acting on an AFM tip is measured as the separation distance z between the tip and substrate is systematically and controllably reduced. Features present (or absent) in a well-executed F(z) experiment provide a fabric-dependent fingerprint that characterizes the relevant forces and interaction mechanisms in play.

Using an AFM, systematic F(z) data were acquired from each fiber under ambient and reduced humidity conditions using the AFM tip as a surrogate for an oxide ENP. Analysis of the results offered useful conclusions that characterize the physical interaction of an oxide ENP in the ~15 nm diam. size range with the individual fibers. Several key findings are summarized:

1. Oxide ENPs should bind weakly to Tyvek and strongest to cotton, with the synthetic fabrics polypropylene and polyester falling somewhere in between. Based on this finding, it might be expected that cotton will shed the fewest ENPs upon wearing by worker with mild motions such as shaking, while Tyvek will shed the largest number of ENPs after motions/shaking.
2. No long-range forces were observed. This implies that tribo-electric induced electrostatic forces between an ENP and each of the fabrics is probably not significant.
3. Analysis of the data for all fibers acquired at low relative humidity (RH) shows the F(z) data is only affected in a subtle way. If a significant water bridge forms under ambient conditions between the ENP and fabric fiber, a large decrease in lift-off force should have occurred as the RH is reduced to near zero. No such change was observed.
4. The data from the two cotton fibers, one extracted from the 100% cotton fabric, the other from the 80/20 polycotton fabric, suggest that treatment of the fabric during manufacture makes a significant difference in how the cotton fibers interact with ENPs. Cotton fiber from the 80/20 polycotton fabric exhibits a strong vdW force of attraction to the AFM tip, while the cotton fiber from the 100% cotton lab coat shows very little in the way of an attractive force. This implies that some currently unknown fabric processing step may have a large influence on ENP adhesion.
5. The contamination layer inferred from the F(z) data on the synthetic fibers indicates these fibers may offer some advantages over cotton to trapping ENPs.
6. The viscoelastic properties shown by all the fabrics except Tyvek suggest alternate routes to a more efficient trapping of ENPs. For example, physically pressing a lab coat exposed to ENP contamination overnight might serve to more firmly embedded ENPs in the contamination layer before the lab coat is used the next day.

Objective 3: Achieve a significant reduction in ENP contamination/exposure by altering surface key properties of the fabric.

The surface chemistry and wettability of these fabrics was tuned using either a C_3F_8 or $H_2O_{(v)}$ plasma and monitored with X-ray photoelectron spectroscopy (XPS) and water contact angle (WCA) analysis. Contamination and release of nanomaterials were quantified by monitoring the

change in mass after contamination and shaking of the fabrics and using scanning electron microscopy (SEM) image analysis. The C_3F_8 plasma deposited a FC coating, increasing the material hydrophobicity, whereas the $H_2O_{(v)}$ plasma implanted O-functionality and etched the surface, nominally increasing the hydrophilicity and roughness of the surfaces. Notably, the latter treatment ultimately resulted in a relatively permanent increase in hydrophilicity of the cotton and Tyvek®, whereas the other two materials exhibited hydrophobic recovery after a month of aging post treatment. Overall, the lowest contamination levels arise from exposure to CNT. Plasma treatment results in differential contamination, with the H_2O(v) plasma treated fabrics demonstrating the lowest CB contamination, whereas the lowest Al_2O_3 contamination and resuspension occurs with the C_3F_8 plasma treated cotton.

Translation of Findings

Overall, Tyvek® is the best fabric for trapping all three types of studied ENPs, which eliminates the resuspension to expose humans. However, this fabric was not durable enough for workers to wear for a long term or the active motions at work might cause wear or tearing of the Tyvek® fabric, reducing its barrier properties and enabling penetration of ENPs. The polypropylene (PP) fabric is the next most effective for trapping ENPs of all three types. In addition, three types of ENPs were found to cause some difference in terms of adhesion onto the fabric surface, and we found that the Al_2O_3 ENPs remained on the fabric the most, especially more on the Tyvek® fabric, after simulated working activities, compared to other CB and CNT ENPs. Cotton and polyester cotton lab coats were found to be the least effective fabric type for trapping ENPs. Although these fabrics are the most durable, comfortable and commonly used in the workplaces, they are not recommended to be used when ENPs are present in work environments.

By monitoring the mass of the contaminated and shaken samples, studies indicate that in general, Al_2O_3 exposure had the largest Δ_{mass}, whereas CNT had the smallest. This suggests that these fabrics work well to protect against contamination and secondary exposure to CNT. The same spot SEM analysis studies reveal that displaced CNT particles on FC plasma treated PP are likely to reattach elsewhere on the fabric, providing an alternative method to limiting secondary exposure. With the concern of the potential carcinogenicity of CNT, the FC surface treatment may support the treated fabric traps CNT, thereby minimizing subsequent exposure.

When considering CB attachment, plasma modification appears to decrease the number of agglomerates attached to the material when compared to the untreated (UT) fabric. In addition, the counts on the shaken fabrics indicate that plasma treatment results in a smaller chance that the ENP will resuspend when the contaminated fabric is shaken. Although the sizes of the attached Al_2O_3 agglomerates seemed dependent on the plasma treatment used, both the FC and $H_2O_{(v)}$ modified Tyvek® had similar agglomerate counts on the contaminated and shaken samples, suggesting that plasma modification is an effective strategy to reduce secondary exposure to Al_2O_3. Results have been translated to two peer-review publications, five conference presentations and two manuscripts to be published.

Publications:

1. Hiyoto, K., Momtaz, S., Maksot, A., Reifenberger, R., Tsai, C.S.J.*, Fisher, E.*, Effects of Surface Hydrophobicity of Lab Coat Fabrics on Nanoparticle Attachment and Resuspension: Implications for Fabrics Used for Making Protective Clothing or Work Uniform, Apr. 21, 2023, ACS Applied Nano Materials, 6,9 7384-7394. [Impact factor: 5.097]
2. Maksot, A., Sorna, S., Blevens, M., Reifenberger, R., Hiyoto, K., Fisher E., Vindell, T., Li, Y., Kipper, M., Tsai, C.S.J.*, Engineered Nanoparticle Release from Personal Protective Clothing:

Implications for Inhalation Exposure, Feb. 11, 2022, ACS Applied Nano Materials, 5, 2, 2558-2568. [Impact factor: 5.097]

Manuscripts to be submitted for publications:

1. Ireland, N., Chen, Y.H., Tsai, C.S.J.*, Understanding engineered nanoparticle penetration of various properties through four types of commonly used lab coat fabrics.
2. Reifenberger, R., Tsai, C.S.J., An Atomic Force Microscope Study to Assess the Fundamental Interaction between ENPs and Fabrics.

Conference papers and presentations:

1. Tsai, CSJ.*, Maksot, A., Momtaz, S., Engineered Nanoparticle Resuspension Contributing to Inhalation Exposure from Contaminated Protective Clothing, Inhaled Particle and NanoOEH Conference, Manchester, England, May 15-18. 2023.
2. Tsai, C.S.J.*, invited panel speaker, Nanotechnology research and safety update panel: personal protective clothing use for nanomaterial exposure. A&WMA 115th Annual Conference & Exhibition, San Francisco, CA, Jun. 27-30, 2022.
3. Maksot, A., Momtaz, S., Blevens, M., Tsai, CSJ.*, A study of protective clothing to prevent nanoparticle exposure and surface contamination, podium, American Industrial Hygiene Conference and Exposition (AIHCE), May 24-26, 2021.
4. Momtaz, S., Maksot, A., Hiyoto, K., Fisher, E., Tsai, CSJ.*, Study of nanoparticle interaction with untreated and plasma treated lab coat fabric, poster, American Industrial Hygiene Conference and Exposition (AIHCE), May 24-26, 2021.
5. Maksot, A., Momtaz, S., Blevens, M., Tsai, CSJ.*, A Study of Protective Clothing to Prevent Nanoparticle Exposure and Surface Contamination, podium, 9th Nano Conference, Sustainable Nanotechnology Organization, Nanotechnology Occupational Environmental Health and Safety, virtual conference, Nov. 12-13, 2020.

Research Outcomes/Impact

Notably, different surface treatments resulting in materials repellent to airborne particles could be used in treating fabrics used for making protective clothing or work uniforms to minimize the contamination and spread of unwanted particles. With the concern of the potential carcinogenicity of CNT, the FC surface treatment may support the treated fabric traps CNT, thereby minimizing subsequent exposure.

Ultimately, the differences of the ENP behavior on the UT and plasma modified fabrics indicate that both fabric weave pattern and surface chemistry impact nanomaterial attachment and resuspension. These efforts toward understanding the role of material properties on the attachment of ENP may lead to strategies for determining what types of fabric are best for protecting the wearer from adverse health effects from exposure to nanomaterials.

It’s worthy to note that novel biobased nanoparticles such as cellulose nanocrystal were made for engineering applications and reinforcement agent in polymer and synthetic materials; our results may aid evaluations of such biobased nanoparticles. Although further work is needed to optimize the hydrophilic treatments of some of the fabrics and fully understand the effect of the surface modifications, these data demonstrate that plasma treatment is a viable route to creating improved materials for protective clothing. In conclusion for implications, the surface treatment resulting in materials repellent to airborne particles could be used in treating fabrics used for making protective clothing or work uniforms to minimize the contamination and spread of unwanted particles.

SECTION 2 OF THE REPORT

CHAPTER 1: Quantitatively document the severity of ENP exposure by both the dermal and inhalation routes from contamination of major fabrics used in laboratory clothing.

Introduction

The nanotechnology market is expected to grow 17% annually up to 2024[1], leading to the production of a variety of products using nanomaterials. The development of new applications with nanomaterials gives rise to risks and uncertainties regarding the exposure and adverse effects to human health and the environment[2]. One main concern with the growth of nanotechnology is the protection of frontline researchers in laboratories and workers in production facilities from exposure to engineered nanoparticles (ENPs) through inhalation or skin contact. Workers wearing contaminated clothing are at high risk of inhaling ENPs resuspended from clothing without any awareness of the potential danger. Moreover, when leaving the laboratory or production line, researchers and workers are unaware of possible ENP exposure from the contaminated clothing that they bring back to the office, home, or public places. That indicates the risk to non-workers outside of the workplace settings. It is well-documented in the previous studies that a mixture of monodisperse particles with the median sizes of 3, 5, and 10 μm has the ability to resuspend from contaminated clothing surfaces during human physical activities[3,4]. ENPs have diameters that are three orders of magnitude smaller, and volumes that are 10^{-9} smaller, than microparticles. Therefore, ENPs represent many times more particles than an equivalent mass or volume of microparticles resuspended from contaminated clothing.

In a pilot study, Tsai et al. studied a few commonly used fabric swatches and measured the level of nanomaterial release associated with each fabric type[5]. A substantial amount of particles were released from these contaminated fabric swatches during the constant manual manipulation of the fabric in both regular room and cleanroom settings[5]. A significant fraction of particles deposited onto clothing are subsequently resuspended into the air due to physical activities. This resuspension contributes to inhalation exposures[4,6]. Exposure to individual and small agglomerates of ENPs can evoke higher inflammation when compared with micrometer sized agglomerates of ENPs[7]. This evidence emphasizes the importance of understanding the resuspension of nanoparticles and the status of trapping and adhesion of ENPs on the protective clothing.

To date, there are no published studies that evaluate the severity of ENP exposure associated with commonly available protective clothing fabrics or determine the affecting factors for contamination and resuspension of ENPs from the contaminated clothing. Thus, the objectives of this study are to study potential exposure contributed by human activities when wearing the ENP contaminated personal protective clothing, and quantitatively evaluate relative ENP to each fabric type. Moreover, this research aims to evaluate the primary factors responsible for ENP adhesion and release from these fabrics and identify optimal fabric characteristics for protection against toxic ENPs. With this study, workers in different fields can readily choose appropriate personal protective clothing when working with certain types of ENPs, as suggested from our results.

Methodology

This study was comprised of two evaluations that include (1) ENP potential exposure at the breathing zone associated with simulated motions of workers walking with various contaminated protective clothing and (2) qualitative evaluation regarding the characteristics attribute to ENP adhesion, retention and resuspension from these fabrics.

Materials

Three common types of ENPs were studied, they were multi – walled CNTs (MWCNTs), aluminum oxide (Al_2O_3), and carbon black, representatives of popular ENPs in categories of high aspect ratio, hydrophilic/insulating sphere metal oxides, and hydrophobic/conducting sphere ENPs, respectively. MWCNTs are routinely produced in industrial settings by popular chemical vapor deposition (CVD) process. The primary diameter of MWCNT (purity > 95 %, Nanolab, Waltham, MA, USA) is between 10 to 30 nm, and the lengths are in the micrometer ranges. Aluminum oxide (Al_2O_3) (purity 100 %, Nanophase Technologies Corporation, Romeoville, IL, USA) ENPs are spherical with an average primary size of 40 nm. Carbon black (Printex grade) is widely used in a dry powder form in printer toners and ink. The average primary size of carbon black (purity 100 %, carbon black-Printex powder, Orion, Germany) is 40 nm. Four popular types of lab coat fabrics with woven vs. non-woven structures, tested in this study include cotton twill woven, polyester/cotton blend (80% polyester and 20% cotton) plain woven, polypropylene spunbond nonwoven, and polyethylene spunbond nonwoven (DuPont™ Tyvek®), respectively. All lab coats were purchased in adult size S through a commercial vendor of protective clothing. Isopropyl alcohol, distilled water and cleanroom wipes were used to carefully clean the equipment and surfaces of the enclosure in the fume hood where experiments were performed.

Facilities, Equipment and Procedure

The research was conducted in a class 100 level cleanroom to eliminate background aerosols and to provide the accurate measurements of ENPs. The cleanroom was operated at slightly negative pressure, enclosed to contain particles, and exhausted to a HEPA filter with an emergency evacuation remote controller. The background particle level in this cleanroom was approximately 0 – 70 particles/cm^3 in the 10 – 420 nm size range and less than 10 particles/cm^3 in the 0.3 – 10 µm size range. A special enclosure was designed and placed inside the fume hood in the cleanroom to contain generated aerosols and provide a controlled environment for each experiment. The enclosure was made from acrylic plastic and had two removable panels at the front to access the equipment and two filter panels (40.6 cm × 63.5 cm each) at the back to pre-filter and collect airborne ENPs, which captured particles as small as 0.3 µm, before venting through the HEPA filter of the fume hood exhaust as illustrated in Figure Ch1-1 (a).

(a)

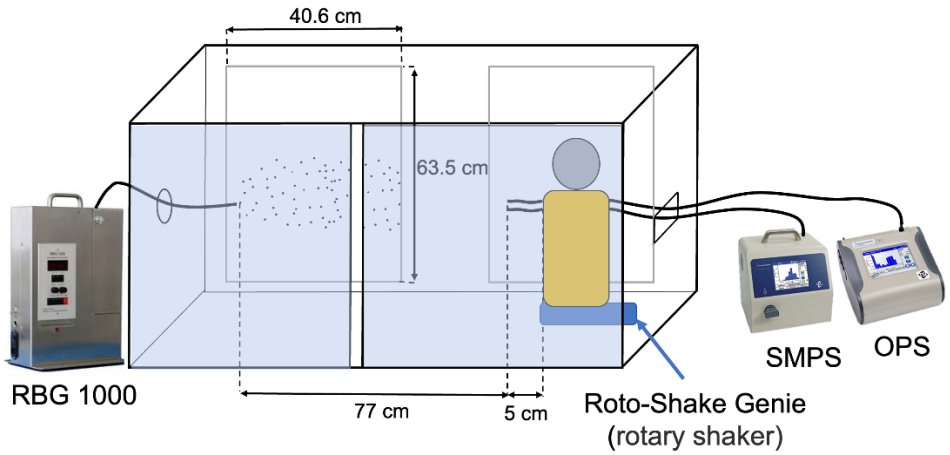

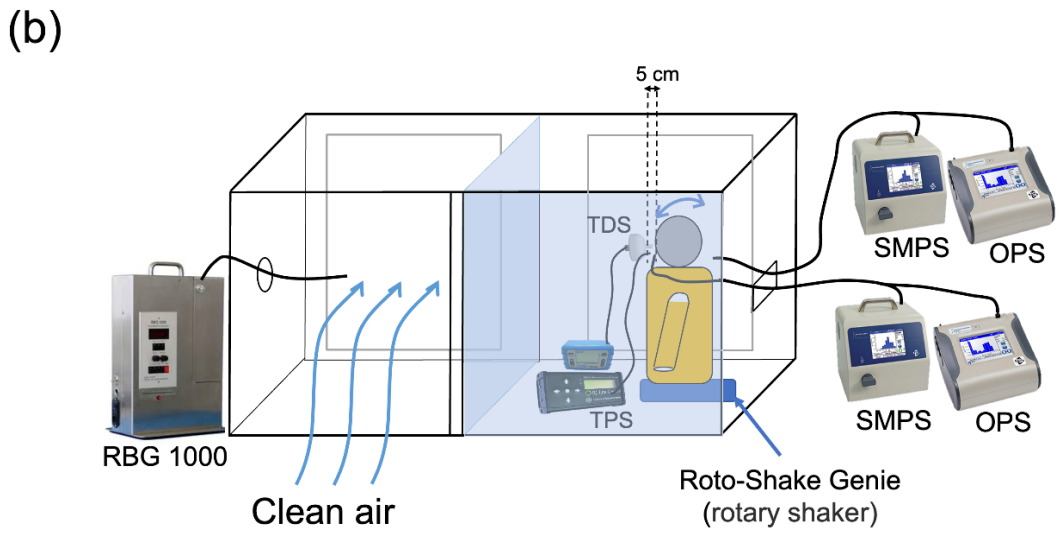

Figure Ch1-1. Illustrations of the contamination and resuspension processes and experimental setups. Clean air flew from the cleanroom toward the enclosure placed inside the fume hood. (a) Engineered nanoparticles (ENPs) aerosolization for contamination on lab coats. (b) Resuspension of ENPs through shaking the mannequin and particle samplings. Note: the shaker was kept underneath the mannequin all the time, but only operated for resuspension tests.

RBG 1000 – dust generator; SMPS – NanoScan Scanning Mobility Particle Spectrometer (SMPS); OPS – Optical Particle Sizer; TPS – Thermal Precipitation Sampler; TDS – Tsai Diffusion Sampler.

The main reason for having removeable panels at the front was for access to the mannequin and equipment; and during the experiments for evaluating ENP resuspension, the left side panel was relocated to the center of the enclosure to contain the mannequin and ENP resuspension at the right side as seen in Figure Ch1-1 (b).

ENPs were aerosolized by powder dispersion generator (RBG 1000, Palas GmBH, Germany), dispersing particles with the sizes between 0.1 µm and 100 µm, to contaminate lab coats worn by the mannequin. When the contamination was completed, the contaminated lab coat was kept on the mannequin in the rightmost compartment of the enclosure. This compartment was further isolated with a separation panel (Fig. Ch1-1b). The remaining aerosols (left side of the enclosure) outside of the isolated mannequin chamber were purged to lower the background aerosol concentration as much as possible. The separation panel was then reinserted to permit the particle resuspension measurements.

A shaker (Roto-Shake Genie rotary shaker, Scientific Industries, Bohemia, NY) was placed underneath the mannequin and held it to create movement on the mannequin to simulate gentle motions of workers and the subsequent resuspension of ENPs from contaminated lab coats. The shaker was operated at 70 cycles/min with the rocking angle of 10 degrees horizontally to simulate workers' motion such as walking-related vibrations causing particle resuspension from the contaminated lab coats.

The right and left side of the enclosure each has a hole to allow the conductive tubing of the direct reading instrument (DRIs) and cables of equipment to go through (Fig. Ch1-1). Particle number concentrations and size distributions of airborne ENPs during aerosolization and shaking the contaminated lab coat were measured with DRIs, including the NanoScan Scanning Mobility Particle Sizer (SMPS), a nanoparticle sizer suitable for low concentration measurement in a cleanroom setting (TSI Model 3910, Shoreview, MN, USA, 10 – 420 nm, 13 channels, concentrations 0 to 10^6 particles/cm^3) and the Optical Particle Sizer (OPS) (TSI Model 3330, Shoreview, MN, USA, 0.3 – 10 μm, 16 channels). The sampling flow rates for NanoScan SMPS and OPS were 0.9 L/min and 1.0 L/min, respectively. Both DRIs when operated together measure particle concentrations for diameters from 10 nm to 10 μm with a 1 min response time. The instruments were connected with conductive tubing (Model 3001901, TSI, Shoreview, MN, USA) which was approximately 1 m length (I.D. of 0.48 cm) to reach the measuring locations. Mass concentrations of resuspended ENP aerosols were calculated with mass differences of sampling filters before and after particle collections, the sampling flowrates and durations. We used a NIOSH Manual of Analytical Methods (NMAM) 5040 to analyze the amount of elemental carbon (organic carbon and total carbon) for the collected airborne MWCNT and carbon black[8]. We also used NMAM 0500 for analyzing mass concentration of Al_2O_3 nanoparticles and NMAM 7402 for mass concentration of MWCNT. NMAM 7402 is typically used for the evaluation of fiber-based particles such as asbestos and recently for CNT[9], while NMAM 0500 is used for the analysis of airborne particulates not otherwise regulated[10]. A thermal anemometer (VelociCalc® 9545, TSI, Shoreview, MN, USA) was used to measure the humidity, temperature and air velocity to ensure all work is done in a carefully controlled environment.

Two types of nanoaerosol samplers, a Tsai Diffusion Sampler (TDS)[11] and a thermal precipitation sampler (TPS) (RJLee, Monroeville, Pa, USA)[12,13], were used to collect airborne particles during the release process. The flow rate of the TDS was 0.3 L/min; it collected nano and respirable sized particles with cut off aerodynamic diameter of 3.8 μm[11]. A Transmission Electron Microscope (TEM, JEOL JEM – 2100F, Peabody, MA, USA) copper grid (SPI 200 mesh, carbon filmed) was taped onto a 25 mm diameter polycarbonate membrane filter (0.2 μm pore) and mounted in the TDS cassette. The TDS pulls air in with a sampling pump and directly collects ENPs on the grid and filter for TEM and Scanning Electron Microscope analysis (SEM, JEOL JSM 6500 FE—SEM, Peabody, MA, USA) to obtain morphology of ENPs. The TPS also collects ENPs directly onto a TEM grid with a flow rate of 0.05 L/min; the grids were analyzed using TEM. Due to the ferromagnetic ability, a nickel carbon filmed TEM grid was used to sample TPS.

Experimental process

Aerosolization of protective clothing with ENPs

ENP powders were dispersed approximately 77 cm in front of the mannequin dressed in a lab coat, which was attached with five swatches of the same lab coat fabric on the top of it to allow contamination to occur on the removable five swatches (Fig. Ch1-1). A powder dispersion generator RBG 1000 was operated at a dispersing pressure of 2 bar, the piston velocity of 5 mm/h and a rotational brush frequency of 1194 rpm. Five fabric swatches (20 cm × 20 cm) were used for each experiment, which represented the similar surface area of the lab coat where ENPs would deposit. Four fabric swatches were placed on the front side of the mannequin wearing a lab coat, and one fabric swatch was placed on the back side of the mannequin. Each swatch was weighed before and after experiments to obtain the mass changes. A set of DRIs were placed in front of the mannequin wearing protective clothing to measure the total number concentrations of exposed

ENPs. According to published data regarding occupational exposure concentrations of metal oxide particles, they were typically in the range of 10^4 to 10^5 particles/cm^3, including background particles[14], [15–19]. Thus, we dispersed ENP aerosols with concentrations ranging from 10^4 to 10^5 particles/cm^3 to simulate the practical contamination of a person wearing a lab coat in such a workplace. Background concentration measurements were taken for 10 min before the experiment to determine a clear baseline to compare the concentration increase during the contamination and resuspension processes.

Resuspension of particles from contaminated clothing

After surface contamination on the lab coat, the contaminated lab coat on the mannequin was then subsequently measured the suspension of ENPs, as shown in Figure Ch1-1 (b). Two sets of DRIs were used, one set to measure at the mannequin's nose and the other set to measure at 10 – 15 cm horizontally away from the back of the head, representing the breathing zone and bystander particle exposure. TDS and TPS collected particles during the release process at the same locations as DRIs at the front of the mannequin. The contaminated fabric swatches attached on the mannequin were shaken by the motion of the mannequin sitting on an automatic shaker to simulate a typical worker's motion. No air exchange occurred during this resuspension of ENPs. The ENPs deposited on the fabric surface were resuspended into the air through shaking. DRIs monitored concentrations of the whole process "at the breathing zone of the mannequin representing the particle release from the fabric to be inhaled by a worker" including background before contamination, during contamination, post-contamination, during resuspension and post-resuspension. The weight of the fabric swatches was measured before the aerosolization of ENP and after the resuspension process to evaluate the amount of ENPs trapped on the fabric swatches.

At the end of each experiment, fabric swatches were stored in a sealed bag then disposed of as hazardous waste. All surfaces were cleaned using distilled water and alcohol following standard cleanroom cleaning procedures to ensure no cross-contamination and overall safety.

Fabric descriptive property measurements and airborne particle sampling using standard methods are described in Supporting Information (SI).

Electron Microscopy Analysis

Fabric samples, plain and contaminated, were analyzed using SEM. For SEM analysis, the sample piece was held on a substrate with carbon tape, coated with different thicknesses of gold alloy and imaged with different accelerating voltage due to the thickness of each type of fabric. Tyvek® and polypropylene samples were coated with 25 nm of gold at 10 kV and cotton and polyester cotton samples were coated with 50 nm at 5 kV for high-resolution images. Similar specifications were used for TEM analysis.

Statistical Analysis

The airborne concentrations of ENP contamination and resuspension were further analyzed to interpret the statistical significances. Statistical analysis was conducted with the R and RStudio software package (version 1.4.1106, BCorps™, Boston, MA, USA). The aerosolized particle number concentration of different ENPs and release of ENPs from different fabrics were assessed and evaluated for correlation analysis. The mass change per unit mass of contaminated fabric swatches was assessed and evaluated using standard ANOVA techniques followed by Tukey's honestly significant difference test. At a 95% confidence level, p-values < 0.05 were considered statistically significant.

Results And Discussion

Resuspension Status of Nanoparticles from Contaminated Clothing

According to the contamination levels of each ENP studied, the average normalized number concentration of ENPs produced by the Powder Dispersion Generator RBG 1000 was measured in the size range between 10 – 420 nm by Nanoscan SMPS and 0.3–10 µm OPS. Measurements were repeated three times. The average measured normalized distribution for each of three ENPs was plotted in Figure S1, and data are further described in SI. The fabric structure and the contaminated fabric were illustrated in Figure Ch1-2. Small individuals and large agglomerates of particles were scattered across the surface of the fabric. Various morphologies of particle contaminate were observed on all types of fabric fibers.

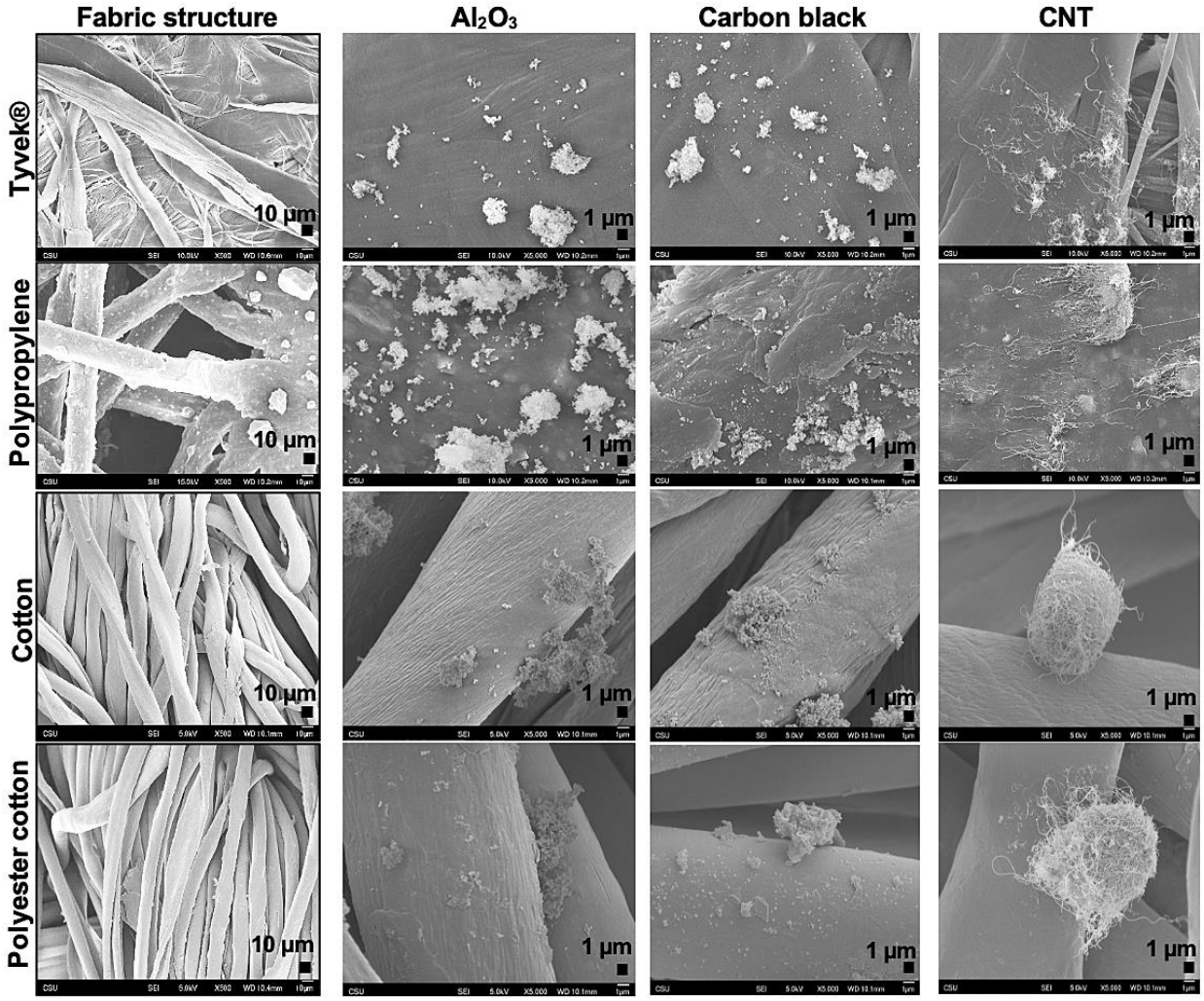

Figure Ch1-2. SEM images of the structure of each type of fabric and surface of the fabrics contaminated with three types of ENPs.

To minimize risks of secondary exposure through contaminated clothing, it was important to determine the level of ENPs resuspension and identify the fabric that would release least ENPs after contamination. Furthermore, any size-dependent adhesion of ENPs to a given fabric would be revealed by comparing the size distributions of resuspended particles to the generated ENPs

which contaminated the fabric. If the released distribution of ENPs was proportional to the contamination distribution, then the ENP size does not play a significant role in adhesion. If the size distribution of the released nanoparticles is significantly different from the size distribution of the generated ENPs, this might indicate that the fabric preferentially traps and/or releases ENPs as a function of size, implying a size-dependent adhesion mechanism that depends on the interaction between the ENPs and fabrics.

To investigate these questions further, the number concentration of airborne particles released from the contaminated protective clothing for each type of ENPs was measured by shaking the fabric after the contamination process. Two studies were analyzed. The first was a gravimetric study in which five fabric swatches attached onto the lab coat worn by the mannequin, initially contaminated by a specific ENP (Al_2O_3, carbon black, or CNTs), were weighed on a balance to determine its mass m_o, then shaken and reweighed to measure its mass m after shaking. The fractional mass change $\Delta m/m_o$ ($\Delta m=m_o - m$) was then calculated. In the second study, the size distribution of the ENPs released by the shaking of the mannequin attached with five contaminated fabric swatches was then determined for each of the fabrics under study using the DRI instrumentation shown in Figure 1. This analysis allowed a detailed size distribution of the released ENPs to be determined. Using these two analyses provided an estimate for the ENPs released by shaking, the amount of ENPs retained on the fabric and an integrated snapshot of the released ENPs irrespective of ENP size.

Mass change analysis

The mass change of a fabric swatch after shaking is a straightforward way to measure the extent that ENPs of different types adhere to each fabric. Because the thickness of each fabric type studied is different, it is difficult to directly compare the fractional mass change of a given ENP between fabrics. Instead, the gravimetric data are most useful to assess the trends between the different types of ENPs released by one fabric. The mass change data per unit mass of fabric are provided in Figure Ch1-3.

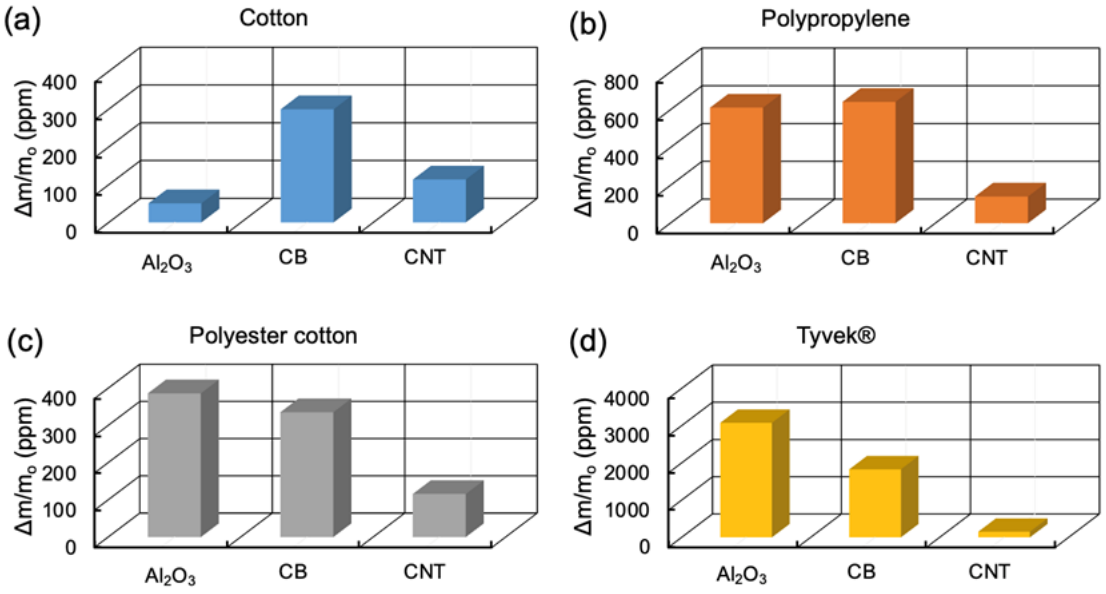

Figure Ch1-3. The fractional mass change after contamination and release of different ENPs from the four fabrics studied. (a) Cotton, (b) Polypropylene, (c) Polyester cotton, (d) Tyvek®.

According to Figure Ch1-3, Tyvek® fabric showed the highest mass change per unit mass from the Al_2O_3 ENPs contamination (3078 ppm), while polypropylene, polyester cotton and cotton presented lower mass change per unit mass of 611.6, 386.3 and 50.6 ppm respectively. Cotton and polyester cotton fabric were much thicker with higher weight m_o than Tyvek® and polypropylene resulting a lower mass change per unit mass of fabric. From the contamination and release of carbon black ENPs, Tyvek® was also found to be the fabric with the highest mass increase per unit mass with the value of 1821.2 ppm, followed by polypropylene with 642.1 ppm, polyester cotton with 335.5 ppm and cotton with 299.6 ppm of mass increase per unit mass. However, the mass change per unit mass of CNT ENPs was similar for all fabrics.

Based on statistical analysis shown in Figure S2 (a) in the supplementary material (see Appendix), there is a significant difference between the mass change per unit mass of Tyvek® compared with polypropylene, cotton and polyester cotton ($p < 0.05$) with 95% confidence level. However, cotton, polyester cotton and polypropylene are not significantly different from each other ($p > 0.05$). Figure S2 (b) shows similar results for the mass change per unit mass from the contamination and release of carbon black ENPs. The results are quite similar to the results from Al_2O_3 (Fig. S1 (a)). The main difference is the mass change per unit mass of Tyvek® fabric is not significantly different from the mass change per unit mass of polypropylene fabric ($p > 0.05$). It is clearly seen from Figure S2 (c), there is no significant difference between fabrics from CNT ENPs contamination and release tests.

Size distributions analysis of released nanoparticles

The number concentrations of released airborne particles from contaminated protective clothing for each type of ENPs are presented in Figure Ch1-4. It is significant that the concentrations of the released nanoparticles in the 10 – 100 nm size range are about a factor of 1000 less than the contaminating concentrations plotted in Figure 2, indicating the high degree of nanoparticle adhesion to all the fabrics studied. Consistently for all studied ENPs, the cotton fabric showed the highest level of particle release, compared with other fabric types. The highest number concentration of Al_2O_3 ENPs released from cotton fabric were 134 particles/cm^3 at particle size of 115 nm, whereas polypropylene fabric released the least number of particles, with number concentrations less than 33 particles/cm^3. The highest number concentrations of airborne Al_2O_3 ENPs released from polyester cotton fabric and Tyvek® fabric were 101 and 37 particles/cm^3 at size 48 nm and 37 nm, respectively. According to Figure Ch1-4 (b), the number concentrations associated with carbon black ENP release from cotton and polyester cotton fabric were lower compared with Al_2O_3 ENP release. Figure Ch1-4 (c) shows that Tyvek®, polypropylene and polyester cotton fabric materials showed approximately similar levels of CNT ENPs release concentration during manipulation; the cotton fabric released the most, followed by the Tyvek®, polyester cotton and polypropylene fabric based on the average release concentrations.

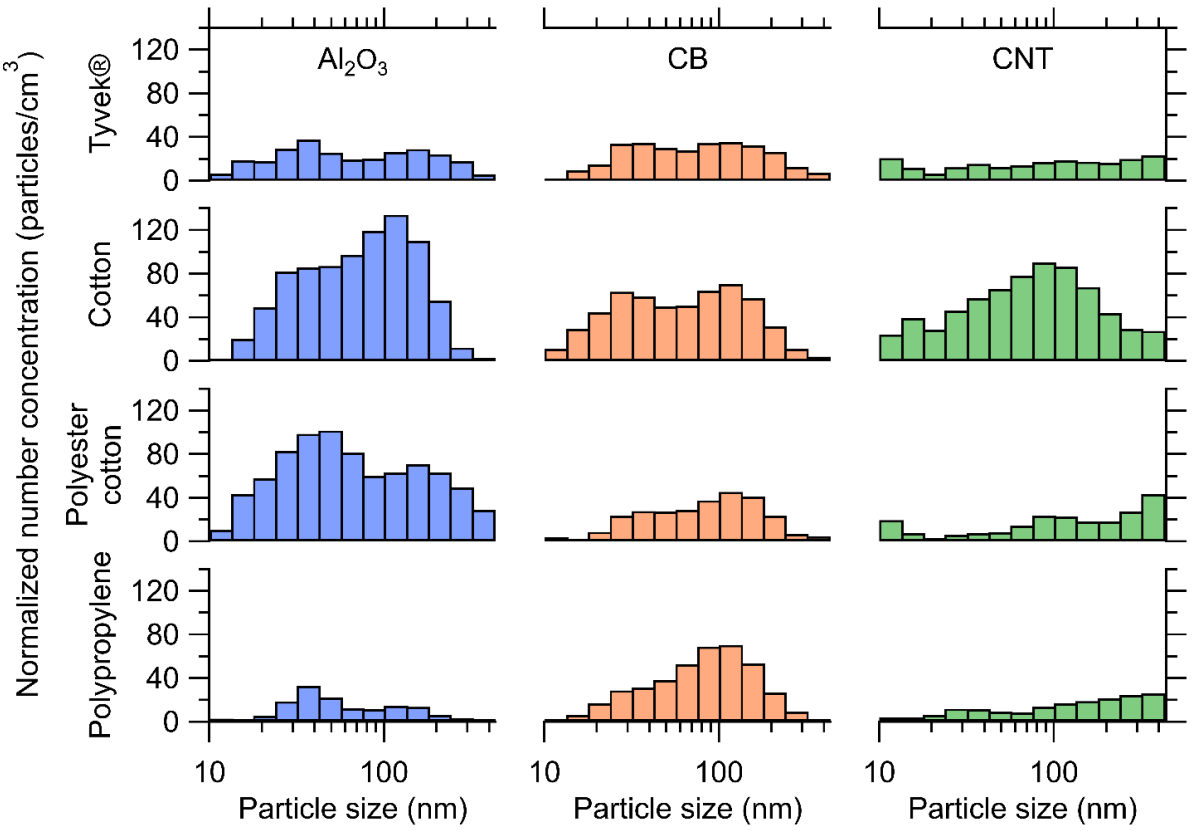

Figure Ch1-4. Measured normalized particle concentrations released after the shaking of contaminated lab coats made from Tyvek®, cotton, polypropylene and polyester cotton. Graph columns present (a) for Al_2O_3 release, (b) for carbon black (CB) and (c) for carbon nanotube (CNT).

Three important conclusions can be drawn that (1) a higher release of Al_2O_3 ENPs was from cotton and polyester cotton fabrics compared to the release of either carbon black or CNT ENPs from the same fabric, (2) cotton fabric was distinctive because it showed an increased concentration of released Al_2O_3 and CNT ENPs when compared to the other fabrics studied, and (3) the release of Al_2O_3 and carbon black ENPs from all fabrics appears to have a bi-modal distribution that is apparently a different size distribution which is not related to the contaminating distribution plotted in Figure 2. This result is especially pronounced for cotton fabric, indicating that Al_2O_3 and carbon black ENPs contaminating cotton likely have a size-dependent adhesive character.

By comparing the normalized distributions in Figures Ch1-4(a), (b) and (c), it is clear that the release concentrations of cotton and polyester cotton in Figure 4(a) have a higher concentration of released Al_2O_3 ENPs when compared to released carbon black and CNTs found in Figures Ch1-4(b) and (c). This result can be understood by the higher concentration of contaminating Al_2O_3 ENPs as shown in Figure Ch1-2. In addition, from Figure 4(a), the cotton fabric released the highest level of Al_2O_3 ENPs of all fabrics studied. This would suggest that when dealing with metal-oxide ENPs, a polypropylene and Tyvek® fabric would offer clear advantages in trapping the ENPs over cotton, polyester-cotton or polypropylene fabrics.

For the case of carbon black contamination, Figure Ch1-4(b) indicated that the overall concentration associated with carbon black release from cotton and polyester cotton fabric was about a factor of 1.5 lower when compared with Al_2O_3 ENP release, even though Figure Ch1-2 indicates the contaminating concentration of carbon black is comparable to that for Al_2O_3. Polypropylene and Tyvek® were found to have the lowest carbon black ENP release. The data in Figure Ch1-4(b) further suggests a bimodal distribution of carbon black ENP release from all fabrics studied, a trend that is most clearly evident for the cotton fabric. The measured released distributions are distinctly different in shape from the contamination distribution as shown in Figure Ch1-2, indicating that 60-70 nm sized carbon black ENPs adhere more strongly to cotton fabric than either a smaller or larger sizes.

For the case of CNT contamination, Figure Ch1-4(c) shows that Tyvek®, polypropylene and polyester cotton fabric showed approximately similar levels of CNT ENP release during manipulation. The release concentration of CNT ENPs for cotton was the highest when compared to Tyvek®, polypropylene or the polyester cotton fabric. These levels of resuspension were associated with a short-term contamination and release time. When prolonged contamination and exposure occurs, the risk of affecting human health will be raising with further results presented in this study.

The mean differences in particle release concentration were found to be statistically significant at the $p = 0.05$ level. According to Table S2 (see Appendix), the Al_2O_3 total number concentrations resuspended from the cotton and polyester cotton fabrics were found to be significantly different from Tyvek® and polypropylene, while cotton is not significantly different from polyester cotton with the p-value of 0.80. Similar for carbon black total number concentrations, cotton and polyester cotton fabrics were significantly different from Tyvek® and polypropylene; however, based on total number concentration results of CNT ENPs, cotton was turn out to be significantly different from all other fabrics at the $p = 0.05$ level. Statistical analysis on correlation was made on the resuspension concentrations of Al_2O_3, carbon black and CNT ENPs. Based on Table S3 and S4 from supplementary material, the strong correlation between the fabrics can be observed for particle size distributions of resuspended Al_2O_3 and carbon black ENPs with low *p*-values, meaning that there is a strong relationship between the particle size distribution of manipulated fabrics. According to the Table S5 related to the results of particle size distributions of released CNT ENPs, the negative or low correlation factor and high p-values can be seen from the comparison between the cotton and other fabrics, which indicate that there is no significant relationship between the variables.

Integrated analysis of released particle sizes, morphology, and concentrations

The resuspended particles collected on the polycarbonate filters of TDS samples are presented with SEM images in Figure 5. Large agglomerates and individual particles of Al_2O_3, with many smaller than 1 μm, were released from the surface of Tyvek® fabric, as shown in Figure Ch1-5(a). Limited amounts of carbon black particles were seen with some individual particles at approximately 50 nm (Fig. Ch1-5(b)). As seen in Figure Ch1-5(c), small CNT clusters containing single fibers were collected during the release process of Tyvek® fabric. The limited amount of CNT ENPs collected imply a low resuspension concentration during the shaking process, whereas the larger amount of Al_2O_3 ENPs and carbon black released from the surface of the fabric was

consistent with the higher total number concentration of released particles presented in Figure 4.

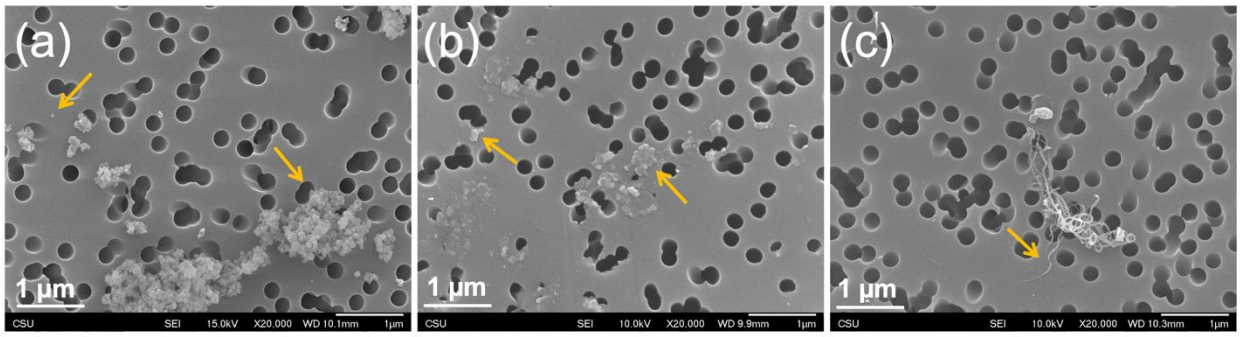

Figure Ch1-5. SEM images of resuspended ENPs collected on polycarbonate membrane filter (0.2 µm pore) of TDS samples (a) Al_2O_3. (b) carbon black. (c) CNT. Arrow marks note single ENPs or agglomerates.

Data presenting airborne particle mass concentrations by filter-based sampling and the total number concentrations from Figure Ch1-4 were listed in Table Ch1-1 for comparisons. Based on the released total number concentrations measured by SMPS, where it is clearly seen that the release concentration measured from the front side of the mannequin was higher than the release concentration measured at the back of the mannequin. Based on the total number concentrations at the front and back sides of the mannequin, the highest release concentration of Al_2O_3 and CNT ENPs was found from manipulating cotton fabric, while polyester cotton fabric release concentration was the highest for carbon black ENPs. The total number concentration during the release of Al_2O_3, carbon black and CNT ENPs for Tyvek® and polypropylene fabrics were found to be the lowest.

Table Ch1-1. Released level of airborne ENPs number and mass concentrations of various types of lab coat.

ENPs	Lab coat fabric type	At front # (30 min)	At back # (30 min)	At front + (6 h)	At front (6 h)	At front Total carbon*	
		Number conc. 10-420 nm (particles/cm^3)			Mass conc. (µg/m^3)	µg/ sample	µg/ m^3
Al_2O_3	Cotton	174 ± 64	30 ± 7	258	29.8[a] ± 0.1	-	-
	Polypropylene	83 ± 41	61 ± 41	73	1.2[a] ± 0.1	-	-
	Polyester cotton	163 ± 46	101 ± 54	210	21.3[a] ± 0.2	-	-
	Tyvek®	88 ± 37	45 ± 22	75	2.2[a] ± 0.4	-	-
Carbon Black	Cotton	96 ± 21	91 ± 22	198	89.9[b] ± 0.3	20[c]	27[c]
	Polypropylene	74 ± 13	69 ± 16	121	10.8[b] ± 0.1	12[c]	16[c]
	Polyester cotton	102 ± 17	86 ± 19	254	79.4[b] ± 0.1	16[c]	22[c]
	Tyvek®	90 ± 36	61 ± 5	114	22.2[b] ± 0.1	19[c]	27[c]
CNT	Cotton	126 ± 58	108 ± 47	223	12.3[b] ± 2.4	16[c]	23[c]
	Polypropylene	52 ± 15	42 ± 12	72	7.8[b] ± 4.5	13[c]	18[c]
	Polyester cotton	59 ± 7	37 ± 7	105	10.8[b] ± 2.5	16[c]	22[c]
	Tyvek®	42 ± 6	32 ± 23	87	2.9[b] ± 1.3	12[c]	17[c]

a: Mass concentration calculated using NIOSH Manual Analytical Method (NMAM) 0500 close face for collecting airborne particles for 6 hours at a flowrate of 2 L/min.

b: Mass concentration calculated using NMAM 7402 open face for collecting airborne particles for 6 hours at a flowrate of 2 L/min.

c: Mass concentration measured using elemental carbon analysis for 6 hours at a flowrate of 2 L/min.

#: Data are the average of three experiments. Each experiment has 30 sets of data.

+: Data are the average from one experiment with 360 sets of data.

*: Released total carbon is the sum of released elemental carbon and organic carbon, analyzed using NMAM 5040 collecting for 6 hours.

Two major conclusions can be made from Table Ch1-1. First of all, the level of generated CNT aerosols was lower compared with Al_2O_3, which was an affecting factor showing a lower mass increase for all fabrics exposed with CNT ENPs. Since our focus was evaluating the difference between fabric types with the same ENP, the small variation in the generated ENP concentrations could be neglected. Moreover, CNT ENPs are considered the lightest nanoparticles among the other used ENPs, therefore the mass increase for each type of fabric was lower compared with Al_2O_3 and carbon black ENPs data. Based on these results, Tyvek® is the best fabric for trapping Al_2O_3 and carbon black ENPs, resulting in less resuspension of particles from the contaminated lab coat. There is not much difference in trapping ENPs between polypropylene, polyester cotton, and cotton fabrics. Secondly, the difference in resuspended total number concentrations between the front and back of the mannequin, as was expected the concentrations of released particles at the breathing zone (front side) are higher than particles released from the back side of the worker wearing the contaminated protective clothing.

Table Ch1-1 also presented the results for the long-term exposure of released nanoparticles, with one hour of exposure followed by six hours of shaking. The 6-hr shaking represents the time when worker wear contaminated clothing/lab coat performing gentle motion of task such as walking, moving arms siting in office or operating equipment during a work shift. The measurements were taken at the breathing zone presenting the particle release to be inhaled by a worker, it would have minimal effects by the room size. It is clearly seen that the release number concentration level after one hour of exposure was much higher than the concentration after 30 minutes of exposure. The total number concentration during six hours of release from the manipulation of cotton and polyester cotton fabric were around two times higher than 30 minutes of release, while there was small difference between the six hours and 30 minutes of release of Tyvek® and polypropylene.

Table Ch1-1 also presented the mass concentrations of released airborne particles following the NMAM 0500 protocol for collecting Al_2O_3 ENPs, and the NMAM 7402 and 5040 protocols for carbon black and CNT ENPs. Note that a large amount of carbon black and CNT ENPs were collected because an open-face cassette for inhalable-sized particles was used, while the Al_2O_3 collection was conducted using a closed-face cassette. The highest amount of released ENPs were collected from the surface of cotton and polyester cotton fabrics for all types of ENPs, while least amount of ENPs were collected from the surface of polypropylene and Tyvek® fabrics.

It seems clear that cotton fabric released the highest amount of carbon black ENPs based on the release mass concentration of total carbon with the value of 27 $\mu g/m^3$ or 20 µg/sample, while the least released fabric was polypropylene with the total carbon mass concentration of 16 $\mu g/m^3$. The released total carbon of Tyvek® and polyester cotton fabric from the exposure of carbon black were 19 µg/sample and 16 µg/sample respectively. Based on the CNT ENPs released total carbon results, cotton fabric was also found to be the most released fabric with the total carbon of 23

μg/m^3 and Tyvek® fabric was observed with the lowest released of 17 μg/m^3. The current recommended exposure limit set by U.S. NIOSH for CNTs is 1 μg/m^3 of total carbon.

The evidence of nanometer sized particles resuspended from was further characterized using TEM and SEM as shown in Figures Ch1-6. Individual particles and agglomerates of airborne Al_2O_3, carbon black and CNT fibers released from the surface of the fabric were clearly seen in Figure Ch1-6.

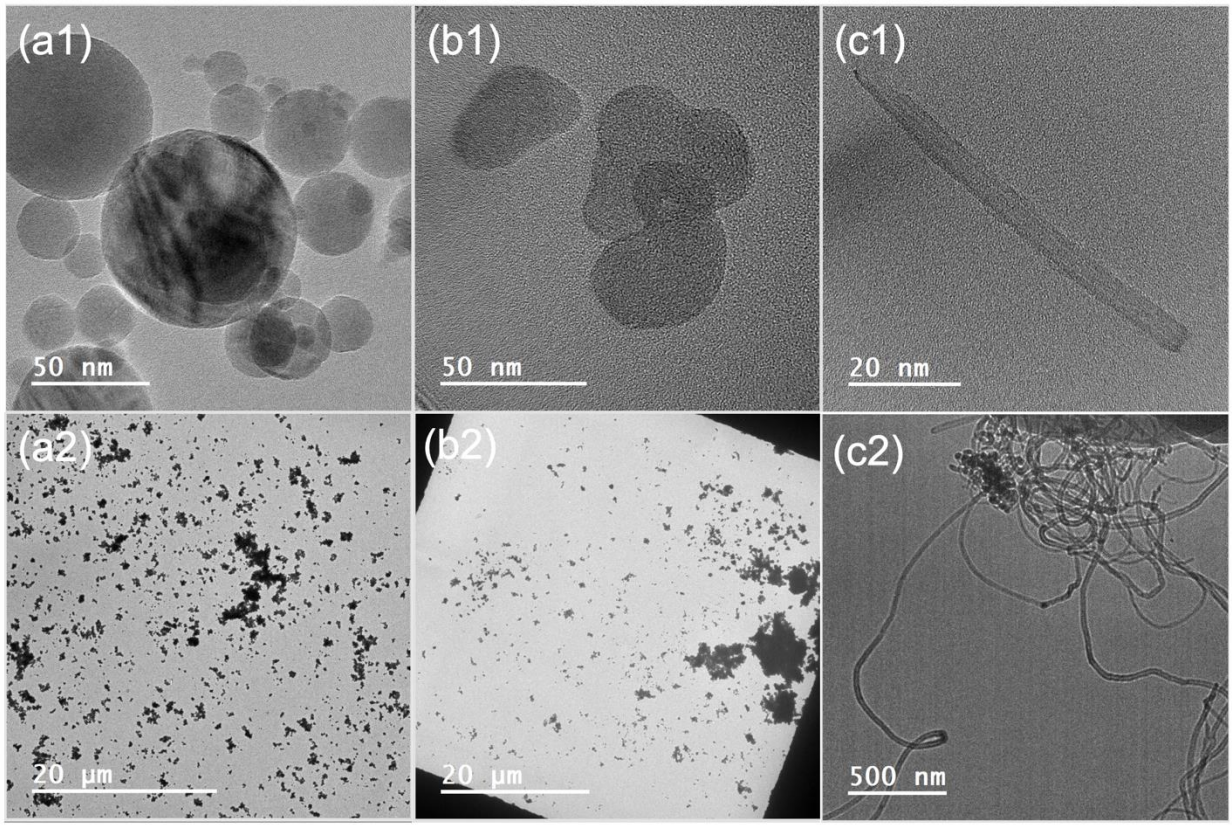

Figure Ch1-6. TEM images of sampled ENPs on grid collected on TDS samples (a1) and (a2) Al_2O_3 at 50 nm and 20 μm scale bars. (b1) and (b2) carbon black at 50 nm and 20 μm scale bars. (c1) and (c2) CNT at 50 nm and 500 nm scale bars.

Theoretical discussion of particle-fabric adhesion

The released number concentration of ENPs is ultimately determined by the strength of the nanoparticle adhesion to each fabric. A detailed accounting of the interaction between an ENP and a fabric surface is complicated because it depends upon many variables, most of which are unknown and difficult to accurately determine. For this reason, rather than focusing on numerical predictions for adhesion forces, we look for trends that can be inferred from the measurement of ENP release. A further complication is that a number of different physical forces can contribute to adhesion. While electrostatic charging may attract an ENP to a fabric, once in contact, other forces usually control how strongly an ENP adheres to the fabric. These forces can depend on the elemental chemical composition of both the ENP and fabric as well the separation distance between an ENP and the fabric. In the case of uncharged ENPs that do not chemically bond to a fabric surface, the dominant particle-substrate interaction is usually attributed to either (1) a surface force that arises from inter-molecular van der Waals (vdW) interactions or (2) a capillary force due to a thin water bridge that forms between the ENP and the fabric surface. The influence of any electrostatic forces due to electrostatic charging are expected to dominate only when the ENP is separated from the substrate by a distance of ~10 nm or more.

The integral form of the vdW molecular interaction (often called the Hamaker force) is typically larger than electrostatic forces and thus is often invoked as the dominant force that attracts nanometer-sized particles toward a surface. Once in contact, the force that holds the two bodies together is termed an adhesive force. If the interaction between the ENP and fabric is perfectly elastic so no energy is dissipated during their interaction, and if no chemical reaction occurs, then the adhesive force will be equal in magnitude to the vdW surface force. The theoretical forces related to particle fabric adhesion are described with details in SI, the estimated Hamaker constants are presented in Table Ch1-2.

Table Ch1-2. In a), the Hamaker constants for the materials used in this study. In b), estimates for the interaction Hamaker constants H_{12} calculated using Eq. 2 in Supplementary Information (SI) in Appendix.

(a) Hamaker Constants for Materials of Interest

	ENP or fabric	**Equivalent material**	**Value (in J)**
H_{11}	Al_2O_3	alumina	15.0×10^{-20}
	Carbon black	carbon	47.0×10^{-20}
H_{22}	Cotton	cellulose	5.8×10^{-20}
	Polypropylene	polypropylene	6.0×10^{-20}
	Tyvek®	HD polyethylene	6.3×10^{-20}
	Polyester cotton	poly(ethylene terephthalate)	8.8×10^{-20}

(b) H_{12} (in J), from Eq. 2 (Appendix, Chapter 1 SI)

	Al_2O_3	**Carbon black**
Cotton	9.3×10^{-20}	16.5×10^{-20}
Polypropylene	9.5×10^{-20}	16.8×10^{-20}
Tyvek®	9.7×10^{-20}	17.2×10^{-20}
Polyester cotton	11.5×10^{-20}	20.3×10^{-20}

Note: H_{12} is the Hamaker constant describing the interaction between the ENP 1 and the planar surface 2. H_{11} and H_{22} describe the interaction between a material 1 (or 2) with itself.

With estimates for H_{12}, checks can be made to determine if vdW interactions alone can qualitatively account for the trends observed for the release of ENPs presented in Figure 4. For example, if vdW interactions largely determine the adhesion of Al_2O_3 ENPs to the fabrics studied, then from the estimates of H_{12} in Table 2(b) we see that to a first approximation, all H_{12} are about the same, i.e. $H_{12}^{polyester-cotton} \approx H_{12}^{polypropolyene} \approx H_{12}^{polyethylene} \approx H_{12}^{cotton}$. Thus, if the vdW interaction is the dominant adhesive force, all the Al_2O_3 ENP release distributions from the various fabrics should have roughly the same shapes and magnitudes, especially for smaller values of the ENP diameter D_s. However, the measurements in Fig. 4 showed that cotton preferentially released a significantly higher concentration of Al_2O_3 ENPs implying that the vdW interaction for Al_2O_3 ENPs and cotton should be the weakest. This contradicts the predictions made on the basis of Table 2(b) where all the H_{12} have similar values.

A similar conclusion can be drawn by considering CB ENPs. As seen from Table 2(b), the Hamaker constant H_{12} describing the interaction of CB ENPs with each fabric is ~1.8 times larger than for Al_2O_3. This implies that if vdW forces are dominant, the vdW adhesion force for a CB ENP to a fabric fiber should be about 1.8 times greater than that of an Al_2O_3 ENP of the same size. This would then further imply that the released number concentration of CB ENPs after shaking should be reduced by a factor of roughly 1/1.8= 0.6 when compared to the released distribution of Al_2O_3 ENPs. Since the initial contamination distribution of CB and Al_2O_3 are very similar (see Fig. 2), if vdW forces are dominant, the release concentration of CB ENPs should be roughly 0.6 the number concentrations measured for Al_2O_3 ENPs. Figure 3 indicates that while this expectation is approximately true for CB on cotton and polyester cotton, the expectation is not met for CB on Tyvek® or polypropylene.

Taken together, an analysis of the systematics between the measured number concentrations of released Al_2O_3 and CB ENPs do not support the hypothesis that vdW forces constitute the dominant adhesive force for the various combinations of ENP/fabrics studied. A similar analysis for CNT ENPs was not attempted because the long tubular shape of the tangled CNTs is not well approximated by the sphere/plane geometry as required in Eq.1 above.

After ruling out vdW forces as the dominant adhesion force, the next interaction between an ENP and a fabric fiber we consider is capillarity. This interaction is related to the formation of a small bridge of moisture between an ENP and the fabric that supports it. A thin equilibrated water layer that depends on the relative humidity (RH) is present on all surfaces exposed to ambient conditions and this thin water layer aids the water bridge formation. The RH in the lab then control the amount of water that will spontaneously condense in the small volume near the contact region

between the ENP and the fabric surface. The water bridge serves to bind the ENP to the surface. In the limit of high humidity, complete immobilization of ENPs often result.

In the case of very low humidity, or if the surface chemistry of either the ENP or the fabric acts to prevent water condensation, the capillary force will be greatly reduced. Since cotton absorbs water, while polyester, polypropylene and polyethylene do not, an ENP resting on a cotton fiber should show a reduction in the capillary force when compared to the other three fabric surfaces. This observation would in turn predict a significantly weaker adhesion of ENPs to cotton, resulting in a greater release of these ENPs when compared to the three other fabrics. This trend is in fact observed for the Al_2O_3, CB, and CNT ENPs in Figure 4, a result that strongly suggests that capillarity likely plays a dominant role in affixing ENPs to the fabrics under study.

A secondary trend can be discerned by examining the ENP release data from polyester cotton fabric in Figure 3. The measured released number concentrations from polyester cotton are somewhat larger than the release distributions from polyethylene and polypropylene. The implication is that the 20% cotton fibers present in the polyester cotton blend fabric play a role in ENP adhesion. It is likely that the 20% cotton fibers interwoven between the 80% majority of polyester fibers enhances the wicking of condensed moisture, thereby reducing the effects of capillary forces between ENPs and the polyester cotton fabric surface.

Mechanical properties (durability) of lab coat fabrics

Figure S3 (see Appendix) showed representative strain-stress curves of the four untreated fabrics including cotton woven, polyester cotton woven, Tyvek® nonwoven, and polypropylene nonwoven. The stress-strain curves of cotton and polyester cotton woven were similar while those of Tyvek® and polypropylene nonwoven were similar. The curves of two woven fabrics can be divided into two zones at the yield point: the first zone corresponds to situation when the yarns within the fabrics move due to friction, resulting in deformation of weaves; the second zone is associated with the elongation of the yarns until the yarns break at the point of breaking shown on the strain-stress curves. Higher tensile strength, was found in the polyester cotton (39.74 ± 6.50 MPa) than in the cotton (30.39 ± 4.00 MPa), suggesting that the polyester cotton fabric is stronger than the cotton fabric. The addition of polyester yarns to cotton enables reinforcement of cotton fabric. The polyester cotton Young's modulus (97.85 ± 10.00 MPa) is lower than the Young's modulus of cotton (152.15 ± 10.00 MPa).

On the other hand, the two nonwoven fabrics (Tyvek® and polypropylene) showed significantly different behaviors when they were stretched in comparison with the woven fabrics. They were stretchy without true breaking during the test. Tyvek® fabric demonstrated immediate plastic deformation and the stress flattens at approximately 0.5% strain. Polypropylene fabric showed plastic deformation during the entire test. The tensile strengths of the Tyvek® and polypropylene fabrics were 11.64 ± 3.35 MPa and 3.11 ± 0.81 MPa, respectively. Although they were notably lower than those of cotton and polyester cotton fabrics, the Tyvek® still showed a considerable strength against stretching compared to polypropylene. No Young's modulus was reported for the nonwoven fabrics, suggesting that both nonwoven fabrics are soft.

In summary, the cotton and polyester cotton woven have high strength and stiffness and hence would have substantial durability in the workplace when compared to the Tyvek® and polypropylene lab coats. Comparing Tyvek® to polypropylene, Tyvek® showed appreciable durability when being used in lab coats.

Abrasion resistance is the ability of a fabric to resist surface wear caused by flat rubbing and can also be used to measure fabric durability. Table S6 showed abrasion resistance measuring average cycle before fabric failure that was defined by onsite of visible holes on fabric surface. The woven fabrics showed significantly higher abrasion resistance than the nonwoven fabrics. In addition, cotton was nearly twice as strong as polyester cotton against rubbing. First, the cotton fabric was thicker than the polyester cotton. Secondly, it was because the cotton woven has a twill structure that has more interlacing than a plain weave. Therefore, twill woven hold yarns together more efficiently than plain woven. The Tyvek® and polypropylene coats both have substantially low abrasion resistance. The results were in a good agreement with the strain-stress curve results, suggesting that the cotton and polyester cotton fabrics have superior mechanical properties, while the Tyvek® and polypropylene fabrics are weak materials and would be used to make disposable lab coats.

WCA analysis of the four fabrics were shown in Table S7. These data revealed that the Tyvek® and polypropylene coats are hydrophobic (with static WCA of 125.9 ± 4.5° and 121.7± 6.3°, respectively) and the cotton polyester and cotton coats are hydrophilic (absorption rates of 4.24 ± 0.75 and 18.9 ± 3.5 μL/s, respectively). From the known chemical structures and XPS analysis, these results are expected as polypropylene and Tyvek® (patented type of high-density polyethylene) are synthetic fibers composed of hydrocarbon polymers, while the woven materials contain some oxygen functionality.

Conclusion

This study showed substantial particle release results for all types of tested fabrics. The release concentration for cotton and polyester cotton fabric were determined to be the highest from the aerosolization of Al_2O_3 and carbon black ENPs, while Tyvek® and polypropylene showed the lowest amount of release concentration. From the exposure of CNT ENPs, the cotton fabric showed the highest release concentration compared with other tested fabrics. The release concentration of cotton and polyester cotton were significantly different from Tyvek® and polypropylene for Al_2O_3 and carbon black ENPs, while for CNT ENPs cotton fabric turned out to be significantly different from all other fabric. Moreover, for all types of tested fabrics the total number concentrations of resuspended ENPs at the breathing zone are higher than particles released from the back side of the worker wearing the contaminated protective clothing. Regarding exposure to multiple ENPs, it will require further studies to discover the rules of contamination based on chemical composition, particle size and other surface properties of a mixture.

The total number concentration from one hour contamination and six-hour release processes could represent the exposure of full-shift work presenting risk of human exposure. Based on results of mass change measured before contamination and after the release processes, Tyvek® fabric indicated the statistically highest value of mass change per unit mass from the exposure of Al_2O_3 and carbon black; for CNT ENPs all fabrics showed a statistically similar level of mass change per unit mass. Some of the ENPs stay on the surface of the fabric due to the ENP adhesive forces. Two fundamental forces might be responsible for Al_2O_3 and carbon black ENP adhesion are van der Waals force and capillary force, but it was difficult to determine for CNT ENPs due to their non-circular shape. Our analysis presented, the dominant force for adhesion of ENPs with fabric fiber varies by the environmental condition (such as humidity). Capillary force can differ greatly with fabric absorbing moisture. A further study is ongoing investigating the mechanisms of adhesion and surface interactions between ENPs and fabric surface.

Overall, Tyvek® is the best fabric for trapping all three types of studied ENPs, which eliminates the resuspension to expose humans. However, this fabric was not durable enough for workers to wear for a long term or the active motions at work might cause wear or tearing of the Tyvek® fabric, reducing its barrier properties and enabling penetration of ENPs. The polypropylene fabric is the next most effective for trapping ENPs of all three types. In addition, three types of ENPs were found to cause some difference in terms of adhesion onto the fabric surface, and we found that the Al_2O_3 ENPs remained on the fabric the most, especially more on the Tyvek® fabric, after simulated working activities, compared to other carbon black and CNT ENPs. Cotton and polyester cotton lab coats were found to be the least effective fabric type for trapping ENPs. Although these fabrics are the most durable, comfortable and commonly used in the workplaces, they are not recommended to be used when ENPs are present in work environments.

References

(1) Global Nanotechnology Market Outlook 2024 - Research and Markets https://www.researchandmarkets.com/reports/4991720/global-nanotechnology-market-outlook-2024 (accessed 2021 -01 -17).

(2) Clemente, A.; Jiménez, R.; Encabo, M. M.; Lobera, M. P.; Balas, F.; Santamaria, J. Fast and Simple Assessment of Surface Contamination in Operations Involving Nanomaterials. *Journal of Hazardous Materials* **2019**, *363*, 358–365. https://doi.org/10.1016/j.jhazmat.2018.10.011.

(3) McDonagh, A.; Byrne, M. A. The Influence of Human Physical Activity and Contaminated Clothing Type on Particle Resuspension. *Journal of Environmental Radioactivity* **2014**, *127*, 119–126. https://doi.org/10.1016/j.jenvrad.2013.10.012.

(4) McDonagh, A.; Byrne, M. A. A Study of the Size Distribution of Aerosol Particles Resuspended from Clothing Surfaces. *Journal of Aerosol Science* **2014**, *75*, 94–103. https://doi.org/10.1016/j.jaerosci.2014.05.007.

(5) Tsai, C. S. J. Contamination and Release of Nanomaterials Associated with the Use of Personal Protective Clothing. *The Annals of occupational hygiene* **2015**, *59* (4), 491–503. https://doi.org/10.1093/ANNHYG/MEU111.

(6) Licina, D.; Nazaroff, W. W. Clothing as a Transport Vector for Airborne Particles: Chamber Study. *Indoor Air* **2018**, *28* (3), 404–414. https://doi.org/10.1111/ina.12452.

(7) Liang, X.; Xu, Z.; Grice, J.; Zvyagin, A.; Roberts, M.; Liu, X. Penetration of Nanoparticles into Human Skin. *Current Pharmaceutical Design* **2013**, *19* (35), 6353–6366. https://doi.org/10.2174/1381612811319350011.

(8) NIOSH Manual of Analytical Methods (NMAM), Fourth Edition.

(9) ASBESTOS by TEM 7402. **1989**.

(10) CDC; Niosh. NMAM 0500: PARTICULATES NOT OTHERWISE REGULATED, TOTAL.

(11) Tsai, C. S. J.; Theisen, D. A Sampler Designed for Nanoparticles and Respirable Particles with Direct Analysis Feature. *Journal of Nanoparticle Research* **2018**, *20* (8), 1–14. https://doi.org/10.1007/s11051-018-4307-2.

(12) Thayer, D.; Koehler, K. A.; Marchese, A.; Volckens, J. A Personal, Thermophoretic Sampler for Airborne Nanoparticles. *Aerosol Science and Technology* **2011**, *45* (6), 744–750. https://doi.org/10.1080/02786826.2011.558943.

(13) Leith, D.; Miller-Lionberg, D.; Casuccio, G.; Lersch, T.; Lentz, H.; Marchese, A.; Volckens, J. Development of a Transfer Function for a Personal, Thermophoretic

Nanoparticle Sampler. *Aerosol Science and Technology* **2014**, *48* (1), 81–89. https://doi.org/10.1080/02786826.2013.861593.

(14) Tsai, S. J.; Ada, E.; Isaacs, J. A.; Ellenbecker, M. J. Airborne Nanoparticle Exposures Associated with the Manual Handling of Nanoalumina and Nanosilver in Fume Hoods. *Journal of Nanoparticle Research* **2009**, *11* (1), 147–161. https://doi.org/10.1007/s11051-008-9459-z.

(15) Methner, M. M. Effectiveness of Local Exhaust Ventilation (LEV) in Controlling Engineered Nanomaterial Emissions during Reactor Cleanout Operations. *Journal of Occupational and Environmental Hygiene* **2008**, *5* (6), D63–D69. https://doi.org/10.1080/15459620802059393.

(16) Methner, M.; Hodson, L.; Dames, A.; Geraci, C. Nanoparticle Emission Assessment Technique (NEAT) for the Identification and Measurement of Potential Inhalation Exposure to Engineered Nanomaterials—Part b: Results from 12 Field Studies. *Journal of Occupational and Environmental Hygiene* **2010**, *7* (3), 163–176. https://doi.org/10.1080/15459620903508066.

(17) Hameri, K.; Lahde, T.; Hussein, T.; Koivisto, J.; Savolainen, K. Facing the Key Workplace Challenge: Assessing and Preventing Exposure to Nanoparticles at Source. *Inhalation Toxicology*. Taylor & Francis 2009, pp 17–24. https://doi.org/10.1080/08958370902942525.

(18) Park, J.; Kwak, B. K.; Bae, E.; Lee, J.; Kim, Y.; Choi, K.; Yi, J. Characterization of Exposure to Silver Nanoparticles in a Manufacturing Facility. *Journal of Nanoparticle Research* **2009**, *11* (7), 1705–1712. https://doi.org/10.1007/s11051-009-9725-8.

(19) Miller, A.; Drake, P. L.; Hintz, P.; Habjan, M. Characterizing Exposures to Airborne Metals and Nanoparticle Emissions in a Refinery. *The Annals of Occupational Hygiene* **2010**, *54* (5), 504–513. https://doi.org/10.1093/annhyg/meq032.

CHAPTER 2: Quantitatively document the severity of ENP exposure by penetrating fabric from contamination of major fabrics used in laboratory clothing.

Introduction

Protective clothing provides protection against nanoparticle (NP) dermal absorption, and protection against settling and resuspension from street clothing into the environment. To protect the health of people working within the ENP manufacturing sector, personal protective equipment (PPE) is recommended. The Center for Disease Control and Prevention (CDC) and the National Institute of Occupational Safety and Health (NIOSH) recommend wearing long pants and long sleeved shirts, lab coats not made from cotton woven material, nitrile gloves, closed toe shoes, and safety goggles when working with ENPs (NIOSH, 2016).[4] PPE is an important control measure against human exposure to NPs when other administrative and engineering controls are insufficient. It is important to wear a lab coat that has a high nanoparticle capture efficiency, low nanoparticle penetration, and is comfortable to wear for the duration of a working day. Determining the most effective type of protective lab coat fabric against NP penetration is important to consider when implementing a nanomaterial safety program.

Previous studies have shown ENP contamination for certain fabrics is substantial. Maksot et al. (2022) reported large amounts of ENP adhesion and release from four tested fabrics (polypropylene, Tyvek, cotton, and polyester cotton), with the cotton fabric releasing the highest amount of ENPs after shaking. A study by Tsai (2015) found that the mass ratio of release to deposited nanoparticles was about 50% for cotton, polyester, and Tyvek fabrics. Licina and Nazaroff (2018) found that clothing can serve as a vector for transporting small aerosols from one location to another, increasing the chance of airborne particle exposure for humans. Clothing and other fabrics can be highly contaminated with ENPs, and can release these particles into the environment at a later time, therefore it is important to study the penetration potential of fabrics used as protective clothing. Penetration of protective lab coats can lead to the contamination of undergarments or street clothing worn under the protective coats, which can lead to resuspension of the ENPs and secondary exposure through inhalation well after someone has left the laboratory or manufacturing floor.

Most NPs are captured onto media by diffusion since they are smaller than 100 nm. Ultrafine particles move in a random pattern defined as Brownian motion, where small aerosol particles move irregularly due to the bombardment of gas molecules against the particle. Brownian motion increases the likelihood that a small particle will collide with and stick to a fiber (Golanski et al., 2009). Larger particles would be captured onto media by interception or impaction (Hinds & Zhu, 2022). Many NPs form larger agglomerates of about 1 μm to over 20 μm, so the processes of interception, impaction, and settling are important to consider when determining the efficiency of fabrics to capture ENPs.

Several previous studies have tested the penetration and filtration efficiencies of fabrics commonly used as PPE against NPs under a wide range of conditions (Gao et al., 2011; Golanski et al., 2009; He et al., 2020; Jamriska, 2009; Konda et al., 2020; Rengasamy et al., 2010). One study conducted by Rengasamy et al. (2010) found that cloth face masks and cotton clothing items had 40-90% penetration when challenged with polydisperse sodium chloride (NaCl) aerosols. Konda et al. (2020) compared the filtration efficiencies of cotton with high thread counts to cotton with lower thread counts, and found the higher thread count cotton is more efficient with 65-90% efficiency for 10 nm - 6 μm particle sizes compared to 5-55% efficiency for cotton with lower

thread counts when challenged with NaCl aerosols. Golanski et al. (2009) tested nonwoven polypropylene, cotton, and Tyvek fabrics against graphite nanoparticles sized between 10-100 nm, and observed the highest penetration percentages were for cotton fabric, and the lowest were for Tyvek. Nonwoven fabrics exhibited lower penetration percentages compared to woven fabrics. Lee and Liu (1980) have predicted the minimum efficiency and most penetrating particle size (MPPS) for filters, and determined MPPS decreases with increasing filter volume fraction and decreasing filter fiber size. (Lee & Liu, 1980).

Fabric characteristics such as fiber and fabric thickness, porosity, fiber diameter, and packing density play a major role in determining the filter efficiency and penetration percentages of common PPE. The four fabric types chosen for this study represent commonly used PPE for protection against NP exposure with varying physical characteristics. NP characteristics also play an important role in penetration and filtration efficiency of fabrics. The ENPs tested in this study were chosen as challenge aerosols due to their differing properties and wide use in industry.

To date, no systematic study has been conducted to evaluate the filtration efficiency of four types of fabrics commonly used as PPE against three types of NPs involving agglomerates and individual NPs representing the real time exposure scenarios. This study aims to quantitatively evaluate penetration percentages of commonly available protective clothing (with fabric made of Tyvek, cotton, polypropylene, and polyester cotton) with ENPs (CNT, CB, and Al_2O_3), in order to inform those who routinely interact closely with different ENPs on the most effective protective clothing to wear. This research also aims to elucidate the mechanisms behind particle capture of spherical and non-spherical ENPs on different types of protective fabrics, and the role fabric characteristics play in particle capture mechanisms.

Methodology

Materials

Three different types of ENPs and four different types of protective clothing were evaluated in this study. Multi-walled carbon nanotubes (MWCNTs), aluminum oxide (Al_2O_3), and carbon black (CB) were chosen as they are common ENPs used in industry whose properties differ from each other. CNT and CB are hydrophobic, while Al_2O_3 is hydrophilic. Both CB and Al_2O_3 are circular shaped while CNT can be characterized by having an aspect ratio of greater than 3:1(Birch et al., 2017). CNT and CB are chemically similar to each other, however, they differ in size and shape (Hiyoto et al., 2023). The MWCNTs were obtained from Nanolab (Waltham, MA, purity >95%), with a primary diameter between 10-30 nm, and lengths in the micrometer range, and are usually produced by chemical vapor deposition. The Al_2O_3 nanoparticles were obtained from Nanophase Technologies Corporation (Romeoville, IL, purity 100%). These ENPs are spherical with an average primary size of 40 nm. The CB nanoparticles were obtained from Printex (Orion, Germany, purity 100%), with an average size of 40 nm. CB nanoparticles are usually used as dry powder in printers and toners.

Four common types of lab coats were tested in this study, with both woven and nonwoven fabrics included. The woven fabrics include cotton twill, and polyester cotton blend (80% polyester, 20% cotton) plain woven. The nonwoven fabrics include polypropylene spun bond, and polyethylene spun bond (DuPont Tyvek). The lab coats were purchased through a commercial vendor of protective clothing in an adult size small. Fabric characteristics such as fabric structure, fiber size, fabric thickness, porosity, water contact angle and absorption rate, and water vapor transmission rate (WVTR) were determined for each fabric. Fiber size was increased in the non woven fabrics compared to the woven fabrics, while thickness and water vapor transmission rate

decreased in the non woven fabrics. Porosity varied between the fabrics, with polypropylene being the most porous, followed by polyester cotton, cotton, and Tyvek. According to Hiyoto et al. (2023), the nonwoven fabrics polypropylene and Tyvek are composed mostly of carbon, while the woven fabric cotton and polyester cotton contained about 10-15% more oxygen.

Facilities, Equipment, and Procedure

A schematic diagram of the experimental setup can be found in Figure 1a. The research was conducted in a closed glove box (89 cm × 61 cm × 64 cm) with a ventilated ultra-filter-system (Terra Universal, Fullerton, CA, USA) to eliminate background aerosols. The filter system on the glove box ran overnight between each ENP trial, then background particle levels inside the glovebox were measured. Background particle levels were determined to be negligible in both the 10-420 nm particle size range and the 0.3-10 µm particle (~10 particle/cm^3) for CNT, and were corrected for during CB and Al_2O_3 trials (<100 particle/cm^3). An enclosure made of acrylic plastic with a removable top was placed inside the glovebox to provide a second layer of control during the experiment. The filter holder was then placed inside this enclosure.. The aerosol generator used was the Wright Dust Feeder II (WDF II) (CH Technologies, USA) . Two direct reading instruments (DRIs), the Nanoscan Scanning Mobility Particle Sizer (SMPS) (TSI Model 3910, Shoreview, MN, 10− 420 nm) and the Optical Particle Sizer (OPS) (TSI Model 3330, Shoreview, MN, 0.3− 10 µm) were used to monitor and record aerosol concentrations. The WDF II was placed inside the glovebox and connected to the sampling enclosure with conductive tubing. The DRIs were placed outside of the glovebox, and connected to the sampling enclosure with conductive tubing. One set of DRIs was located 10 cm upstream of the filter cassette within the sampling enclosure, and the other set of DRIs was connected to the downstream end of the cassette, as shown in Figures Ch2-1a and 1b. A thermal anemometer (VelociCalc 9545, TSI, Shoreview, MN) measured humidity and temperature at 46-48%, and 75-75.4°F respectively. Particle number concentrations and size distributions were measured both upstream and downstream using two DRIs each, as shown in Figure Ch2-1a.

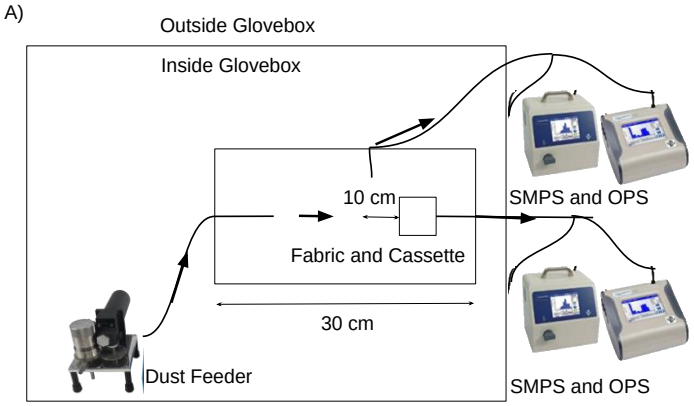

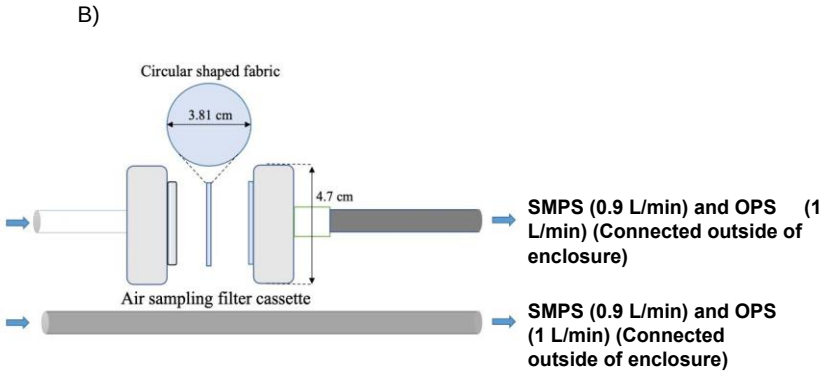

Figure Ch2-1. Schematic diagram of the experimental setup. (a) Diagram of the entire experimental setup. (b) Close up diagram of the fabric inside the air sampling cassette. Dust feeder - Wright Dust Feeder II; SMPS- Scanning Mobility Particle Sizer; OPS- Optical Particle Sizer.

Fabric Preparation

Before fabric sample preparation, the surfaces of tools and lab bench were wiped off with isopropyl alcohol and deionized water. With gloved hands, each fabric swatch was cut into a circular shape with a diameter of about 3.81 cm. The fabric samples were then placed in clean petri dishes and transferred to the glove box. Each fabric was placed in a 47 mm in-line filter holder (Pall Corp., Port Washington, NY, USA), and secured flat over the entire opening of the filter holder as shown in Figure 1b. In order to reduce the loss from fabric particles downstream, clean air was run over each fabric sample for 30 minutes inside the glove box. This was done to clean the fabric and ensure the downstream particle concentrations measured by the SMPS and OPS did not contain a significant amount of fabric particles.

Aerosolization of ENPs

ENP aerosolization was achieved by using the dry powder disperser WDF II. The WDF II was packed with ENPs and manually stamped down before each trial. Clean air was pumped through the dust feeder at a rate of 20 psi, while the WDF II was operated at a speed of 2.00 -4.00 rpm in order to disperse the ENPs in the range 10^3-10^5 particles/cm^3. The Nanoscan SMPS and OPS ran at a sampling flow rate of 0.9 L/min and 1.0 L/min respectively. Together, the instruments measured particles ranging from 10 nm - 10 µm with a collective sampling flow rate of 1.9 L/min. The face velocity was calculated as 0.028 cm/s. This face velocity represents typical face velocities at the surface of protective clothing due to fabric resistance and blunt body airflow patterns (Gao et al., 2011). Since the face velocity was low, particle concentrations did not immediately stabilize. Thus, the experiment was run for an average of 10 minutes before particle concentrations stabilized. After the initial 10 minutes, upstream and downstream data was collected for 30 minutes. Each fabric trial was replicated three times under the same operating conditions. The enclosure inside the glovebox was wiped down with deionized water, and the outside surface of the conductive tubing was wiped with Sani wipes, between each of the trials to minimize background concentrations. Penetration was determined by comparing the upstream concentration

to the downstream concentration. The penetration percentage ((D/U)x 100) was then calculated. This investigation also analyzed the penetration size distribution of the four fabrics in order to determine the most penetrating particle size (MPPS) for each ENP across the different fabrics.

Scanning Electron Microscopy (SEM) Analysis

Both ENP contaminated and clean fabric samples from each fabric type were analyzed using SEM. Each fabric sample was taped to a substrate using carbon tape, coated with gold alloy, and imaged. The SEM images were used to compare the upstream versus downstream contamination of each piece of fabric, and to compare the contaminated fabrics to the uncontaminated fabrics.

Statistical Analysis

The penetration of three different types of ENPs against four different types of fabrics was further analyzed for statistical significance. One way ANOVA analysis was conducted to determine the statistical significance between fabric penetration of each ENP, and across the same fabric when challenged with different ENPs. Statistical analysis was conducted with the Stata BE software package (version 17.0, StataCorp, College Station, TX). At a 95% confidence level, p-values <0.05 were considered statistically significant.

Results And Discussion

Fabric Characteristics

Certain physical characteristics, such as fabric structure, fiber size, fabric thickness, water vapor transmission rate (WVTR), porosity, static water contact angle (WCA), absorption rate, and pore volume, were calculated or measured in order to better understand the mechanisms behind why each ENP, with different morphologies and chemical properties, is captured or penetrates through each type of fabric. The measured descriptive properties are shown in Table Ch2-1. Fabric structure, fiber size, thickness, porosity, and pore volume provide insight into the specific fabric's ability to trap large and small particles. Thicker nonwoven fabrics that are with low porosity and large fiber size should have a higher particle capture efficiency when compared to fabrics without these characteristics. Tyvek fabric is the least porous, while cotton is the thickest fabric. Polypropylene is the most porous fabric. The static WCA and absorption rate measurements were used to determine the hydrophilicity or hydrophobicity of each fabric. Polyester cotton, Tyvek and polypropylene were all found to be hydrophobic, while cotton was found to be hydrophilic. More information on how each descriptive property was calculated to be available in the prepared manuscript. SEM images of each non contaminated fabric tested in this study are shown in Figure Ch2-2. The two woven fabrics (cotton and polypropylene) were composed of layers of individual fibers in a defined pattern. The Tyvek non-woven fabric had no discernable individual fibers, and instead consisted of multiple layers forming a consistent web of material, which was consistent throughout the fabric swatch. The polypropylene non-woven material did not have a consistent pattern throughout. Some areas consisted of fibers with large gaps in between, and other areas were composed of a consistent web of material. The SEM images support the data that polypropylene fabric is the most porous with the highest pore volume.

Table Ch2-1. Measured descriptive properties of the four fabrics tested.

Fabric	Fabric Structure	Fiber Size (μm)	Thickness (mm)	WVTR (g/m^2xday)	Porosity	Static WCA	Absorption Rate (μL/s)	Pore Volume (m^3/kg)
Cotton	Twill Woven	18.1±1.4	0.66±0.01	7561±196	0.464	—	18.9±1.2	0.00101
Polyester Cotton	Plain Woven	Polyester= 12.0±0.8 Cotton= 21.5±2.5	0.41±0.01	7070±561	0.431	—-	4.24±0.25	0.00101
Tyvek	Non Woven	Single Fiber= 13.9±1.4 Entire Fabric= 28.2±7.1	0.15±0.01	3216±61	0.498	125.9± 1.5	—-	0.00105
Polypropylene	Non Woven	29.2±3.5	0.25±0.01	6121±149	0.232	121.7± 2.1	—-	0.00368

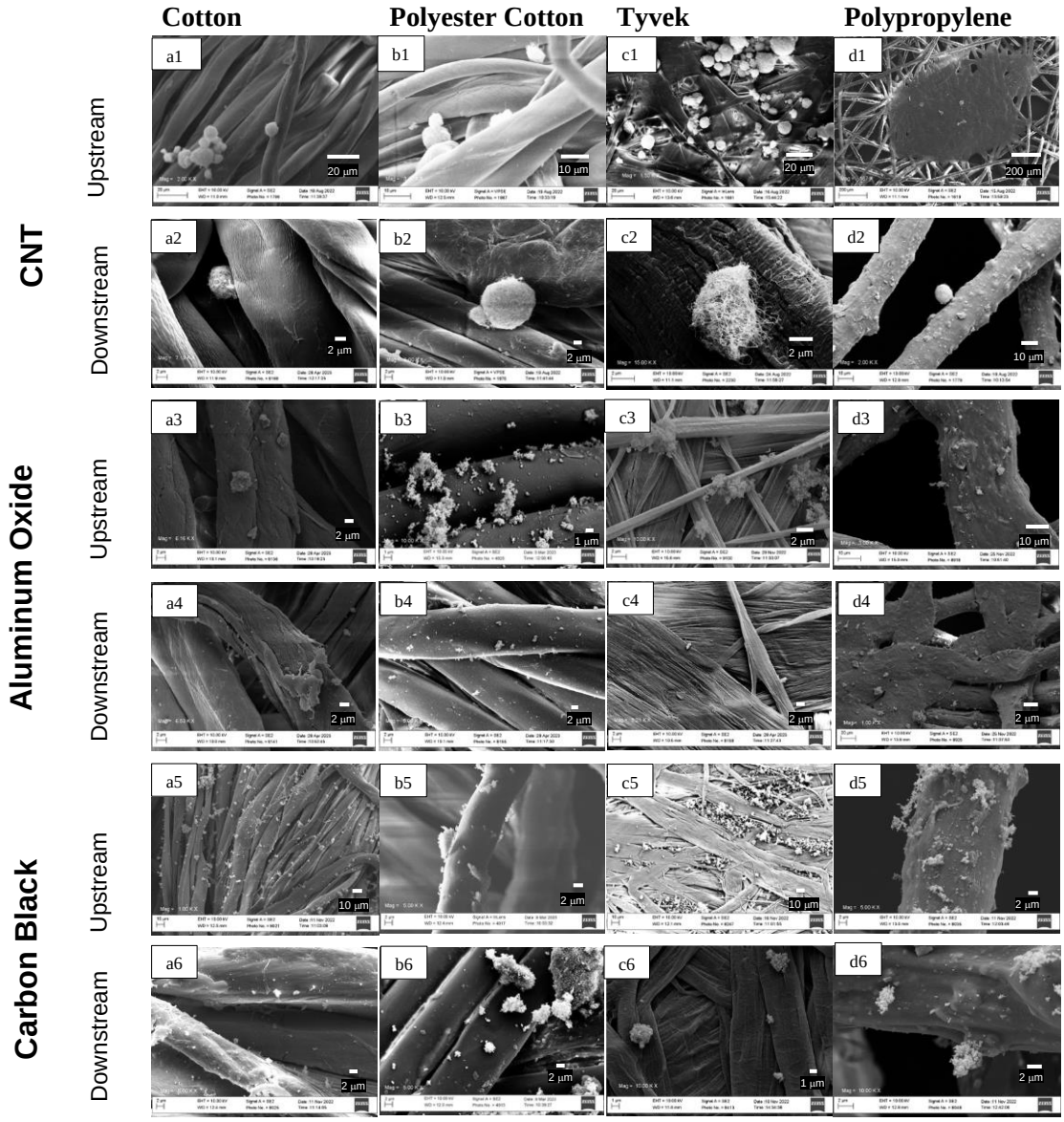

Figure Ch2-2. SEM images of the upstream and downstream sides of each of the four fabrics when challenged with CNT, aluminum oxide, and carbon black ENPs

Penetration of Different Fabrics Against the Same ENP

Comparing the penetration percentages of each type of fabric for one type of ENP is helpful in determining the most protective fabric against different types of nanoparticles. Using this data along with each fabric's physical and chemical characteristics, the mechanisms by which each fabric captures particles will be elucidated. The particle size fractioned penetration percentages for each type of fabric when challenged with CNT are shown in Figure Ch2-3a-b. Overall, all four fabrics had very similar penetration percentages across the range 48.7-154 nm. The MPPS for all fabrics was 154 nm, with penetration percentages between 3-5%. Overall, no fabric had statistically significant higher penetration percentages. It can be concluded that all four fabric types are equally protective for CNT nanoparticles between the sizes 48.7-154 nm. For larger CNT

particles between 0.3-1 µm, the cotton fabric had the highest penetration percentages, at 31% in the 0.35 µm size range. Cotton had significantly higher penetration percentages than Tyvek in the 0.3 µm size range (p=0.046), but penetration was not statistically significant between cotton, polypropylene, and polyester cotton. CNT particles tend to stick together and form very large agglomerates, greater than 10 µm. One of the reasons penetration percentages are so low for all fabrics may be because many of the larger particles were out of the particle size range for this investigation, and had settled onto the fabric or penetrated without being counted.

The particle size fractioned penetration percentages for each type of fabric when challenged with Al_2O_3 are shown in Figure Ch2-3c-d. The MPPS across the size range 48.7-154 nm were 154 nm. At 154 nm, the polypropylene fabric had the highest penetration of about 32%, followed by cotton (18%), 80/20 (9%), and Tyvek (0.1%). However, none of the fabrics were significantly different from each other at these size ranges. The MPPS across the size range 0.3 µm to 1 µm was 0.35 µm for all fabrics, with polypropylene fabric having the highest penetration at 64%, followed by cotton (47%), 80/20 (29%), and Tyvek (0.08%). The Tyvek fabric penetration was significantly lower compared to the other three fabrics in this size range. For Al_2O_3 particles, Tyvek is the most protective fabric, while polypropylene and cotton are the least protective fabrics.

The particle size fractioned penetration percentages for each type of fabric when challenged with CB nanoparticles are shown in Figure Ch2-3e-f. The MPPS was 48.7 nm for all fabrics. There was also a slight increase in penetration at the 115.5 nm size range for all fabrics except polyester cotton. At the 48.7 nm size range, polyester cotton had the highest penetration at about 51%, followed by polypropylene (33%), cotton (4%), and Tyvek (0.09%). At the 115.5 nm size range, polypropylene had the highest penetration at 22.4%, followed by polyester cotton (15%), cotton (3%), and Tyvek (0.06%). At both of these size ranges, none of the fabrics were statistically different from each other. In the 0.3 - 1 µm size range, the MPPS was 0.35 for all fabrics. Polypropylene, polyester cotton, and cotton all had very similar penetration percentages at 96%, 93%, and 89% respectively. Tyvek penetration at this size range was 0.6%. Tyvek fabric penetration was significantly lower compared to the other three fabrics at this size range.

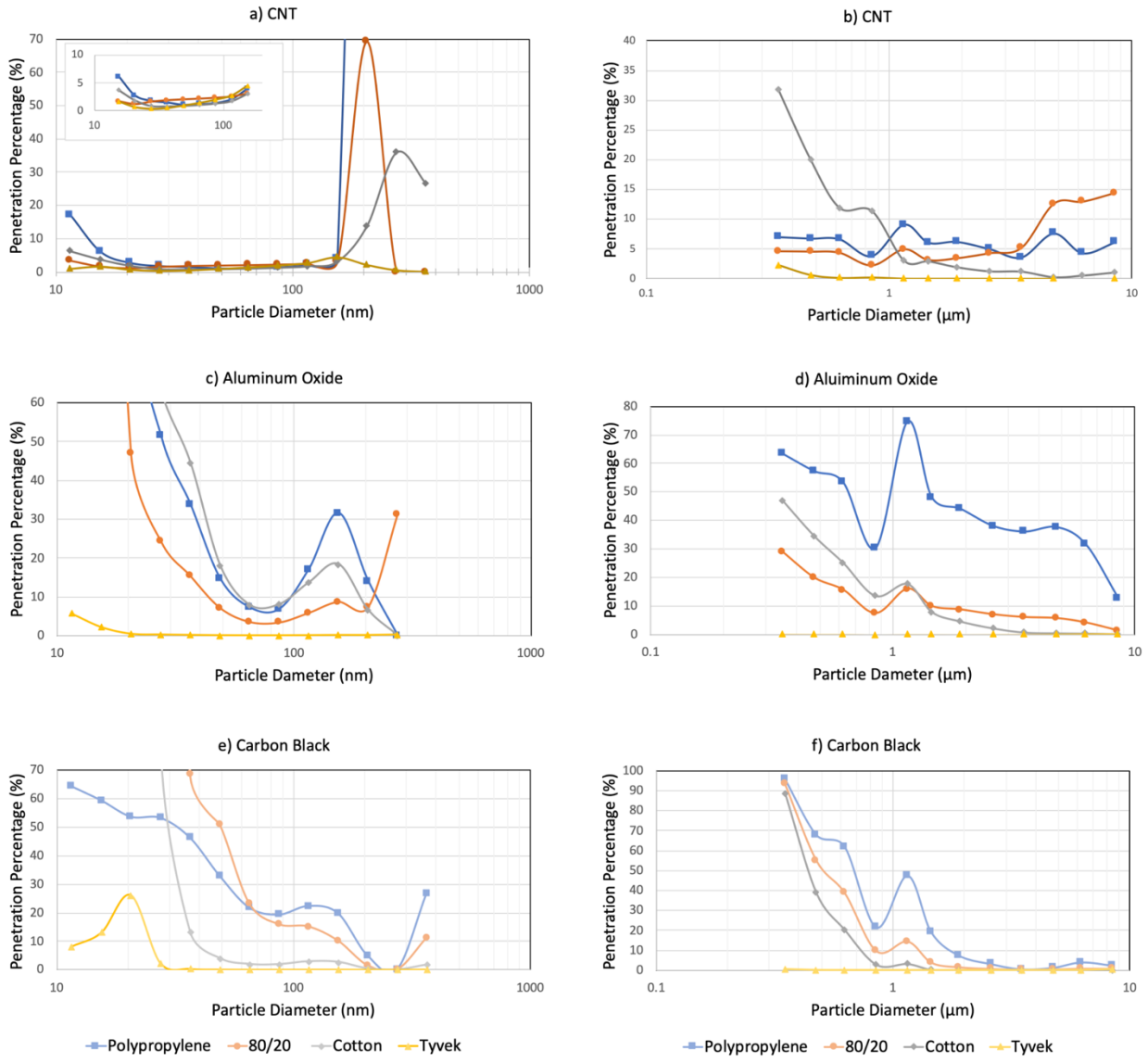

Figure Ch2-3. Particle fractioned size penetration for each fabric against a) CNT in the size range 10-420 nm; b) CNT in the size range 0.3-10 µm; c) aluminum oxide in the size range 10-420 nm; d) aluminum oxide in the size range 0.3-10 µm; e) carbon black in the size range 10-420 nm; and f) carbon black in the size range 0.3-10 µm.

Relationships Between ENP Penetration and Fabric Type

Figure Ch2-4 shows the penetration percentage of each fabric when challenged with each nanoparticle averaged over thirty minutes and three trials over the size range 10 nm-10 µm. The highest penetration overall occurred in the polypropylene fabric when challenged with CB nanoparticles (52%), while the lowest the Tyvek fabric experienced the lowest penetration overall when challenged with CB (0.1%). It is interesting to note that all four fabrics when challenged with CNT experienced less that 10% penetration, further characterizing CNT as the least penetrating nanoparticle for all fabrics. CNT penetrated cotton fabric significantly less when compared to aluminum dioxide penetration. CB nanoparticles penetrated cotton fabric less when

compared to Al_2O_3, and this finding was nearly significant. Cotton fabric is hydrophilic, while both CNT and CB are hydrophobic. This difference in chemical compositions may increase the capture efficiency of cotton fabric against hydrophobic particles. Polypropylene fabric was able to significantly capture more CNT particles when compared to CB particles. Since CNT particles form large agglomerates, it is possible that the particles are captured onto the fibers more easily than the smaller and more rounded CB particles. Tyvek fabric had significantly increased capture efficiency when compared to cotton when challenged with CNT, polypropylene and cotton when challenged with Al_2O_3 and polypropylene when challenged with CB nanoparticles. Tyvek was the most protective fabric over all three ENPs, which can be explained by the low porosity and low pore volume of the fabric. Nanoparticles of different physical and chemical morphologies cannot move through the individual fibers of the Tyvek fabric very well, causing the particles to attach to the surface of the fabric.

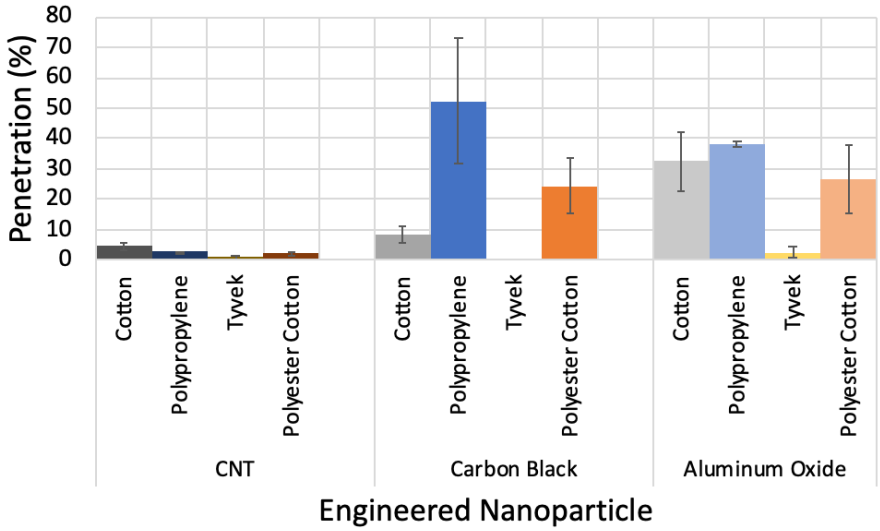

Figure Ch2-4. Average penetration percentages over 30 minutes for each fabric and each engineered nanoparticle over the size range 10 nm-10 µm.

Conclusions

Four important conclusions can be made from this investigation. First, Tyvek fabric was shown to be the most protective. Tyvek consistently showed the lowest penetration percentages when challenged with all three different types of ENPs, and some results showed that Tyvek had statistically significantly lower penetration than all three other fabrics. Most of the other data when comparing Tyvek fabric to the other four types of fabric was suggestive that Tyvek was more protective, however, the data was not significant at the 0.05 significance level. Second, polypropylene had the highest penetration percentages when challenged with Al_2O_3 and CB nanoparticles in the 100 nm-1 µm size range, and when averaged over the entire time period over all the size ranges measured. This may be explained by the fact that polypropylene has the highest calculated porosity when compared to the other three fabrics, and the governing mode of deposition for particles of this size is interception. Third, cotton fabric does better at capturing hydrophobic particles when compared to hydrophilic particles. Since cotton is a hydrophilic fabric, there is a correlation between hydrophilic fabrics increasing the capture of hydrophobic particles Fourth, CNT nanoparticles penetrated all four fabrics significantly less than the other two ENPs

studied. This may be due to the elongated fiber shape of a CNT fiber compared to the spherical shape of the other two particles, and the high agglomeration rate of CNT.

References

Birch, M. E., Wang, C., Fernback, J. E., Feng, H. A., Birch, Q. T., & Dozier, A. K. (2017). Analysis of carbon nanotubes and nanofibers on mixed cellulose ester filters by transmission electron microscopy. *NIOSH Manual of Analytical Methods. 5th ed. Cincinnati,. Department of Health and Human Services, Centers for Disease Control and Prevention, National Institute for Occupational Safety and Health, DHHS (NIOSH) Publication*(2014-151).

Chen, S.-C., Wang, J., Bahk, Y. K., Fissan, H., & Pui, D. Y. H. (2014). Carbon Nanotube Penetration Through Fiberglass and Electret Respirator Filter and Nuclepore Filter Media: Experiments and Models. *Aerosol science and technology*, *48*(10), 997-1008. https://doi.org/10.1080/02786826.2014.954028

Dhaniyala, S., & Liu, B. Y. H. (2001). Theoretical Modeling of Filtration by Nonuniform Fibrous Filters. *Aerosol science and technology*, *34*(2), 170-178. https://doi.org/10.1080/027868201300034763

Ducker, W. A., & Mastropietro, D. (2016). Forces between extended hydrophobic solids: Is there a long-range hydrophobic force? *Current opinion in colloid & interface science*, *22*, 51-58. https://doi.org/10.1016/j.cocis.2016.02.006

Faghihnejad, A., & Zeng, H. (2013). Interaction Mechanism between Hydrophobic and Hydrophilic Surfaces: Using Polystyrene and Mica as a Model System. *Langmuir*, *29*(40), 12443-12451. https://doi.org/10.1021/la402244h

Gao, P., Jaques, P. A., Hsiao, T.-C., Shepherd, A., Eimer, B. C., Yang, M., Miller, A., Gupta, B., & Shaffer, R. (2011). Evaluation of Nano- and Submicron Particle Penetration through Ten Nonwoven Fabrics Using a Wind-Driven Approach. *Journal of occupational and environmental hygiene*, *8*(1), 13-22. https://doi.org/10.1080/15459624.2010.515554

Golanski, L., Guiot, A., Rouillon, F., Pocachard, J., & Tardif, F. (2009). Experimental evaluation of personal protection devices against graphite nanoaerosols: fibrous filter media, masks, protective clothing, and gloves. *Human & experimental toxicology*, *28*(6-7), 353-359. https://doi.org/10.1177/0960327109105157

He, M., Ghee, T. A., & Dhaniyala, S. (2020). Aerosol penetration through fabrics: Experiments and theory. *Aerosol science and technology*, *55*(3), 289-301. https://doi.org/10.1080/02786826.2020.1845297

Hinds, W. C., & Zhu, Y. (2022). *Aerosol technology: properties, behavior, and measurement of airborne particles*. John Wiley & Sons.

Jamriska, M. (2009). *Aerosol penetration through protective fabrics*.

Kanduč, M., Schlaich, A., Schneck, E., & Netz, R. R. (2016). Water-Mediated Interactions between Hydrophilic and Hydrophobic Surfaces. *Langmuir*, *32*(35), 8767-8782. https://doi.org/10.1021/acs.langmuir.6b01727

Konda, A., Prakash, A., Moss, G. A., Schmoldt, M., Grant, G. D., & Guha, S. (2020). Aerosol Filtration Efficiency of Common Fabrics Used in Respiratory Cloth Masks. *ACS nano*, *14*(5), 6339-6347. https://doi.org/10.1021/acsnano.0c03252

Lee, K. W., & Liu, B. Y. H. (1980). On the Minimum Efficiency and the Most Penetrating Particle Size for Fibrous Filters. *Journal of the Air Pollution Control Association*, *30*(4), 377-381. https://doi.org/10.1080/00022470.1980.10464592

Licina, D., & Nazaroff, W. W. (2018). Clothing as a transport vector for airborne particles: Chamber study. *Indoor air*, *28*(3), 404-414. https://doi.org/10.1111/ina.12452

Liu, P. S. K., & Deshler, T. (2003). Causes of Concentration Differences Between a Scanning Mobility Particle Sizer and a Condensation Particle Counter. *Aerosol science and technology*, *37*(11), 916-923. https://doi.org/10.1080/02786820300931

Maksot, A., Sorna, S. M., Blevens, M., Reifenberger, R. G., Hiyoto, K., Fisher, E. R., Vindell, T., Li, Y. V., Kipper, M. J., & Tsai, C. S.-J. (2022). Engineered Nanoparticle Release from Personal Protective Clothing: Implications for Inhalation Exposure. *ACS applied nano materials*, *5*(2), 2558-2568. https://doi.org/10.1021/acsanm.1c04229

Pashley, R. M., McGuiggan, P. M., Ninham, B. W., & Evans, D. F. (1985). Attractive Forces between Uncharged Hydrophobic Surfaces: Direct Measurements in Aqueous Solution. *Science (American Association for the Advancement of Science)*, *229*(4718), 1088-1089. https://doi.org/10.1126/science.4035349

Rengasamy, S., Eimer, B., & Shaffer, R. E. (2010). Simple Respiratory Protection—Evaluation of the Filtration Performance of Cloth Masks and Common Fabric Materials Against 20–1000 nm Size Particles. *The Annals of occupational hygiene*, *54*(7), 789-798. https://doi.org/10.1093/annhyg/meq044

Tsai, C. S.-J. (2015). Contamination and release of nanomaterials associated with the use of personal protective clothing. *The Annals of occupational hygiene*, *59*(4), 491-503. https://doi.org/10.1093/annhyg/meu111

Wang, J., Kim, S. C., & Pui, D. Y. H. (2011). Measurement of multi-wall carbon nanotube penetration through a screen filter and single-fiber analysis. *Journal of nanoparticle research : an interdisciplinary forum for nanoscale science and technology*, *13*(10), 4565-4573. https://doi.org/10.1007/s11051-011-0415-y

Wiedensohler, A., Birmili, W., Nowak, A., Sonntag, A., Weinhold, K., Merkel, M., Wehner, B., Tuch, T., Pfeifer, S., Fiebig, M., Fjäraa, A. M., Asmi, E., Sellegri, K., Depuy, R., Venzac, H., Villani, P., Laj, P., Aalto, P., Ogren, J. A., . . . Bastian, S. (2012). Mobility particle size spectrometers: harmonization of technical standards and data structure to facilitate high quality long-term observations of atmospheric particle number size distributions. *Atmospheric measurement techniques*, *5*(3), 657-685. https://doi.org/10.5194/amt-5-657-2012

Wiedensohler, A., Wiesner, A., Weinhold, K., Birmili, W., Hermann, M., Merkel, M., Müller, T., Pfeifer, S., Schmidt, A., Tuch, T., Velarde, F., Quincey, P., Seeger, S., & Nowak, A. (2018). Mobility particle size spectrometers: Calibration procedures and measurement uncertainties. *Aerosol science and technology*, *52*(2), 146-164. https://doi.org/10.1080/02786826.2017.1387229

CHAPTER 3: Elucidate the mechanism of differential ENP interactions with major laboratory clothing fabrics.

Introduction

Since the mid-1990s, the use and availability of Engineered Nanoparticles (ENPs) has grown rapidly because countless studies have repeatedly shown that ENPs improve performance in many products spanning different business sectors. As a result, ENPs have found widespread use in additives, coatings, battery components, drugs, medicine, and structural materials. However, the use of ENPs poses a potential health risk to those very individuals who are involved in either the manufacturing process or the assembly of a final product. One way to mitigate potential ENP risks is to better characterize the efficacy of protective clothing against ENP exposure. A question that begs to be answered is how to select a particular fabric to help mitigate risk for a specific genre of ENP. Is there an optimal fabric that will maximize protection against exposure to a specific type of ENP?

The work conducted under Aim 2 of this NIOSH grant is intended to provide some fundamental knowledge to help answer this type of question. In particular, by characterizing the nature and strength of the physical interaction between an individual ENP with different fabrics commonly used to make protective clothing, we seek to provide a rational basis for the selection of a particular protective garment for a specific application. The aim of the work performed is to ultimately provide a more basic and fundamental understanding of how ENPs adhere to different fabrics, thereby laying the groundwork for the further optimization of protective garments.

The primary tool employed in this study is the Atomic Force Microscope (AFM). The AFM measures the interaction of a sharp tip integrally attached to a flexible microcantilever as the tip is made to approach, contact, indent and then withdraw from the surface of a fabric of interest. The underlying premise behind our work is that an oxidized Si AFM tip of ~15 nm diameter serves as a useful surrogate for an oxide ENP. The relevant forces that influence an ENP near a fabric surface are expected to be on the order of a few nanoNewtons, well within the range of accurate measurement by an AFM. Thus with this context in mind, it seems natural to investigate what can be quantitatively learned about ENP/fabric interactions using an AFM.

Data acquired during an AFM experiment are often referred to as an *F(z)* curve because the force *F* acting on an AFM tip is measured as the separation distance *z* between the tip and substrate is systematically and controllably reduced. Features present (or absent) in a well-executed *F(z)* experiment provide a fabric-dependent fingerprint that characterizes the relevant forces and interaction mechanisms in play.

By studying the forces acting on the tip as it approaches and makes contact to a fabric surface, considerable insight can be gained about i) the strength of the tip-fabric interaction, ii) the fundamental origin of the interaction, iii) the influence of contamination layers that might coat the fabric, iv) any time-dependent viscoelastic effects that might influence the binding of an ENP once it makes contact with a fiber, and v) estimates of the force required to remove an oxide ENP from the fabric.

With this motivation, systematic measurements using an AFM were conducted to supplement prior work on the effectiveness of various fabrics to protect those who manufacture or otherwise

use ENPs in the work place.[1,2] The AFM work described in what follows quantitatively probes the basic nature and strength of interaction of nanometer-size oxide ENPs with a variety of different fabrics commonly used in the production of lab coats. Of particular interest is to identify those fabrics that most strongly trap ENPs.

Since scanning probe techniques were introduced in 1986, AFMs have enjoyed widespread use in every branch of science and engineering. Only recently have reports appeared where an AFM has been used to study textiles. Topics that have been reported are widespread and diverse and include studies of the micro-structure of woven fabrics, a better characterization of hydrophobic/hydrophilic coatings applied to textiles, maps of the variations in the surface charge on wool, and the imaging of nanocomposite coatings designed to produce anti-bacterial fabrics.[3,4,5,6,7,8,9,10,11]

Methodology

Introductory Remarks

To assess the adhesion of oxide ENPs to different protective lab coats, an Atomic Force Microscope (AFM) study was performed on single fibers obtained from two woven and two nonwoven lab coats all purchased through Global Industrial: 100% cotton (Fashion Seal men's lab coat), polyester/cotton blend (80% polyester 20% cotton, Red Kap® women's button closure lab

[1] A. Maksot, S. Sorna, M. Blevens, R. Reifenberger, K. Hiyoto, E. Fisher, T. Vindell,Y. Li, M. Kipper, C. S-J. Tsai, "Engineered Nanoparticle Release from Personal Protective Clothing: Implications for Inhalation Exposure", ACS App. Nano Mat. **5**(2), 2558-68 (2022).

[2] K. Hiyoto, S. Sorna, A. Maksot, R. Reifenberger, C.S-J.Tsai, E. Fisher, "Effects of Surface Hydrophobicity of Lab Coat Fabrics on Nanoparticle Attachment and Resuspension: Implications for Fabrics Used for Making Protective Clothing or Work Uniform", ACS App. Nano Mat. **6**, 7384-94 (2023).

[3] B. Zimmerman, J. Chow, A.G. Abbott, M.S. Ellison, M.S. Kennedy, D. Dean "Variation of Surface Charge along the Surface of Wool Fibers Assessed by High-Resolution Force Spectroscopy" J Eng Fiber Fabr. **6**(2), 61-66 (2011).

[4] M. Naebe, R. Denning, M. Huson, P. G. Cookson, X. Wang "Ageing effect of plasma-treated wool" J. Textile Ins., **102**(12), 1086-93 (2011).

[5] M. P. Gashti, F. Alimohammadi, G. Song, A. Kiumarsi "Characterization of nanocomposite coatings on textiles: A brief review on microscopic technology", in *Current microscopy contributions to advances in science and technology*: Vol 2, Ed. A. Méndez-Vilas, Formatex Research Centre, Norristown PA, 1424-37 (2012).

[6] N. Behary and A. Perwuelz "Atomic Force Microscopy – For Investigating Surface Treatment of Textile Fibers", in *Atomic Force Microscopy - Imaging, Measuring and Manipulating Surfaces at the Atomic Scale.*, V. Bellitto, Ed., InTech, (2012).

[7] S.K. Koc "Applications of Atomic Force Microscopy in Textiles", J. Engin. Fibers and Fabrics **10**(1), 169-73 (2015).

[8] X. Luo, Y, Weng, S. Wang, J. Du, H. Wang, C. Xu "Superhydrophobic and oleophobic textiles with hierarchical micro-nano structure constructed by sol–gel method" J. Sol-Gel Sci. Tech. **89,** 820-9 (2019).

[9] T. Nakamura, E. A. Q. Mondarte, H. Tahara, R. Chang, T. Hayashi "Chemical force spectroscopic mapping of nanoparticle-embedded polyester fiber by atomic force microscopy", Mol. Crys. and Liq. Crys. 728(1), 52-58 (2021).

[10] O.N. Baranova and L.I. Zolina, " Atomic Force Microscopy Study of Cotton Cloth Modified by Silver Nanoparticles, Fibre Chemistry, **54**(1), 51-53, (2022).

[11] R. Salem, K. Thompson, M. Uttamlal "Bleaching cotton in textile conservation: a closer look using atomic force microscopy", Heritage Science **10**(1), 195 (2022).

coat), Tyvek® (HD polyethylene, Dupont), and 100% polypropylene (Keystone HD polypropylene lab coat). A table listing some properties of these fabrics is given in Table Ch3-1.

Table Ch3-1: A list of the fabrics studied

Fabric	**Chemical formula**	**Density (g/cm^3)**
Tyvek (HD polyethylene)	$[- C_2H_4 -]_n$	0.93 – 0.97
Polypropylene	$[- C_2H_6 -]_n$	0.90
Cotton, primarily cellulose (from 100% cotton fabric)	$[- C_{18}H_{21}N_{11}O_{38} -]_n$	1.35
Polyester (from 80/20 polycotton fabric)	$[- C_{10}H_8O_4 -]_n$	1.38
Cotton, primarily cellulose (from 80/20 polycotton fabric)	$[- C_{18}H_{21}N_{11}O_{38} -]_n$	1.35

Based on preliminary AFM experiments conducted at the beginning of the NIOSH contract, a decision was made to study individual fibers extracted from the above fabrics rather than perform AFM studies on the as-received fabric material. This decision was reached after attempts to scan a fabric surface netted very mixed results. During AFM scans of as-received fabrics, stray randomly protruding fibers would snare the AFM cantilever, often shearing the microcantilever from its support. To get around these problems caused by stray fibers, we studied individual fibers extracted from the fabric of each lab coat. The exception was Tyvek fabric which is made by compressing randomly placed, high density polyethylene fibers to make a non-woven, flexible, and tough fabric material. Therefore the Tyvek fabric itself was studied with no attempt to isolate or mount an individual polyethylene fiber.

It should be clear that we had no control or knowledge of any processing or surface treatments the fabrics may have received during the textile manufacturing and/or subsequent lab coat fabrication steps. *A priori*, we anticipated residual surfactants, solvents, spinning agents, or plasticizers, used in the manufacturing process, might unevenly coat individual fibers in the fabrics. This processing uncertainty places a constraint on the scope of the AFM work that was performed.

As a consequence, it is reasonable to expect that an individual fiber is **not** an ideal sample possessing a homogeneous surface. As a result, uncontrolled variability in any data taken from a randomly selected nanoscale region of an individual fiber should be expected. Thus the AFM study conducted was focused on trends related to attractive forces, adhesive forces, and the nature of the tip/fiber interaction rather than on obtaining precise and statistically significant values for any particular quantity.

Atomic Force Microscope Capabilities

Throughout the course of this study, an Asylum Research AFM Cypher Model S was used. Initially, the AFM was housed in the Birck Nanotechnology Center on Purdue's campus. During the first six months of 2022, the AFM laboratory was relocated to the basement of Purdue's Mechanical Engineering building, at which time the controlling computer was upgraded.

The experimental focus was to obtain systematic force vs. distance (*F* vs. *z* or *F(z)*) data to characterize the interaction of a 14 nm diameter SiO*x* AFM tip with each of the relevant lab-coat fibers of interest. This type of experiment is a common application of any AFM and is often referred to as a nanoindentation experiment. In this mode of operation, the stiffness and viscoelastic properties of a selected material can be measured. For the purposes of this study, *F(z)* data were used to assess the origin and strength of interaction between the tip and fabric fiber, as well as to measure the adhesion between the AFM tip and an individual fiber.

Summary of Experimental Protocols Developed

AFM microcantilevers Model AC240 available from Asylum Research were used throughout. These AFM levers typically had a resonant frequency near 70 kHz and a spring constant between 2 and 3 nN/nm. The SiO_2 tip diameter is specified by the manufacturer to be 14 nm. Before use, each cantilever was exposed to ~10 minutes of UV radiation to reduce any possible hydrocarbon contamination. The individual cantilever spring constant k for each cantilever was calibrated using the well-established thermal method that measures the k_BT thermal vibration spectrum of the cantilever at room temperature.[12] Using the fluctuation dissipation theorem[13] and combining with Sader's hydrodynamic damping method,[14] a reliable value for k and the inverse optical lever sensitivity (invOLS) for each cantilever was obtained. Once the spring constant is known, the cantilever deflection q (what the AFM measures) can be converted to an applied cantilever force using

$$F_{cant} = kq. \quad (1)$$

In preparation for AFM studies, individual fibers around 5 to 10 mm in length were carefully selected from each fabric using tweezers under an optical microscope. An individual fiber typically had a diameter of between 20 μm and 25 μm, making the fiber diameter about 1500 times greater than the diameter of the AFM tip. The synthetic fibers (polyester and polypropylene) appeared to have a uniform cross-sectional diameter when viewed under a compound optical microscope (adjustable magnification between 7.5x to 30x). These fibers were visibly kinked due to their inclusion in the fabric material. The natural cotton fibers, when viewed under the optical microscope, have both a kinked and twisted appearance which gives a clear impression of a non-uniform cross-sectional area.

After a single fiber was successfully extracted from the fabric, it was then placed on a thin steel mounting disc of ~15 mm diameter. Each end of the fiber was firmly held to the supporting steel disc by a tiny drop of glue. Effectively, the crinkled fibers were suspended a few 100 μm above the hard steel support surface. Each disc was then labeled with a unique sample ID number to allow ready identification at a later date. Once prepared, the mounted samples were stored in labelled cardboard boxes which were kept inside a covered desiccator that was backfilled with dry N_2 gas for the duration of the entire study.

[12] M.J. Higgins, R. Proksch, J.E. Sader, M. Polcik, S. Mc Endoo, J.P. Cleveland, S.P. Jarvis, "Non-invasive determination of the optical lever sensitivity in atomic force microscopy", Rev. Sci. Instrum. **77**, 013701 (2006).
[13] The fluctuation-dissipation theorem states that the linear response of a given system to an external perturbation can be understood in terms of the thermal fluctuation of the system in equilibrium with its environment.
[14] J.E. Sader, J.A. Sanelli, B.D. Adamson, J.P. Monty, X. Wei, S.A. Crawford, J.R. Friend, I. Marusic, P. Mulvaney, E.J. Bieske, "Spring constant calibration of atomic force microscope cantilevers of arbitrary shape", Rev. Sci. Instrum. **83** 103705 (2012).

An Asylum Cypher Model S AFM, available in Purdue University's Birck Nanotechnology Center recharge facility, was used throughout. The charge to use this AFM instrument is $45/hour. The AFM electronics were always energized to facilitate a stable operating environment. After the cantilever and fiber sample were mounted in the AFM, the front door of an insulated, double walled metallic enclosure was secured to insure thermal equilibrium. The temperature inside the electrically shielded thermal enclosure box was unregulated and was typically measured to be 26±1^{o}C.

Once mounted, the steel disc was shifted in steps of a few micrometers (using a stick/slip inertial translation mechanism) until the individual fiber was eventually positioned below the AFM cantilever. This alignment was facilitated using the Cypher's view module which includes a Pixelink camera and an Olympus LUCPlanFL objective with a magnification of 20x. After a rough alignment was made, the AFM system was allowed to further equilibrate for ~½ hour before taking data. Acquisition of *F(z)* data commenced after making a final optical alignment. An example of the AFM cantilever positioned over a cotton fiber is given in Figure Ch3-1.

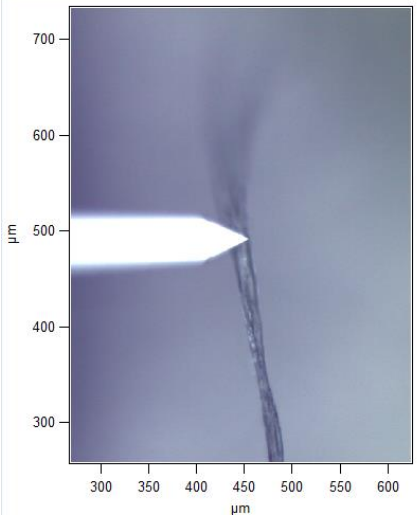

Figure Ch3-1: A photo of the top side of an AFM AC240 microcantilever positioned above a cotton fiber. The AFM tip is located below the cantilever and is not visible in this view.

A sequence of *F(z)* measurements were initially performed under ambient conditions. Following this, the metal enclosure box surrounding the AFM was slowly purged using dry N_2 gas before taking *F(z)* data at a reduced humidity level. The relative humidity (RH) was measured with a Pyle hand-held PTHM20 meter. It required about 30 minutes for the ambient lab humidity (typically near 30%) to reach a value less than 1% inside the steel enclosure.

Results

AFM Results

A number of issues were encountered during the course of this AFM study as detailed in Table Ch3-1 below. All of these issues were successfully resolved during the course of this study.

Approximately 750 *F(z)* data curves were acquired over a five month period of time. Every fiber was studied at least twice to assure reproducibility of results. For each fiber, *F(z)* data were systematically acquired for specified set point forces of 2, 5, and 10 nN. These low set point forces were intentionally chosen because our interest is primarily to study how an ENP interacts with a fiber surface. Presumably, an adsorbed ENP does not indent the surface on which it rests. In addition, other factors affecting the decision to use low loading forces are i) to minimize plastic deformations that might be caused by larger indentations and ii) to reduce the chances of tip damage and wear.

Table Ch3-1: List of major and minor issues encountered during this study		
Fiber/Fabric	**Major issues**	**Minor difficulties**
Tyvek	none	➢ Regions of Tyvek surface were found to be very sticky
Polypropylene	none	➢ Aligning tip over apex of fiber
100% Cotton	none	➢ Fiber moves with changes in RH ➢ Locating an untwisted region of the fiber ➢ Aligning tip over apex of fiber
Cotton (from 80/20 polycotton)	➢ Unambiguous selection of cotton fiber from polycotton fabric	➢ Fiber moves with changes in RH ➢ Locating an untwisted region of the fiber ➢ Aligning tip over apex of fiber
Polyester (from 80/20 polycotton)	➢ Unambiguous selection of polyester fiber from polycotton fabric ➢ Eliminating halo of microfibers surrounding each fiber	➢ Aligning tip over apex of fiber

A standard set point force of 5 nN was selected to compare data from different fibers acquired on different days using different AFM cantilevers. For this force, the maximum indentation of the tip into the fiber can be estimated from the Hertz contact theory to be less than ~1 nm. Thus, the experiments are specifically designed to characterize the interaction of an ENP with the surface of a fiber, thereby providing information that determines how an ENP binds to protective clothing.

Prior studies have shown that for small indentations performed by an AFM, polymers exhibit a depth dependent elastic modulus, an effect that is often referred to as the skin effect.[15] As the indentation increases, an elastic modulus more characteristic of the bulk value is achieved. We expect a similar result will also apply to our data.

Discussion of Important Features in F(z)

While no two *F(z)* curves were exactly identical, it became clear that the *F(z)* from each fiber had a characteristic shape with recognizable features. Before proceeding with the results for all fibers, it is perhaps worthwhile to discuss some typical *F(z)* data, acquired under ambient conditions, from a cotton fiber extracted from the 100% cotton lab coat fabric. The experiments were performed under ambient laboratory conditions (in this case, the relative humidity was ~34%).

The result of an *F(z)* experiment is plotted in Figure Ch3-2. Note that ALL the *F(z)* data acquired during this study are plotted using the same color convention: a red curve represents data as the tip approaches the fabric fiber while the retract data are plotted as blue.

[15] S.A. Chizhik, Z. Huang, V.V. Gorbunov, N.K. Myshkin, and V.V. Taylor, "Micromechanical properties of elastic polymeric materials as probed by scanning force microscopy" Langmuir, 14 2606-09 (1998).

The characteristic shape and features of the *F(z)* data plotted in Fig. Ch3-2 deserves further comment. The force *F* (in nN) acting on the tip is plotted along the y-axis. Forces plotted as positive are considered repulsive, forces plotted as negative are considered attractive. A piezoelectric translator integrated into the AFM moves the fiber toward the tip. The relative position of the fiber with respect of the tip is plotted along the x-axis which is labelled as Z – piezo displacement (in nm). During this motion, the AFM electronics accurately measures the cantilever bending to infer the force on the tip using Eq. 1.

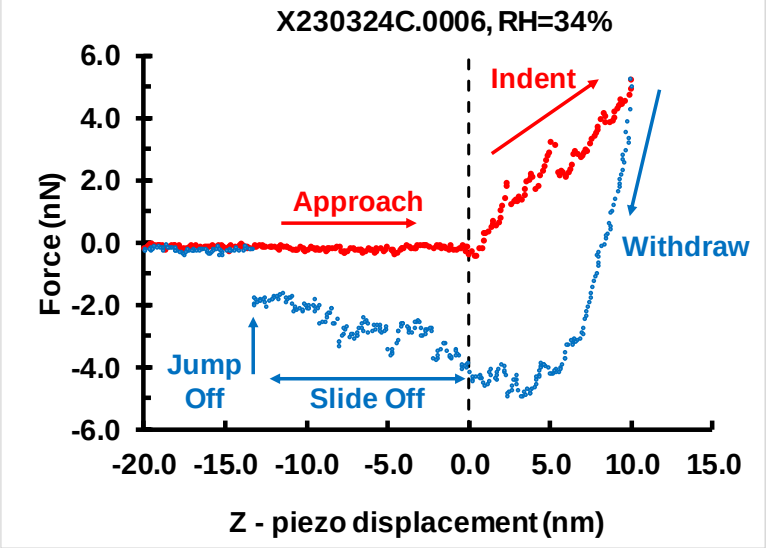

Figure Ch3-2: Typical F(z) data from a fiber extracted from the 100% cotton fabric studied under ambient conditions (RH = 34%). The data were taken by specifying a nominal 5 nN setpoint force (maximum applied force). An AC240 AFM cantilever was used with a SiO_x tip having a nominal diameter of 14 nm and a spring constant of 2.81 nN/nm. The tip approached the surface with a speed of 100 nm/s. Red represents the tip approaching the fiber, blue is the data upon retraction.

Starting with the approach (red) data for z≅-15 nm, the tip is far from the cotton fiber, and there is no force acting on the tip as represented by the appearance of a flat, horizontal line. Note that if a significant long-range force (e.g. from electrostatics) were present, the approach curve would not show a horizontal line but would have a noticeable upward or downward slope.

As the fiber approaches closer to the tip, the tip eventually jumps into contact with the fiber when the strength of the interaction force between tip and fiber overcomes the restoring force offered by the bent AFM cantilever. In Fig. Ch3-2, this is observed as a very small jump downward near z=0 (a negative force implies an adhesive attractive force).The size of this jump indicates the strength of interaction between the tip and substrate and is related to the Hamaker constant of interaction that characterizes van der Waal (vdW) forces. For the case of the cotton fiber from the 100% cotton fabric, the interaction is very weak as evidenced by the small but discernable jump downward near the vertical dashed line at z=0.

Once this jump to contact at z=0 occurs, the tip begins to indent into the fiber and the force on the cantilever transitions from negative to positive until a preset force (in this case 5 nN) is reached. In this indent regime, the tip is pressing into the fiber's surface. Soft surfaces (Young's modulus <1 GPa) exhibit an indentation region extending to z values of ~ +20 to +30 nm or larger. By contrast, hard surfaces (Young's modulus > 50 GPa) show a much smaller indentation region because a harder surface suffers a small indentation, causing the set point force to be rapidly reached. Thus the extent of the indent region in the approach data provides a quick and useful guide about the relevant mechanical properties for the particular fiber under study.

Once the 5 nN setpoint force is reached, the AFM withdraws the tip and the data are now plotted as blue. If the indentation was elastic, the blue data should exactly overlap with the red data. The absence of an overlap indicates the tip is experiencing viscoelastic time-dependent forces that are a function of the prior indentation history as well as the rate of indentation. The observation of viscoelastic behavior upon retraction is an unambiguous sign of an energy dissipative process.

As the tip continues to withdraw, the force exerted by the cantilever becomes negative around z=+7 nm, indicating that the tip is adhering to the fiber surface. Normally, this behavior persists until the restoring force of the downward bent cantilever snaps the tip off the fiber surface. For a clean tip/fiber interface, this jump off event would be signified by a sharp discontinuity as the tip jumps back to the zero force position. Typically, this occurs near z=0.

If a contamination layer is present on the fiber, the tip does not jump off, but rather it gradually slides-off as a "bridge" of contamination forms between the tip and fiber surface. This is the case observed in Fig. 2. The longer the tip stays in contact with the fiber as the tip retracts, the more pronounced the contamination layer. The contamination could well be related to adsorbed water on the surface of the tip and/or fiber or to unknown surfactants contaminating the fiber surface. Measurements at low RH have been conducted to assess the extent that adsorbed water plays in this slide-off behavior.

Eventually, the contamination layer breaks and the tip snaps off the fiber and returns to its F=0 position, indicating no forces are acting between the tip and fiber. For the data in Fig. 2, this occurs around z = -13 nm. In general terms, the withdrawal data is useful because it provides an indication of the maximum force required to separate the tip from the fiber. For the data plotted in Fig. 2, the most negative region of the blue withdrawal data is about -5 nN and this suggests that a force of ~ 5 nN would be required to separate an oxide ENP from this region of the fiber.

Central Results

Following this brief discussion outlining the important features in *F(z)* data from a single fiber, it is worthwhile to plot representative *F(z)* data taken under ambient conditions from all fibers on one graph. This is done in Figure Ch3-3 and represents a major result of the work conducted. The data from each fiber has been offset vertically to aid in viewing. The setpoint force for each curve is nominally the same, i.e. 5 nN. With an understanding of the important features in *F(z)* data in mind, this composite graph allows a quick comparison between the interaction of an oxide ENP with different fabrics and reveals interesting systematic trends.

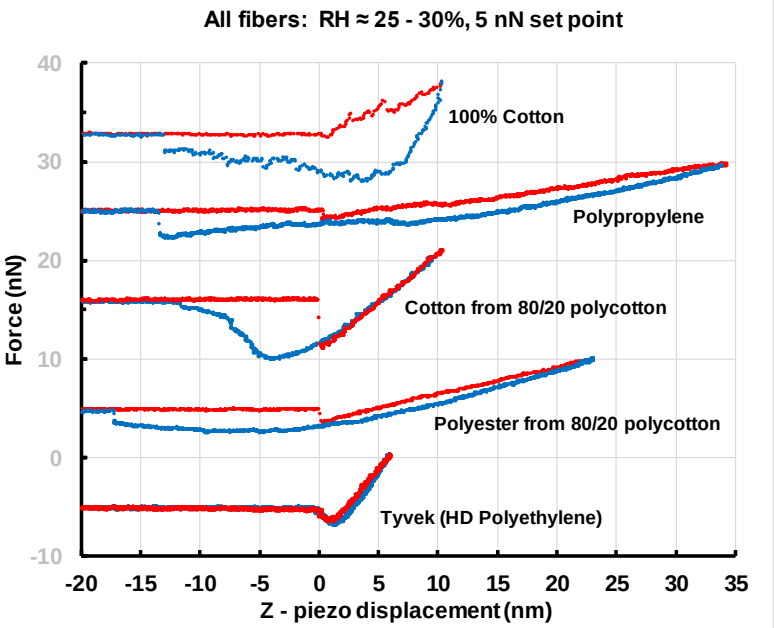

Figure Ch3-3: A collection of typical F(z) data for all fibers studied under ambient conditions (RH between ~25% to ~30%). All data have a nominal 5 nN setpoint force (maximum applied force) using an AFM cantilever with a SiO_x tip having a nominal diameter of 14 nm. Red represents the tip approaching the fiber, blue is the data upon retraction. All data curves were horizontally aligned so that the x-axis zero corresponds to the point of first contact between the tip and fiber. Each curve has been displaced vertically for ease in viewing.

The data plotted in Fig. Ch3-3 were chosen carefully. An effort was made to deselect those curves which demonstrated recognizable anomalies. Based on experience gained during the course of this study, the reasons to disregard an *F(z)* curve as suspicious include

i) The observation of abrupt jumps in the approach curve that presumably indicate a tip slip event during indentation. While not usually a problem when using an AFM to study smooth, flat substrates, this becomes an issue when using an AFM to study individual textile fibers of ~20 μm diameter.

ii) The observation of large adhesion upon tip withdrawal from a textile fiber. This usually indicates that the contact area became uncontrollably larger than expected for the ideal case when the apex of the AFM tip alone contacts the apex of the fiber. The origin of the high adhesion is presumably caused when a portion of the tip shank comes into contact with the fiber surface. Thus, any *F(z)* data from a fiber that shows low adhesion tends to gain preference over similar data that exhibits a significantly higher adhesion.

iii) Generally, the observation of an extended retract curve containing features and/or jumps suggest that the *F(z)* data might be unreliable. The presence of features/jumps suggest that different contact points are breaking at different times during the retraction. Such events are generally not reproducible.

Discussion

Taken as a whole, the data in Fig. Ch3-3 reveal a number of interesting features worth comment.

- None of the data follow the idealized *F(z)* behavior (no hysteresis between approach and retract, a sharp snap off upon retraction) that would indicate a clean interface between the AFM tip and fiber.
- All the data except that from Tyvek show a loading curve (red, approach) which does not overlap with the unloading data (blue, retract). This hysteretic behavior provides good evidence that the fibers except Tyvek exhibit viscoelastic behavior even for small indentations.
- The behavior of the *F(z)* data for the synthetic fibers (polypropylene and polyester) are considerably different than observed for the natural cotton fibers in two important ways: i) the synthetic fibers are significantly softer than the natural cotton fibers, and ii) the synthetic fibers require a much larger retract distance of about -15 nm beyond first contact (z=0) to release the tip from the fiber surface. Both these features suggest the synthetic fibers likely have a viscous contamination layer.
- Surprisingly, there is a significant difference in the *F(z)* data between the two cotton fibers suggesting that the fabrics made from these fibers may have been manufactured and processed in different ways.

Significant features in each curve also deserve further comment.

- *F(z)* taken on a fiber from the 100% cotton lab coat offers little evidence to support a significant vdW attractive force. This cotton fiber shows a large adhesive force upon retraction, suggesting that ENPs will strongly adhere to cotton.
- *F(z)* taken on the fiber from the polypropylene lab coat shows an extended indentation region. The z-piezo requires a displacement of about +35 nm before the 5 nN setpoint is reached. This behavior, coupled with the extended slip-off behavior on retraction indicates that the polypropylene fiber is likely coated with a contamination layer of unknown origin.
- *F(z)* taken from the cotton fiber extracted from the polycotton (80/20) lab coat shows the largest jump to contact, indicating the strongest attractive vdW force of all fibers studied.
- *F(z)* taken from the polyester fiber extracted from the polycotton (80/20) lab coat shows a trend similar to that for polypropylene. Both synthetic materials seem to be coated with a contamination layer.
- *F(z)* taken from the Tyvek lab coat is closest to ideal and shows little hysteresis. The indentation region extends about +6 nm before the setpoint is reached, indicating Tyvek is the stiffest fabric studied. This observation further suggests the Tyvek lab coat may not have a significant contamination layer. Significantly, Tyvek also shows the smallest adhesion force, suggesting that ENPs will not strongly adhere to this material.

Conclusions

The above narrative provides a preliminary analysis of *F(z)* data collected from individual fibers extracted from four different lab coat fabrics. Using an Atomic Force Microscope, systematic *F(z) data* were acquired from each fiber under ambient and reduced humidity conditions using the AFM tip as a surrogate for an oxide ENP. At this time, a preliminary analysis of the results offer some general and useful conclusions that characterize the physical interaction of an oxide ENP in the ~15 nm diam. size range with the individual fibers.

1. Oxide ENPs should bind weakly to Tyvek and strongest to cotton, with the synthetic fabrics polypropylene and polyester falling somewhere in between. Based on this finding, it might be

expected that cotton will shed the fewest ENPs upon shaking, while Tyvek will shed the largest number of ENPs after shaking.

2. No long range forces were observed. This implies that tribo-electric induced electrostatic forces between an ENP and each of the fabrics is probably not significant.
3. Preliminary analysis of the data (not discussed above) for all fibers acquired at low relative humidity (RH) shows the *F(z)* data is only affected in a subtle way. If a significant water bridge forms under ambient conditions between the ENP and fabric fiber, a large decrease in lift-off force should have occured as the RH is reduced to near zero. No such change was observed.
4. The data from the two cotton fibers, one extracted from the 100% cotton fabric, the other from the 80/20 polycotton fabric, suggest that treatment of the fabric during manufacture makes a significant difference in how the cotton fibers interact with ENPs. Figure 3 shows the cotton fiber from the 80/20 polycotton fabric exhibits a strong vdW force of attraction to the AFM tip, while the cotton fiber from the 100% cotton lab coat shows very little in the way of an attractive force. This implies that some currently unknown fabric processing step may have a large influence on ENP adhesion.
5. The contamination layer inferred from the F(z) data on the synthetic fibers indicates these fibers may offer some advantages over cotton to trapping ENPs.
6. The viscoelastic properties shown by all the fabrics except Tyvek suggest alternate routes to a more efficient trapping of ENPs. For example, physically pressing a lab coat exposed to ENP contamination overnight might serve to more firmly embed ENPs in the contamination layer before the lab coat is used the next day.

Future Work

All indications of data are that useful results will be obtained which include quantitative estimates for the maximum adhesion force, Hamaker constants characterizing the van der Waals force of interaction for each of the lab coat fibers studied, the influence of relative humidity on adhesion, and a better characterization of the observed viscoelastic effects using an on-line AFM *F(z)* simulator called VEDA. A first draft manuscript describing the final results is also being prepared for publication.

CHAPTER 4: Achieve a significant reduction in ENP contamination/exposure by altering surface key properties of the fabric

Introduction

Nanomaterials have become widespread in various applications, such as healthcare, energy storage materials, sensing devices, and catalysis because of their unique physicochemical properties and diverse morphologies and compositions.[1-12] Although some nanomaterials can originate from natural processes, many of these applications utilize engineered nanoparticles (ENP) to ensure control over properties like morphology, size, and composition. Prevention of adverse health effects arising from exposure to ENP is vital for both workers in facilities producing/using these materials and researchers in laboratories. Although the National Institute for Occupational Safety and Health (NIOSH) provides general guidelines for handling nanomaterials,[13] secondary exposure from contaminated personal protective equipment (PPE) and recommendations for using these PPE have not been widely studied. Specifically, ENPs released from PPE (e.g., lab coats) can contact skin and cause dermal exposure or can be released back into the air and inhaled, leading to harmful respiratory and cardiovascular effects.[14-16]

McDonagh, et al. studied the effect of particle size, level of physical activity, and fabric type on the resuspension of tagged silica particles.[17-18] The authors used 3, 5, and 10 μm silica nanoparticles and found that the smallest particles (3 μm) were easily deposited on the fabrics. The number of particles released during shaking increased as particle size increased or when higher levels of physical activity occurred during resuspension. In addition, the weave pattern, rather than the fabric composition, had a more significant impact on particle release. Although these studies thoroughly examined several factors impacting particle adhesion and release, the authors only employed micron sized silica and did not study the behavior of nanomaterials. Examination of nanoparticles could be useful, as Brownian motion can influence nanoparticle interaction (either adhesion or resuspension) and change the probability of secondary exposure. Previous work in our lab demonstrated the adhesion and resuspension of Al_2O_3 ENP with several common lab coats (polyester/cotton, Tyvek®, and polyester).[16] The polyester/cotton coats exhibited the highest level of contamination and release, whereas polyester displayed the lowest. Although this previous work examined both woven and nonwoven fabrics, these studies were only performed with one type of nanomaterial morphology; thus, further work exploring more morphologically complex materials such as carbon nanotubes (CNT) is needed to determine if nanomaterial morphology also plays a role in ENP interaction. Notably, CNT can also be used as building blocks to construct electromagnetic composites.[19] Expansion of previous work including studying the underlying mechanisms of ENP adhesion and release from the contaminated PPE fabric requires further study to minimize secondary exposure. We chose to study two ENP, namely Al_2O_3 and CNT, for comparison with previous work and because of their extensive use in a range of applications; CB was selected as a direct comparison to CNT with respect to chemistry, but with a different particle morphology.

In addition to examining different nanomaterial morphologies, the role of surface properties of the fabrics themselves was also explored. As seen in the above noted studies, fabric texture dominates when determining particle release. Even if the fabrics have a similar weave pattern or chemical composition, direct comparison between the different materials introduces a level of complexity such that the role of surface chemistry cannot be dismissed. Low-temperature plasma

treatment is a useful strategy for tailoring surface properties as it allows for modification of the surface while maintaining the bulk properties. Plasmas have been used to both deposit a conformal thin film and to functionalize a variety of textiles and polymers.[20-22] By keeping the overall weave pattern of the fabrics the same and only modifying the surface chemistry, a direct comparison can be made to evaluate if this is an effective strategy to decrease secondary ENP exposure. Thus, the aims of this study were to (1) expand our knowledge of the impact of ENP morphology on adhesion and release; (2) utilize plasma surface modification to decrease secondary ENP exposure; and (3) to formulated mechanisms for ENP adhesion and release on common laboratory fabrics (coated and uncoated). The implications of studied surface treatments could be used in treating fabrics used for making protective clothing or work uniforms to minimize contamination and avoid migration of unwanted and toxic substances. Here, we propose initial answers to the many questions posed above, as we describe the results of a systemic study of ENP adhesion and release from untreated (UT) and plasma treated fabrics commonly used to fabricate lab coats. The novelty of the work is highlighted by the extensive surface characterization performed on the materials, the use of plasma-based coatings to change the surface chemistry, but not the morphology of the underlying materials, the use of multiple ENP materials (from both a chemical and morphological perspective), and the explicit study of the adhesion and release of the particles. Thus, this comprehensive study provides the basis for formulating hypotheses regarding the mechanisms for interaction of nanoparticles with laboratory fabrics.

Methodology

Materials

Two woven and two nonwoven lab coats were selected for this study and were all purchased through Global Industrial: 100% cotton (Fashion Seal men's lab coat), polyester/cotton blend (80% polyester 20% cotton, Red Kap® women's button closure lab coat), Tyvek® (Dupont), and 100% polypropylene (Keystone HD polypropylene lab coat). Before use, all fabrics were cut into circular fabric samples (1.375 in diameter) by using a punch-out cutter, enabling homogenous sample sizes for all plasma studies. Contamination studies used CNT (industry grade 10 – 30 nm outer diameter, >95% purity, Nanolab, Waltham, MA), Al_2O_3 (40 nm, 100% purity Nanophase Technologies, Romeoville, IL), and carbon black (CB) (40 nm, 100% purity, carbon black-Printex powder, Orion, Germany).

Plasma modification of fabric swatches

All plasma surface modification processes were performed in a home-built glass barrel style reactor, described previously, Figure Ch4-1a.[23-25] Briefly, discharges were ignited by applying radio

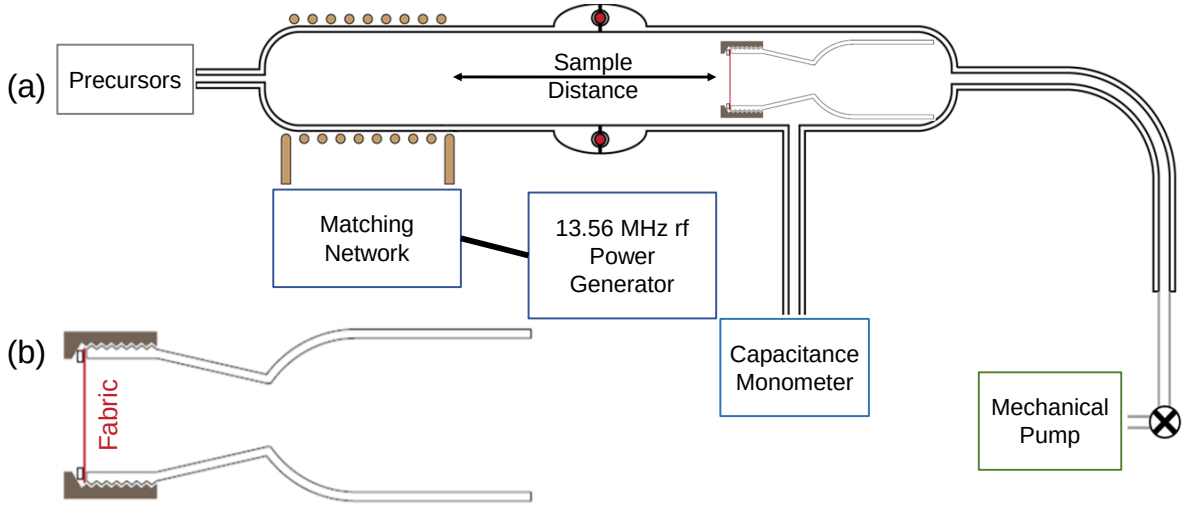

Figure Ch4-1. Schematic representation of the (a) rf plasma reactor and (b) holder constructed to mount fabrics perpendicular to gas flow.

frequency (rf) power (*P*) through a 13.56 MHz power supply via a matching network to a Ni-plated copper induction coil. Vacuum was maintained with a mechanical pump and pressure (*p*) was monitored by a Baratron® capacitance monometer. The reactor stabilized at base pressure (<1 mTorr) before introduction of plasma precursors. After the introduction of gaseous or high vapor pressure liquid precursors, the pressure stabilized at pressures indicated for at least 5 min before plasma ignition and for at least 5 min after plasma treatment to quench surface active sites. For fluorocarbon (FC) plasma treatments (p = 30 mTorr, P = 50 W, 5 min treatment time), C_3F_8 (Advanced Specialty Gases, >95%) was used as received and introduced to the system using mass flow controllers. An O_2 (Airgas, 99.9%) plasma (p = 100 mTorr, P= 100 W) was used to remove potential FC film growth on the plasma reactor walls between C_3F_8 treatments. Prior to use, ultra-pure H_2O (reverse osmosis purified, ≥18 MΩ) in a side arm vacuum flask was freeze-pump-thawed at least 4 times and during $H_2O_{(v)}$ plasma treatment (p = 15 mTorr, P = 30 W, 5 min treatment time), water vapor flowed into the reactor via a needle metering valve.

An additional, cylindrical glass substrate holder (1.5 in diameter) was used to orient the fabric perpendicular to the gas flow with the outside of the lab coat facing toward the coil, Figure Ch4-1b. To reduce damage to the fabrics, the holder was placed 10 and 16.5 cm downstream from the end of the coil region for the FC and $H_2O_{(v)}$ treatments, respectively.

Fabric contamination with ENPs

For all contamination studies, four samples of each type of fabric and plasma treatment (UT, FC, and $H_2O_{(v)}$) were prepared at one time and within 48 h of plasma exposure. Fabrics contaminated with Al_2O_3 and CB were prepared in a ultra-filtered custom-built glovebox (Terra Universal). A steel wire mesh was used to evenly distribute ~0.20 g of Al_2O_3 or ~0.14 g of CB onto the 12 fabric swatches. Excess ENP were then removed by gently tilting the fabric patch.

Based on the safety protocol for CNT, fabrics were contaminated with CNT in an enclosed hood in a class 100 cleanroom and using a Powder Dispersion Generator RBG 1000 (operated at p = 2 bar and 10 mm/h feeding rate for 10 minutes) to limit CNT agglomeration.[26] After patch contamination, the air was purged/cleaned inside the enclosure. Two of the four contaminated patches were each shaken manually for 2 min to release the ENP from the fabrics (these samples are referred to as "shaken" or "after shaking"). The shaking experiments were performed in the same environment as the contamination process, normally inside a glovebox for Al_2O_3 and CB and inside a cleanroom enclosed hood for CNT. All samples were weighed before and after the indicated contamination process. The change in mass (Δ_{mass}) was calculated by subtracting the mass of the uncontaminated sample from the mass of the same sample after contamination or shaking.

Materials characterization

i. Scanning electron microscopy (SEM).

Images were taken on a JEOL JSM-6500F with a field emission source, using an accelerating voltage of 5 – 15 kV and a working distance of 10.1 – 10.9 mm. Prior to imaging, samples were cut into ~2 cm × 2 cm pieces from the center of the circular fabric samples and coated with 25 – 50 nm of Au. A range of 3 – 7 images were taken of each sample after contamination or contamination and shaking ~3 days after plasma treatment. For the 100% polypropylene (PP) and polyester/cotton blend (blend) samples, SEM analysis was used to image the fabric after ENP contamination and the same spot after manual shaking. These fabrics were chosen because of their unique fiber patterns to allow for high confidence that the same spot was imaged both times. For analysis of same spot images, a counting grid was placed over the SEM images, and individual NPs were outlined in circles using WSXM software.[27] The circles were then sorted by size and counted, and a histogram was generated for each type of fabric/ENP combination. For the ENP counting analysis, SEM images were uploaded into the software Fiji and a line tool was used to measure the longest side of the agglomerates and the measurements were exported into Excel. Due to the different shape of the CNT compared to the spherical CB and Al_2O_3, the number of CNT clusters and individual fibers were counted instead of agglomerates, as a function of size.

ii. X-ray photoelectron spectroscopy (XPS).

XPS was performed on a Physical Electronics PE5800 ESCA/AES system equipped with an Al K monochromatic X-ray source (1486.6 eV), hemispherical electron analyzer, and multichannel detector to elucidate surface composition. Samples were secured to the sample holder with metal clips and spectra were collected using a 45° angle. A minimum of two spots on three samples (n = 6) was collected to analyze surface and sample reproducibility; a mean value and its standard deviation are reported. CasaXPS v2.3 software was used to process all high-resolution spectra with Gaussian-Lorentzian (30:70) fits and FWHM of each component was constrained to ≤2.0 eV. Small amounts (<1 nm) of Au were sputtered onto the fabric samples prior to XPS analysis to allow collection of gold (Au_{4f}) high-resolution spectra for charge correction by setting the Au $4f_{7/2}$ component to 84.0 eV. The FC treated glass slide samples were not coated with Au, so all components and regions were charge corrected by assigning the F-C peak in the F_{1s} high resolution spectra to 689.0 eV. The glass slide data provides a baseline for understanding the composition of the fluorocarbon material being deposited within the reactor to ensure a true comparison with what is deposited on the fabrics.

iii. Water Contact Angle (WCA) goniometry.

Experiments were performed using a Krüss DSA30 goniometer under ambient laboratory conditions (22 ± 2 °C and <25% relative humidity) to measure the wettability of the uncontaminated fabrics, described previously.[26] Briefly, static WCA measurements were collected with a 2 μL drop of ultra-pure H_2O (Millipore, ≥18 MΩ) and absorption rates using a 4 μL drop. The absorption rate was calculated by dividing the drop volume by the time it took for the drop to be fully adsorbed by the material. WCA measurements were performed <1 h after plasma treatment for the fresh samples and after 48 h and 28 days for the aged samples (2-day and 1 month, respectively). Aged samples were stored in ambient laboratory conditions with minimal exposure to light. All WCA data are averages of at least 3 spots on 3 samples (n = 9). As noted further below, the fabrics are all porous materials and measurement of contact angles on porous fabrics are notoriously difficult.[31]

Results And Discussion

A significant goal of this work seeks to utilize plasma processing to deposit conformal coatings or to functionalize fabrics, ultimately improving potential PPE materials with respect to ENP contamination. Fluorocarbon plasmas have been extensively used to create hydrophobic surfaces through formation of a FC film, wherein the film deposition process is hypothesized to be more efficient at lower y/x ratios of C_xF_y precursors.[28] C_3F_8 was thus selected as the precursor gas, as we have previously documented FC film formation on various substrate architectures, including semiconductor wafers (Si, ZrO),[29-30] zeolites,[23] and complex polymer structures (e.g. scaffolds, electrospun fibers).[31-32] As these FC coatings result in hydrophobic surfaces, $H_2O_{(v)}$ plasma treated fabrics were also used to create a highly hydrophilic surface for comparison and to determine the role of hydrophobicity on nanomaterial attachment. Prior work examined the effect of $H_2O_{(v)}$ plasma treatment on a range of polymeric membranes[25, 33-35] and found this system successfully implants O-containing functional groups with less substrate etching and damage than O_2 plasmas system. For both FC and $H_2O_{(v)}$ plasmas, we have previously discussed the mechanisms for plasma modification, [25, 31-35] as well as the impact of the raw materials on the gas-phase chemistry. Briefly, for the materials and conditions employed here the raw materials do not appreciably alter the gas-phase chemistry.

Atomic composition information obtained from fitting high-resolution XPS spectra are included in Table Ch4-1 for the UT and plasma modified fabrics. A more complete analysis and results of the UT and FC plasma treated materials is included in the Supporting Information (SI) and Figure S1 which presents the high-resolution C_{1s} XPS spectrum of a glass slide after FC treatment. Briefly, as expected from the Table 1 chemical compositions, the PP and Tyvek® were primarily carbon, whereas the 100% cotton (cotton) and blend fabrics had increased O% and additional O-containing binding environments (Fig. S2, presents high-resolution C1s XPS spectra of the UT fabrics).

Table Ch4-1. XPS atomic composition of the UT and plasma treated fabric samples[a]

Plasma Precursor Gas	Fabric	C (%)	O (%)	Si (%)	F (%)
UT	PP	89.2 (0.4)	10.8 (0.4)	--	--
	Tyvek®	82.8 (1.0)	17.4 (1.0)	--	--
	blend	70.3 (0.3)	24.9 (0.4)	4.8 (0.3)	--

	cotton	65.9 (0.4)	33.9 (0.4)	--	--
FC	PP	82.0 (1.5)	9.8 (0.8)	--	8.1 (1.2)
	Tyvek®	77.0 (0.4)	11.3 (0.8)	--	10.5 (0.8)
	blend	71.0 (0.9)	20.8 (0.4)	--	8.2 (0.5)
	cotton	64.9 (1.0)	22.7 (0.8)	--	12.5 (0.4)
	glass	32.1 (0.1)	28.9 (1.5)	11.1 (0.4)	27.8 (2.0)
$H_2O_{(v)}$	PP	85.6 (0.5)	14.3 (0.5)	--	--
	Tyvek®	82.3 (0.2)	17.7 (0.3)	--	--
	blend	71.0 (0.3)	29.0 (0.3)	--	--
	cotton	55.1 (0.3)	44.9 (0.3)	--	--

[a]All analyses were performed for an n = 6-9; error are reported in parentheses.

After FC plasma treatment, all fabrics gained ~10% F and the high-resolution C_{1s} spectra retain the distinct C-C/C-H peak, arising from the underlying fabric. Because of the overlap of the C-CF with the C-O peak and the C-F with the C=O peak, the C_{1s} spectra in Fig. S3 were fit attributing these peaks to both pairs of binding environments.

Similar to the FC treatment, only minor changes in the atomic composition of the fabrics are observed after $H_2O_{(v)}$ plasma exposure. Except for Tyvek®, this treatment resulted in all samples displaying a 4 – 10% increase in surface O. Figure Ch4-2 contains the high-resolution C_{1s} spectra of the $H_2O_{(v)}$ plasma treated materials, showing the treatment of PP and Tyvek® samples increased C-O functionality and resulted in an additional peak corresponding to a C=O binding environment.

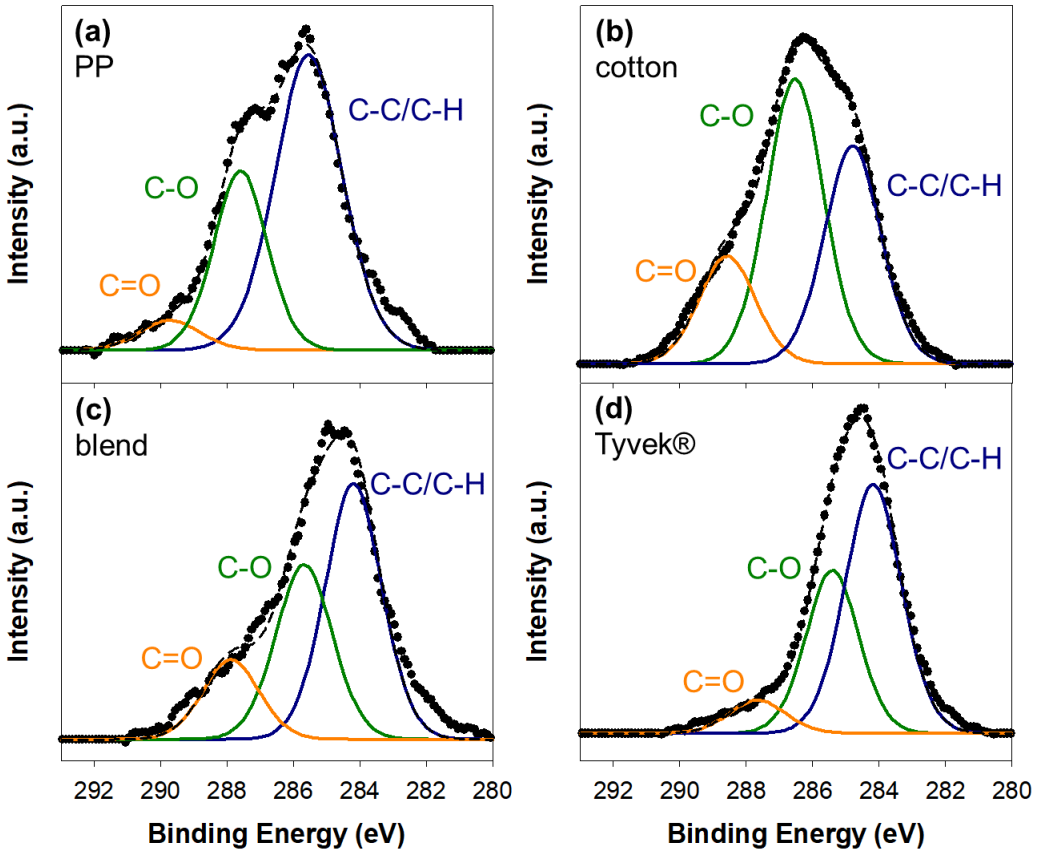

Figure Ch4-2. High-resolution C_{1s} XPS spectra for (a) PP, (b) cotton, (c) blend, and (d) Tyvek®, after $H_2O_{(v)}$ plasma treatment (P = 30 W, p = 15 mTorr).

At three of the nine spots analyzed, the Tyvek® C_{1s} spectra looked identical to the UT fabric, indicating that O-functionalization was not consistent throughout the sample. The uneven functionalization could account for this being the only sample that did not have increased percent O after plasma treatment.

WCA analysis revealed changes in surface wettability of the fabrics resulting from plasma surface modification. As discussed previously,[31] measuring WCA on porous hydrophilic materials is challenging as the water drop tends to wick through the material, causing the WCA to change with time. As such, here we report static contact angles for nominally hydrophobic materials with water drops that do not appreciably change during the measurement and we utilize dynamic WCA measurements to calculate absorption rates (volume of water absorbed per unit time) for nominally hydrophilic materials where the water drop disappears during analysis. In this way, we can compare treatments by understanding either the change in static WCA and/or differences in water absorption rates. The static and dynamic WCA measurements of UT and FC samples listed in Table S1 reveal that UT PP and Tyvek® coats are hydrophobic (with static WCAs of 121.7 ± 2.1° and 125.9 ± 1.5°, respectively) and the UT blend and cotton coats are hydrophilic (absorption rates of 4.24 ± 0.25 and 18.9 ± 1.2 μL/s, respectively).

From the known chemical structures and XPS analysis, these results align with expectations as PP and Tyvek® (a patented type of high-density polyethylene) are synthetic fibers composed of hydrocarbon polymers, whereas the cotton contains some oxygen functionality, nominally rendering cotton-containing materials more hydrophilic.

After FC plasma exposure, all materials have a static WCA above 120°, except for the blend, which has an absorption rate of 0.101 ± 0.006 μL/s. Although the Tyvek® and PP have the same WCA before and after FC plasma exposure, the cotton becomes a very hydrophobic material (WCA = 139.4 ± 0.9°), and the absorption rate of the blend is significantly reduced, indicating these materials are more hydrophobic compared to their UT counterparts. Previous work in our labs using similar treatment conditions suggests these coatings have a relatively smooth and amorphous morphology and are stable after long periods under ambient conditions.[29,32] Iriyama, et al. similarly treated white Nylon-6 fabric with various FC plasmas.[36] In their studies, the UT Nylon-6 "absorbed water immediately," but after C_3F_8 plasma exposure, the authors measured a static WCA of ~130°.[36] Another study successfully transformed cotton into a superhydrophobic material using chemical vapor deposition.[37] The polyaniline-coated cotton had a WCA of 156 ± 2°, which was only reduced to ~146° after washing 30 times, indicating a robust coating. Although the Iriyama, et al. modification strategy resulted in a more hydrophobic material than the FC plasma-treated cotton in this work, their process required cleaning, rinsing, and drying steps and took over an hour to complete. In contrast, the method presented here does not require any extra sample preparation and takes ~15 min for the entire treatment process.

One possible explanation for why the FC plasma treated blend still absorbs the water drop may be related to the weave pattern of natural fiber fabrics. Figure S4 contains low magnification SEM images of all UT samples and inset photographs of the same materials. The blend (Fig. S4c) displays a plain weave, whereas the cotton (Fig. S4b) has a twill weave. Twill is typically the denser and more compact of the two weaves, potentially allowing a better blanket coverage with the FC coating, whereas the plain weave can have large gaps that the water can pass through. Visual inspection of the two fabrics-cotton and blend (inset images in Fig. S4b for cotton and c for blend) also shows these larger gaps in the blend fabric, suggesting that even if the individual fibers have a hydrophobic coating, the material is porous enough to still allow water to pass through it.

Table Ch4-2 lists WCA data of $H_2O_{(v)}$ plasma treated materials, clearly showing the increase in hydrophilicity compared to UT fabrics. The only sample that did not have a measurable

Table Ch4-2. WCA for fresh and aged $H_2O_{(v)}$ treated fabrics.[a]

Fabric	**Fresh**	**Aged – 2 Days**	**Aged – 1 Month**
Static WCA (°)			
PP	103.7 (2.9)	111.5 (1.5)	118.1 (1.7)
Absorption Rate (μL s^{-1})			
Tyvek®	4.36 (1.24)	4.27 (1.07)	4.78 (1.41)
blend	8.42 (0.44)	6.09 (0.58)	4.64 (0.53)
cotton	46.4 (1.7)	48.8 (1.6)	44.3 (1.7)

[a]All analyses were performed for n = 9; error are reported in parentheses.

absorption rate after $H_2O_{(v)}$ plasma exposure is PP. The WCA of this sample decreased by ~18° after plasma treatment, from ~122° (Table Ch4-2) to ~104°; nevertheless, this material is still considered hydrophobic.[31, 38] Harsher plasma parameters (higher *P* and *p* and sample distance closer to the coil region of the plasma) were briefly explored, but resulted in the plasma burning a hole in the material within one minute of exposure to the plasma. Thus, further optimization of treatment conditions is needed to balance increasing the wettability of the PP while not significantly damaging the fabric.

For the remaining samples, an absorption rate was calculated after $H_2O_{(v)}$ plasma treatment. Similar to the UT materials, the $H_2O_{(v)}$ cotton exhibits a much faster absorption rate than the blend (~46 and ~8 μL s^{-1}, respectively). The Tyvek® became very hydrophilic after $H_2O_{(v)}$ plasma modification, evidenced by the shift from a static WCA of ~126° to an absorption rate of 4.36 ± 1.24 μL s^{-1}. The larger error reported with these data comes from the absorbance rates ranging from 0.704 – 12.5 μL s^{-1}. Even with a more extensive sampling size (n = 18), the variability of these rates did not decrease, suggesting that the interaction of the $H_2O_{(v)}$ plasma with the Tyvek® is less uniform than with the other materials. These data support the XPS results discussed above, wherein some sample locations showed additional C-O and C=O functionality, whereas other spots remain unchanged compared to the UT fabric. Again, this can be attributed to the challenge of treating substrates with complex morphologies.

Because WCA measurements reflect both the surface chemistry and morphology of the material,[31] morphological changes can aid in explaining the observed WCA data of $H_2O_{(v)}$ treated samples. SEM images of UT and plasma treated fabrics, Figure 3, show that although all the samples experienced some degree of etching from $H_2O_{(v)}$ plasma exposure (indicated by the visually rougher and pitted surface), the Tyvek® visually seems to have the most substantial morphological change. This plasma treatment enhanced the already existing texture of the fabric

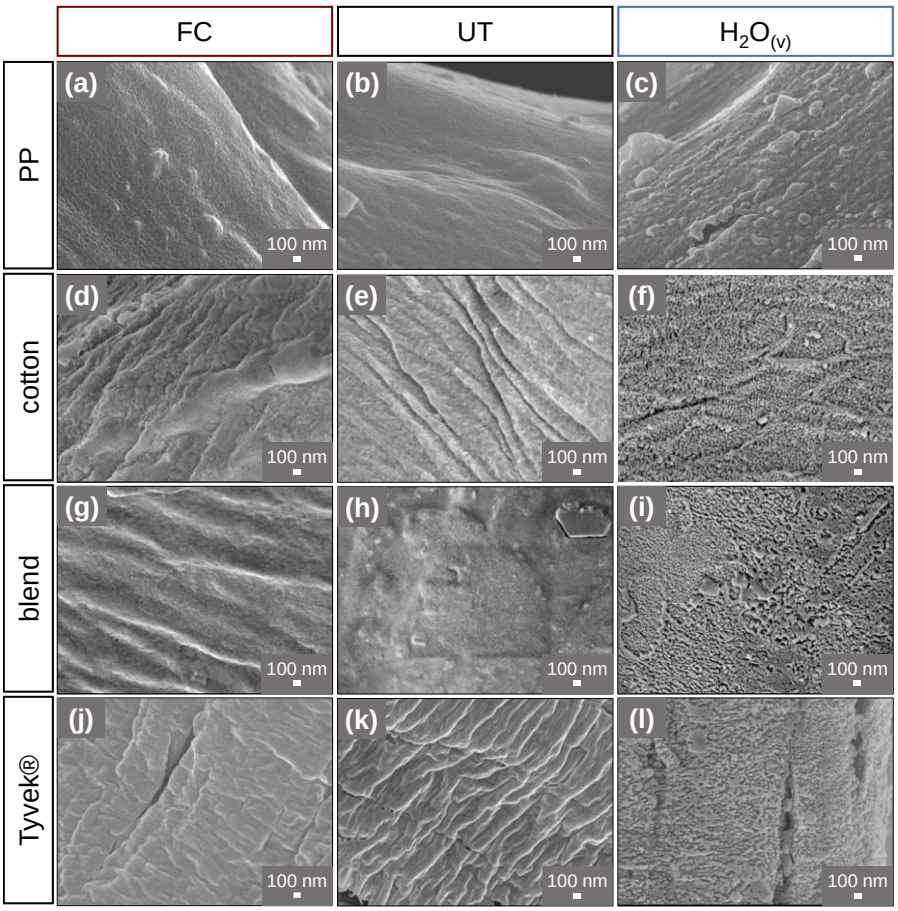

Figure Ch4-3. SEM images of (a-c) PP, (d-f) cotton, (g-i) blend, and (j-l) Tyvek® fabrics. The (b, e, h, k) UT, (a, d, g, j) FC and (c, f, I,l) $H_2O_{(v)}$ plasma treated samples were all Au coated prior to imaging. All images taken at ×30,000 magnification and inset scale bars represent 100 nm.

and sporadically formed deep grooves on the material. Similar features are seen in some of the other fabrics (blend, cotton), but to a lesser degree. Thus, surface morphology may not be uniform between samples and even at different areas on the same sample, potentially contributing to the larger error in the measured absorbance rates. As with the $H_2O_{(v)}$ treated Tyvek®, the natural fibers (Fig. Ch4-3f and i) also have increased surface roughness after plasma treatment and demonstrated an increase in hydrophilicity when compared to the UT fabrics. Notably, the PP sample (Fig. Ch4-3c) does not have the same pitting observed on the other $H_2O_{(v)}$ plasma treated fabrics, and this is the only material with a static WCA after plasma treatment. These results are comparable to previous work in our lab with H_2O plasma treating PP sheets (p = 50 mTorr, P = 25 W, 2 min treatment time, 9 cm downstream).[25] Although those samples were 0.060 in. (compared

to the ~0.010 in[26] used in this work) and treated under harsher plasma parameters, SEM images of the treated PP did not appear to have the same scale of increased surface roughness when compared to the treated high-density polyethylene. The previously published results also had similar trends to the data presented herein when comparing WCA measurements of PP and high-density polyethylene. The $H_2O_{(v)}$ plasma treated PP still had a static WCA of 71 ± 2° compared to an UT material WCA of ~105° and became less hydrophilic than high density polyethylene after plasma modification (WCA reduced from ~101° to ~18°). Finally, after aging for 1 month, the PP experienced almost full hydrophobic recovery whereas the polyethylene only had an increase of ~30°. As these observations were demonstrated in the present study, the results suggest that it is not specifically the PP used in this work, but it is likely that PP in general is not as easily functionalized or etched via plasma treatment as other fabrics.

Previous work in our lab demonstrated that some plasma-treated polymeric materials experience some hydrophobic recovery after two weeks and up to a month after plasma modification.[25, 39] Hydrophobic recovery is thought to be caused at least partially by the rearrangement, or burying of high surface energy components (e.g., O functionality) over time and/or chemical reactions with atmospheric O_2 and H_2O.[25, 39-40] Sample aging was also observed by Holc et al. when studying O_2 plasma treated polyacrylonitrile. Yet, the authors found that they could prevent some of the reorganization of surface functional groups by storing samples at a lower temperature. All samples exhibited some degree of hydrophobic recovery; nevertheless, storage at 5 °C slowed aging over room temperature storage. This behavior was attributed to the "less intensive" reorientation of surface groups at the lower temperature.[40] Although this storage method might improve the stability of the $H_2O_{(v)}$ treatments in this work, we chose to age the samples at room temperature to better mimic conditions that the fabrics would experience in a store or warehouse. Thus, WCA measurements of $H_2O_{(v)}$ treated samples were made after aging for two days and one month in ambient conditions to determine the relative permanence of the treatments. The shorter time measurement provided data to ensure the treatment was still effective at the time of the ENP exposure studies. The 2-day aged samples still have WCA and absorption rates within experimental error of the freshly treated samples, Table 2, indicating the ENP contamination results were not impacted by a change in wettability caused by the delay between plasma modification and nanomaterial contamination. WCA measurements made on the 1-month aged samples, however, suggest that hydrophobic recovery does occur but is dependent on the material. The 1-month $H_2O_{(v)}$ PP and blend have a WCA of 118.1° and an absorption rate of 4.64 ± 0.53 μL s^{-1}, respectively. These values are within error of the UT materials, meaning there was

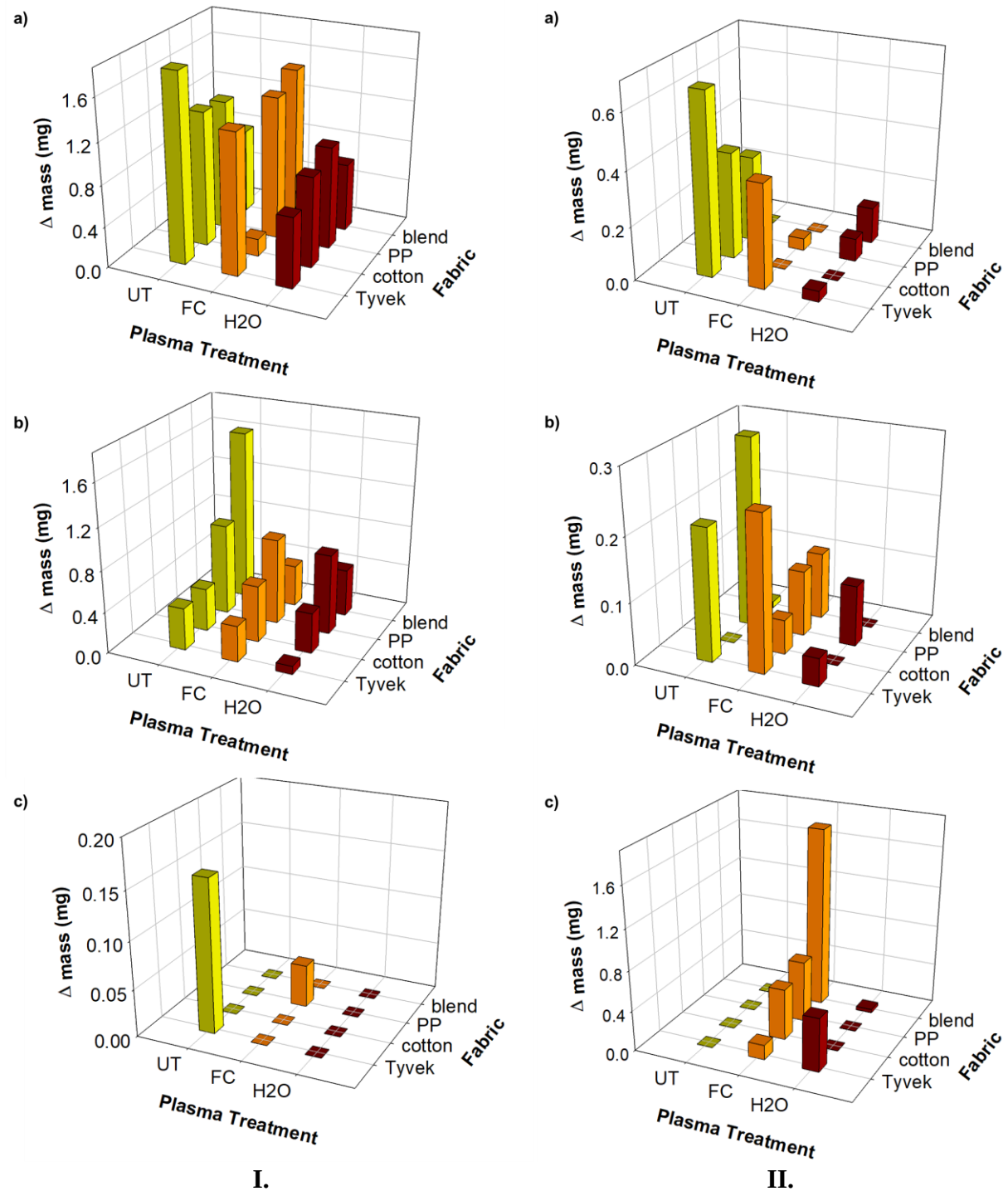

Figure Ch4-4. Change in mass of UT and plasma treated fabrics. I. after contamination with (a) Al_2O_3, (b) CB, and (c) CNT; II. after contamination (a) Al_2O_3, (b) CB, and (c) CNT and shaking samples.

hydrophobic recovery for these fabrics. Notably, the 1-month aged Tyvek® sample continues to

be completely wettable with a measurable absorption rate, whereas the UT material had a static WCA of 125.9°. Likewise, the cotton samples still had an absorption rate of 44.3 ± 1.7 μL s^{-1} compared to the UT material's absorption rate of 4.24 ± 0.25 μL s^{-1}. These results suggest $H_2O_{(v)}$ plasma modification of the Tyvek® and cotton is stable enough to be an effective method to increase the hydrophilicity of these fabrics; however, further treatment optimization is needed for the PP and blend materials.

Table S2 reports the average Δ_{mass} of all the contaminated and shaken samples. These data (without error analysis for clarity) are also shown in Figures Ch4-4. In general, the $H_2O_{(v)}$ plasma treated fabrics had the smallest Δ_{mass} after Al_2O_3 contamination (Fig. 4-I). The FC plasma treated cotton samples exhibited the smallest Δ_{mass}, with an increase of 0.17 mg after contamination. In contrast, the UT Tyvek® had the largest Δ_{mass}, with an increase of 1.81 mg after contamination. Although shaking reduced the Δ_{mass} for all fabrics when compared to the contaminated samples, they still retain some ENP, indicating the nanomaterials are not completely resuspended from these fabrics. Compared to samples contaminated with Al_2O_3, samples contaminated with CB (Fig. Ch4-4-II) had a smaller Δ_{mass} (both after contamination and after shaking) that was somewhat independent of fabric and plasma treatment. Note that the UT blend had significantly more CB attach than any other fabric; however, essentially all of it was removed after shaking, indicating that this combination of fabric/ENP has a high likelihood for causing secondary exposure. For the CNT contaminated samples, the Δ_{mass} was comparable to the CB contaminated fabrics, but many of the samples had $\Delta_{mass} \leq 0$, suggesting that contamination with CNT resulted in a decrease in mass even without shaking the fabric when compared to the mass of the uncontaminated samples. Although this result may be an indication of the low contamination levels of the fabrics with CNT, it is also possible that some fibers from the fabric could have been dislodged by the high air flow of the powder dispersion generator used during the CNT contamination process.

To understand the role of surface chemistry on ENP attachment and resuspension, SEM images were acquired from the same spot on contaminated fabrics before and after shaking. Although this same spot imaging was attempted with all ENP on all the UT and plasma modified

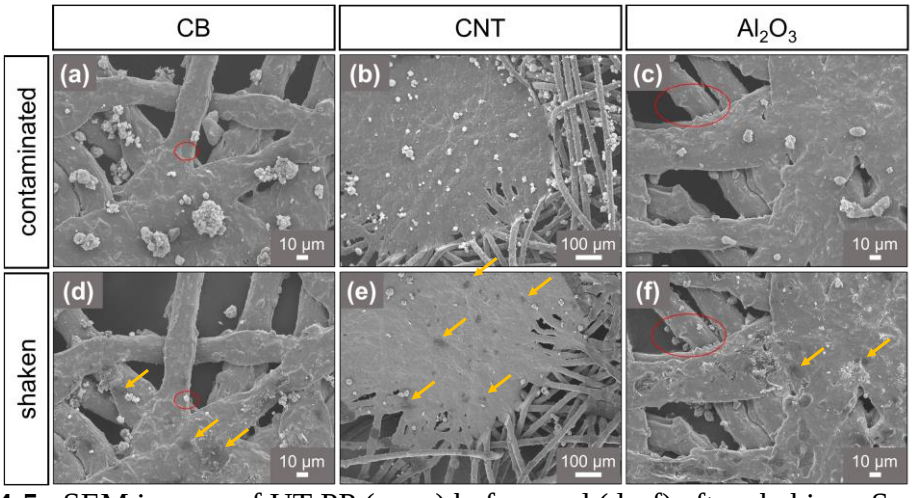

Figure Ch4-5. SEM images of UT PP (a – c) before and (d - f) after shaking. Samples were contaminated with (a, d) CB, (b, e) CNT, and (c, f) Al_2O_3. Images taken at (a, c, d, f) ×500 and (b, e) ×110 magnification. Yellow arrows highlight some areas where ENP were removed, and red circles indicate areas that ENP reattached to.

fabrics, only the PP fabric samples are reported here. This fabric was selected as it has easily identifiable "landmarks" on the material, allowing for confidence that the areas imaged were the same, despite removing the sample from the instrument to perform the shaking experiments. Figure Ch4-5 contains SEM images of the ENP-contaminated UT PP before and after shaking.

Because of the Au coating required for imaging these samples, distinct dark spots where ENP released from the fabrics can be seen in the images and select spots are highlighted using yellow arrows. The red circles in Figure 5 highlight some areas where ENP were displaced from elsewhere and have reattached. This reattachment may be beneficial as it can serve as an alternative method to prevent secondary nanomaterial exposure. Figure Ch4-6 shows the same

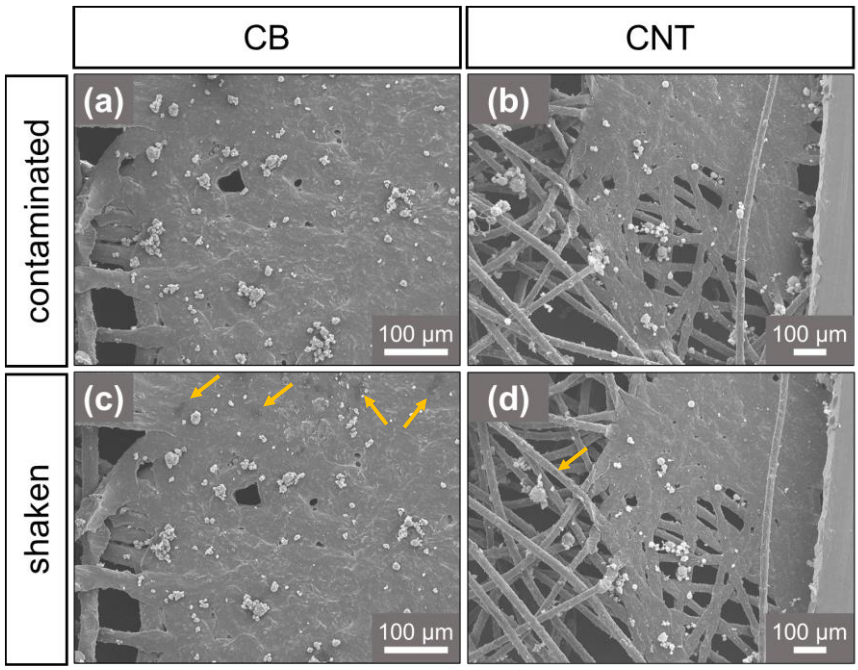

Figure Ch4-6. SEM images of FC PP (a – b) before and (c - d) after shaking. Fabrics were contaminated with (a, c) CB and (b, d) CNT. Images taken at (a, c) ×200 and (b, d) ×100 magnification. Yellow arrows highlight some areas where ENP were removed.

spot imaging of the FC PP fabric contaminated with CB and CNT. These images also contain dark spots where ENP have fallen off or relocated after shaking (also highlighted using yellow arrows). The FC plasma treated fabric samples, do not, however, have as many ENP released after shaking as seen with the UT materials.

The number and size distribution of the aggregates counted in these "same spot" images are plotted in Figure S5. For most agglomerates, shaking the UT PP (Fig.S5a and c) results in ~50% reduction of ENP, a behavior also observed with the FC plasma treated PP contaminated with CB. With the FC PP, the CNT counts do not show as significant a decrease after shaking, and for the smaller clusters, the counts actually increase. This indicates that even though the CNT moves around on the fabric, they are still adhering to the material and not completely falling off or being resuspended. This is a promising result, as the continued attachment of the CNT to the FC PP means that this ENP/fabric combination could represents a lower risk for ENP inhalation by the wearer. This study demonstrates that the deposition of a FC film altered the interaction of the CNT

with the PP, suggesting that the surface chemistry of a material plays an important role in the attachment and resuspension behavior of ENP. Further work is needed to analyze a larger sample size for the UT and FC plasma treated PP and to perform these same spot analyses on all of the fabrics to better understand ENP/fabric interactions to improve PPE.

Because of the difficulties collecting "same spot" images with the other fabrics, preliminary results sampling random spots on contaminated and shaken fabrics were also examined to begin understanding the ENP attachment and resuspension behavior with both the UT and plasma modified materials. Four samples of each type of fabric were contaminated with either Al_2O_3, CB, or CNT and then two of those samples were also shaken. The number and size of ENP agglomerates were determined from SEM image analysis of random areas of the contaminated and shaken samples. Tables S3 and S4 include the size distribution and number of agglomerates (raw counts) for the samples contaminated with CB and Al_2O_3, respectively. Some samples had very low total agglomerate counts. Consequently, only samples with total agglomerate counts >100 were selected for comparison to ensure these values were representative with a relatively large sample size. Figure Ch4-7 shows the number and size distribution of select CB and Al_2O_3 contaminated fabrics. As seen in Figure S5, agglomerates <15 μm have the highest counts for both ENP and fabrics, whereas the larger agglomerates have very little attachment and subsequent release counts. When comparing the CB attachment of the UT and plasma treated blend samples, the UT samples clearly had more nanometer sized agglomerates than the FC and $H_2O_{(v)}$ samples, indicating that both plasma treatments decreased the attachment of CB on the blend fabric. For the larger agglomerates, the UT samples had fewer counts when compared to the plasma treated fabrics. In general, these trends are also seen when comparing the agglomerate counts after shaking the samples. This result may indicate that particle size affects the attachment of these

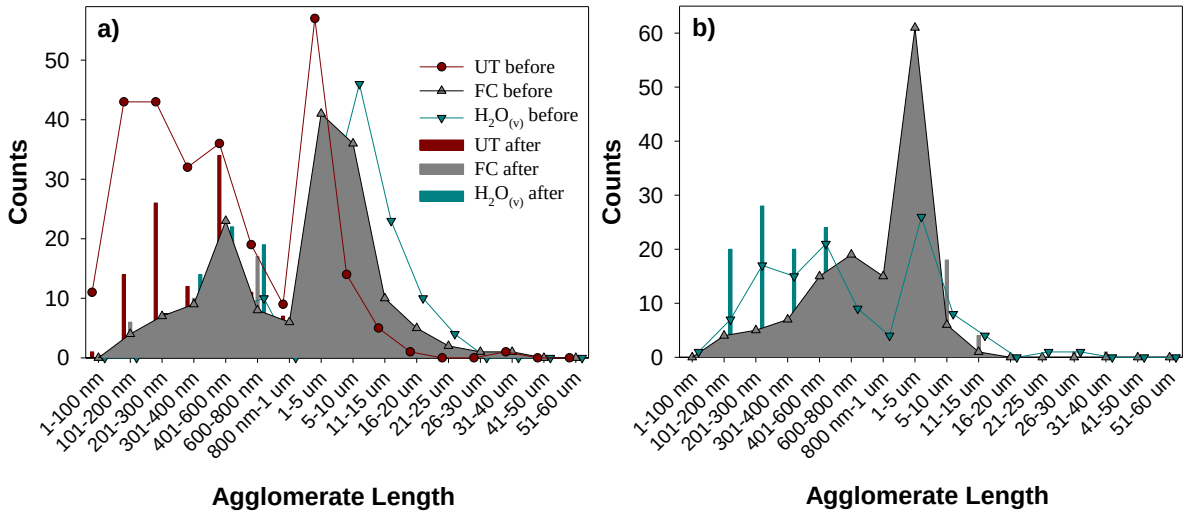

Figure Ch4-7. Number of (a) CB agglomerates on blend and (b) Al_2O_3 on Tyvek®. Fabrics were contaminated with CB and counted (points) before and (vertical bars) after shaking. Red, gray, and teal data represent the UT, FC, and $H_2O_{(v)}$ plasma treated fabrics, respectively.

materials to the fabric. Comparing the counts of the contaminated and shaken samples, the UT samples appear to have the largest decrease for most agglomerate sizes, suggesting the plasma

treated blend fabrics are better at preventing the resuspension of CB. Comparing the Al_2O_3 attachment of the plasma treated Tyvek samples (Fig. 7b), the $H_2O_{(v)}$ samples had larger counts for the nanometer agglomerates and the FC samples had larger counts for the micrometer ENP. The counts of the shaken samples are relatively similar to the contaminated samples, indicating that these treatments can be an effective strategy to prevent secondary contamination of Al_2O_3.

As a final measure of ENP contamination, Table S5 lists the numbers of individual and bundled CNT on the different fabrics. These results are reported without a size distribution because of the irregular shape of the agglomerates not allowing a representative diameter to be determined. Samples were only imaged after shaking, so comparison of the amount before and after shaking cannot be performed. From these data, Tyvek® has the most CNT remaining after shaking, followed by the blend, cotton, and finally the PP. In general, the FC plasma treated samples have the largest number of bundles for each fabric type, whereas the Tyvek® samples have the most individual (i.e., not bundled) CNT.

Similar to the McDonagh, et al. studies,[17-18] larger ENP agglomerates displayed the lowest contamination and resuspension. The data presented here, however, also appear to contradict their finding that the tightness/pattern of the fabric is the sole influencing factor on ENP adhesion.[17] If this were true, the cotton and blend materials would exhibit similar counts before and after shaking, whereas the PP and Tyvek® would have a majority of ENP released after shaking. Predictions that are clearly not borne out in our data. Furthermore, if fabric tightness/pattern was the only factor in ENP adhesion, the UT and plasma treated samples for a given fabric would display no appreciable differences in behavior. Thus, the type and surface chemistry of the material must have significant effects on ENP attachment and release.

There are two forces that can contribute to ENP interactions with fabrics, which we will briefly discuss here. One contributing factor is Hamaker attraction or van der Waals forces between a particle and a substrate.[26] Because of the large relative size difference of the ENP to the fabric threads, this intermolecular force can be approximated using the individual Hamaker constants of the ENP and the fabric interacting with themselves. This calculation, however, is complicated to perform, as finding reliable Hamaker constants for uncommon or modified materials (i.e., the ENP and plasma treated fabrics) are difficult and “equivalent” material substitutions will need to be used. Thus, although this force is not quantified for each ENP fabric pair, it can contribute to the observed contamination and resuspension behavior.

Another force that can impact ENP-fabric interactions is capillary adhesion.[41] Water from the atmosphere can condense on the surface of the materials and form a small water bridge that binds the ENP to the surface of the fabric. Thus, fabrics that absorb water (i.e., cotton, blend, and $H_2O_{(v)}$ plasma treated samples) will have less water on the surface of the fabric and capillary forces will be diminished. Looking at the mass and agglomerate count data, however, the hydrophilic samples do not consistently demonstrate lower resuspension, indicating that capillary adhesion alone does not dominate ENP-fabric behavior. Clearly, ENP attachment and resuspension is a complex phenomenon that can be attributed to a combination of physical and chemical properties of the fabric with which they interact.

Conclusion

The attachment and release of several ENP with four PPE fabrics were investigated to understand how different properties affect their interactions with the ultimate goal of improving the materials by mitigating contamination or risk of secondary exposure. The surface chemistry

and wettability of these fabrics was tuned using either a C_3F_8 or $H_2O_{(v)}$ plasma and monitored with XPS and WCA analysis. The C_3F_8 plasma deposited a FC coating, increasing the material hydrophobicity, whereas the $H_2O_{(v)}$ plasma implanted O-functionality and etched the surface, nominally increasing the hydrophilicity and roughness of the surfaces. Notably, the latter treatment ultimately resulted in a relatively permanent increase in hydrophilicity of the cotton and Tyvek®, whereas the other two materials exhibited hydrophobic recovery after a month of aging post treatment.

By monitoring the mass of the contaminated and shaken samples, studies indicate that in general, Al_2O_3 exposure had the largest Δ_{mass}, whereas CNT had the smallest. This suggests these fabrics work well to protect against contamination and secondary exposure to CNT. The same spot SEM analysis studies reveal that displaced CNT particles on FC plasma treated PP are likely to reattach elsewhere on the fabric, providing an alternative method to limiting secondary exposure. With the concern of the potential carcinogenicity of CNT, the FC surface treatment may support the treated fabric traps CNT, thereby minimizing subsequent exposure. SEM image analysis of the contaminated and shaken fabrics indicate that in general, agglomerates <15 μm have the highest attachment to all the materials studied, and the probability of a particle being released after shaking increases as its size increases. This result seems to support other literature studies that demonstrated attachment and release of micron sized particles increases as their size increase.[18] When considering CB attachment, plasma modification appears to decrease the number of agglomerates attached to the material when compared to the UT fabric. In addition, the counts on the shaken fabrics indicate that plasma treatment results in a smaller chance that the ENP will resuspend when the contaminated fabric is shaken. Although the sizes of the attached Al_2O_3 agglomerates seemed dependent on the plasma treatment used, both the FC and $H_2O_{(v)}$ modified Tyvek® had similar agglomerate counts on the contaminated and shaken samples, suggesting that plasma modification is an effective strategy to reduce secondary exposure to Al_2O_3.

Ultimately, the differences of the ENP behavior on the UT and plasma modified fabrics indicate that both fabric weave pattern and surface chemistry impact nanomaterial attachment and resuspension. These efforts toward understanding the role of material properties on the attachment of ENP may lead to strategies for determining what types of fabric are best for protecting the wearer from adverse health effects from exposure to nanomaterials. Authors will consider other types of nanomaterials such as those with specific high surface area and absorbability for future studies. It's worthy to note that novel biobased nanoparticles such as cellulose nanocrystal[42] were made for engineering applications and reinforcement agent in polymer and synthetic materials; our results may aid evaluations of such biobased nanoparticles. Although further work is needed to optimize the hydrophilic treatments of some of the fabrics and fully understand the effect of the surface modifications, these data demonstrate that plasma treatment is a viable route to creating improved materials for PPE. In conclusion for implications, the surface treatment resulting in materials repellent to airborne particles could be used in treating fabrics used for making PPE or work uniforms to minimize the contamination and spread of unwanted particles.

References

1. Singh, A. K., Chapter 1 - Introduction to Nanoparticles and Nanotoxicology. In *Engineered Nanoparticles*, Singh, A. K., Ed. Academic Press: Boston, 2016; pp 1-18.
2. Jose Varghese, R.; Sakho, E. h. M.; Parani, S.; Thomas, S.; Oluwafemi, O. S.; Wu, J., Chapter 3 - Introduction to Nanomaterials: Synthesis and Applications. In *Nanomaterials for Solar Cell*

Applications, Thomas, S.; Sakho, E. H. M.; Kalarikkal, N.; Oluwafemi, S. O.; Wu, J., Eds. Elsevier: 2019; pp 75-95.
3. Rohilla, D.; Chaudhary, S.; Umar, A. An Overview of Advanced Nanomaterials for Sensor Applications. Eng. Sci. 2021, 16, 47–70. https://doi.org/10.30919/es8d552.
4. Zhang, Y.; Luo, Y. Naturally Derived Nanomaterials for Multidisciplinary Applications and Beyond. ES Food Agrofor. 2021, 4, 1–2. https://doi.org/10.30919/esfaf484.
5. Liu, H.; Mao, Y. Graphene Oxide-Based Nanomaterials for Uranium Adsorptive Uptake. ES Mater. Manuf. 2021, 13, 3–22. https://doi.org/10.30919/esmm5f453.
6. Wu, Y.; Chen, E.; Weng, X.; He, Z.; Chang, G.; Pan, X.; Liu, J.; Huang, K.; Huang, K.; Lei, M. Conductive Polyvinyl Alcohol/Silver Nanoparticles Hydrogel Sensor with Large Draw Ratio, High Sensitivity and High Stability for Human Behavior Monitoring. Eng. Sci. 2022, 18, 113–120. https://doi.org/10.30919/es8d659.
7. Qin, C.; Gong, H.; Sun, C.; Wu, X. Optical Properties of a Core/Shell/Shell Shape Metal-Insulator-Metal Composite Nanoparticle for Solar Energy Absorption. Eng. Sci. 2021, 17, 224–230. https://doi.org/10.30919/es8e509.
8. Prasad, S. R.; Teli, S. B.; Ghosh, J.; Prasad, N. R.; Shaikh, V. S.; Nazeruddin, G. M.; Al-Sehemi, A. G.; Patel, I.; Shaikh, Y. I. A Review on Bio-Inspired Synthesis of Silver Nanoparticles: Their Antimicrobial Efficacy and Toxicity. Eng. Sci 2021, 16, 90–128. https://doi.org/10.30919/es8d479.
9. Kale, S. K.; Parishwad, G. V.; Husainy, A. S. N.; Patil, A. S. Emerging Agriculture Applications of Silver Nanoparticles. ES Food Agrofor. 2021, 3, 17–22. https://doi.org/10.30919/esfaf438.
10. Chen, J.; Zhu, Y.; Guo, Z.; Nasibulin, A. G. Recent Progress on Thermo-Electrical Properties of Conductive Polymer Composites and Their Application in Temperature Sensors. Eng. Sci. 2020, 12, 13–22. https://doi.org/10.30919/es8d1129.
11. Zhao, J.; Wei, D.; Zhang, C.; Shao, Q.; Murugadoss, V.; Guo, Z.; Jiang, Q.; Yang, X. An Overview of Oxygen Reduction Electrocatalysts for Rechargeable Zinc-Air Batteries Enabled by Carbon and Carbon Composites. Eng. Sci. 2021, 15, 1–19. https://doi.org/10.30919/es8d420.
12. Chang, X.; Chen, L.; Chen, J.; Zhu, Y.; Guo, Z. Advances in Transparent and Stretchable Strain Sensors. Advanced Composites and Hybrid Materials 2021, 4, 435–450. https://doi.org/10.1007/s42114-021-00292-3.
13. Ellenbecker, M.; Tsai, S.; Geraci, C.' Schulte, P.; Beaucham, C.; Hodson, L.; Hoover, M.; Zumwalde, R. General Safe Practices for Working with Engineered Nanomaterials in Research Laboratories. National Insitute for Occupational Safey and Health: 2012, DHHS (NIOSH) Publication No. 2012-147.
14. Kan, H.; Pan, D.; Castranova, V., Engineered Nanoparticle Exposure and Cardiovascular Effects: The Role of a Neuronal-Regulated Pathway. *Inhal. Toxicol.* **2018,** *30* (9-10), 335-342. doi:10.1080/08958378.2018.1535634
15. Tang, C.-S.; Chuang, K.-J.; Chang, T.-Y.; Chuang, H.-C.; Chen, L.-H.; Lung, S.-C. C.; Chang, L.-T., Effects of Personal Exposures to Micro- and Nano-Particulate Matter, Black Carbon, Particle-Bound Polycyclic Aromatic Hydrocarbons, and Carbon Monoxide on Heart Rate Variability in a Panel of Healthy Older Subjects. *Int. J. Enviorn. Res. Public Health* **2019,** *16* (23), 4672. doi:10.3390/ijerph16234672

16. Tsai, C. S.-J., Contamination and Release of Nanomaterials Associated with the Use of Personal Protective Clothing. *Ann. Occup. Hyg* **2015,** *59* (4), 491-503. doi:10.1093/annhyg/meu111
17. McDonagh, A.; Byrne, M. A., The Influence of Human Physical Activity and Contaminated Clothing Type on Particle Resuspension. *J. Enviorn. Radioact.* **2014,** *127*, 119-126. doi:10.1016/j.jenvrad.2013.10.012
18. McDonagh, A.; Byrne, M. A., A Study of the Size Distribution of Aerosol Particles Resuspended from Clothing Surfaces. *J. Aerosol Sci* **2014,** *75*, 94-103. doi:10.1016/j.jaerosci.2014.05.007
19. Wu, H.; Sun, H.; Han, F.; Xie, P.; Zhong, Y.; Quan, B.; Zhao, Y.; Liu, C.; Fan, R.; Guo, Z. Negative Permittivity Behavior in Flexible Carbon Nanofibers- Polydimethylsiloxane Films. Eng. Sci. 2022, 17, 113–120. https://doi.org/10.30919/es8d576.
20. Zhao, J.; Song, L.; Shi, Q.; Luan, S.; Yin, J., Antibacterial and Hemocompatibility Switchable Polypropylene Nonwoven Fabric Membrane Surface. *ACS Appl. Mater. Interfaces* **2013,** *5* (11), 5260-5268. doi:10.1021/am401098u
21. Lao, L.; Fu, L.; Qi, G.; Giannelis, E. P.; Fan, J., Superhydrophilic Wrinkle-Free Cotton Fabrics via Plasma and Nanofluid Treatment. *ACS Appl. Mater. Interfaces* **2017,** *9* (43), 38109-38116. doi:10.1021/acsami.7b09545
22. Karaman, M.; GÜRsoy, M.; AykÜL, F.; Tosun, Z.; Kars, M. D.; Yildiz, H. B., Hydrophobic Coating of Surfaces by Plasma Polymerization in an rf Plasma Reactor with an Outer Planar Electrode: Synthesis, Characterization and Biocompatibility. *Plasma Sci. Technol.* **2017,** *19* (8), 085503. doi:10.1088/2058-6272/aa6fec
23. Hanna, A. R.; Fisher, E. R., Tailoring the Surface Properties of Porous Zeolite Constructs Using Plasma Processing. *Microporous Mesoporous Mater.* **2020,** *307*, 110467. doi:10.1016/j.micromeso.2020.110467
24. Hiyoto, K. A. M.; Fisher, E. R., Utilizing Plasma Modified SnO_2 Paper Gas Sensors to Better Understand Gas-Surface Interactions at Low Temperatures. *J. Vac. Sci. Technol., A* **2020,** *38* (4), 043202. doi:10.1116/6.0000029
25. Tompkins, B. D.; Fisher, E. R., Evaluation of Polymer Hydrophobic Recovery Behavior Following H_2O Plasma Processing. *J. Appl. Polym. Sci.* **2015,** *132* (20). doi:10.1002/app.41978
26. Maksot, A.; Sorna, S. M.; Blevens, M.; Reifenberger, R. G.; Hiyoto, K.; Fisher, E. R.; Vindell, T.; Li, Y. V.; Kipper, M. J.; Tsai, C. S.-J., Engineered Nanoparticle Release from Personal Protective Clothing: Implications for Inhalation Exposure. *ACS App. Nano Mater.* **2022,** *5* (2), 2558-2568. doi:10.1021/acsanm.1c04229
27. Horcas, I.; Fernández, R.; Gómez-Rodríguez, J. M.; Colchero, J.; Gómez-Herrero, J.; Baro, A. M., WSXM: A Software for Scanning Probe Microscopy and a Tool for Nanotechnology. *Rev. Sci. Instrum.* **2007,** *78* (1), 013705. doi:10.1063/1.2432410
28. d'Agostino, R.; Cramarossa, F.; Fracassi, F.; Illuzzi, F., 2 - Plasma Polymerization of Fluorocarbons. In *Plasma Deposition, Treatment, and Etching of Polymers*, d'Agostino, R., Ed. Academic Press: San Diego, 1990; pp 95-162.
29. Cuddy, M. F.; Fisher, E. R., Contributions of CF and CF_2 Species to Fluorocarbon Film Composition and Properties for C_xF_y Plasma-Enhanced Chemical Vapor Deposition. *ACS Appl. Mater. Interfaces* **2012,** *4* (3), 1733-1741. doi:10.1021/am2018546
30. Hanna, A. R.; Cuddy, M. F.; Fisher, E. R., Energy Partitioning and its Influence on Surface Scatter Coefficients within Fluorinated Inductively Coupled Plasmas. *J. Vac. Sci. Technol., A* **2017,** *35* (5), 05C308. doi:10.1116/1.4990682

31. Hawker, M. J.; Pegalajar-Jurado, A.; Fisher, E. R., Innovative Applications of Surface Wettability Measurements for Plasma-Modified Three-Dimensional Porous Polymeric Materials: A Review. *Plasma Process. Polym.* **2015,** *12* (9), 846-863. doi:10.1002/ppap.201500035
32. Hawker, M. J.; Pegalajar-Jurado, A.; Fisher, E. R., Conformal Encapsulation of Three-Dimensional, Bioresorbable Polymeric Scaffolds Using Plasma-Enhanced Chemical Vapor Deposition. *Langmuir* **2014,** *30* (41), 12328-12336. doi:10.1021/la502596f
33. Steen, M. L.; Hymas, L.; Havey, E. D.; Capps, N. E.; Castner, D. G.; Fisher, E. R., Low Temperature Plasma Treatment of Asymmetric Polysulfone Membranes for Permanent Hydrophilic Surface Modification. *J. Membr. Sci.* **2001,** *188* (1), 97-114. doi:10.1016/S0376-7388(01)00375-1
34. Steen, M. L.; Butoi, C. I.; Fisher, E. R., Identification of Gas-Phase Reactive Species and Chemical Mechanisms Occurring at Plasma−Polymer Surface Interfaces. *Langmuir* **2001,** *17* (26), 8156-8166. doi:10.1021/la0106642
35. Tompkins, B. D.; Dennison, J. M.; Fisher, E. R., Etching and Post-Treatment Surface Stability of Track-Etched Polycarbonate Membranes by Plasma Processing Using Various Related Oxidizing Plasma Systems. *Plasma Process. Polym.* **2014,** *11* (9), 850-863. doi:10.1002/ppap.201400044
36. Iriyama, Y.; Yasuda, T.; Cho, D. L.; Yasuda, H., Plasma Surface Treatment on Nylon Fabrics by Fluorocarbon Compounds. *J. Appl. Polym. Sci.* **1990,** *39* (2), 249-264. doi:10.1002/app.1990.070390205
37. Zhou, X.; Zhang, Z.; Xu, X.; Guo, F.; Zhu, X.; Men, X.; Ge, B., Robust and Durable Superhydrophobic Cotton Fabrics for Oil/Water Separation. *ACS Appl. Mater. Interfaces* **2013,** *5* (15), 7208-7214. doi:10.1021/am4015346
38. Gao, L.; McCarthy, T. J., Teflon is Hydrophilic. Comments on Definitions of Hydrophobic, Shear versus Tensile Hydrophobicity, and Wettability Characterization. *Langmuir* **2008,** *24* (17), 9183-9188. doi:10.1021/la8014578
39. Steen, M. L.; Jordan, A. C.; Fisher, E. R., Hydrophilic Modification of Polymeric Membranes by Low Temperature H_2O Plasma Treatment. *J. Membr. Sci.* **2002,** *204* (1), 341-357. doi:10.1016/S0376-7388(02)00061-3
40. Holc, M.; Zaplotnik, R.; Mozetic, M.; Vesel, A., Surface Modification and Aging of Polyacrylonitrile Butadiene Styrene Polymer Induced by Treatment in rf Oxygen Plasma. *IEEE Transactions on Plasma Science* **2018,** *46* (10), 3669-3676. doi:10.1109/TPS.2018.2855808
41. Harrison, A. J.; Corti, D. S.; Beaudoin, S. P., Capillary Forces in Nanoparticle Adhesion: A Review of AFM Methods. *Part. Sci. Technol.* **2015,** *33* (5), 526-538. doi:10.1080/02726351.2015.1045641
42. Mohd Amin, K.N.; Hosseinmardi, A.; Martin, D.J.; Annamalai, P.K. A mixed acid methodology to produce thermally stable cellulose nanocrystal at high yield using phosphoric acid. *J. Bioresources and Bioproducts.* 2022, 7 (2), 99-108. doi: 10.1016/j.jobab.2021.12.002

Appendix

Chapter 1 supplementary materials

Fabric descriptive property measurements

To further correlate ENP retention and resuspension corresponding to different fabric materials, each clean and uncontaminated fabric was also characterized following standard methods. Fabric characterizations were conducted according to ASTM standard testing methods for textiles. Fabric thickness was measured using a thickness tester (Custom Scientific Instruments, Easton, PA USA) according to ASTM method D1777. Five square fabric swatch (5 cm × 5 cm each) samples of each lab coat were cut out to determine fabric thickness. In addition, tensile testing and abrasion resistance testing were used to measure fabric durability. ASTM D3884 and ASTM D5034 methods were used for testing abrasion resistance and tensile strength, respectively. First, tensile testing was conducted using an Instron tensile tester (Instron Worldwide, Norwood, MA) in accordance with ASTM D5034 standard test method for breaking strength and elongation of textile fabrics (Grab Test). The load cell used in the testing was 500 N. Eight replicates of dog-bone fabric swatches were used for testing each lab coat. The fabric swatches were stretched at a rate of 10 mm/min and stress-strain curves were collected. Abrasion resistance was measured using an abrasion tester in accordance with ASTM D3884 standard guide for abrasion resistance of textile fabrics (Rotary Platform, Double-Head Method). Eight replicates of circular fabric swatches with a diameter of 11 cm were used for testing each lab coat. Each fabric swatch was rubbed until a visible hole on fabric surface was observed and the cycle of rubbing on the platform was recorded.

A Krüss DSA30 goniometer was used to quantify wettability of the uncontaminated fabrics. Substrates did not require further sample preparation for WCA analysis; all data were collected under ambient laboratory conditions at 21 ± 1 °C and < 25% relative humidity. The probe liquid parameters (density 0.9970 g/mL, viscosity = 0.010 P, surface tension = 72.16 mN/m) were programmed into the onboard software and employed for all WCA fitting. Static and dynamic (i.e., time-resolved) WCA data were collected depending on the nature of substrate (i.e., hydrophilic or hydrophobic). Static WCA measurements were collected with a 2 μL drop of ultra-pure H_2O (Millipore, ≥ 18 MΩ cm); 4 μL drops were used in dynamic WCA measurements. Generally, the circle method was employed to fit hydrophilic surfaces and the tangent-1 algorithm was used to fit hydrophobic surfaces. Water absorption rates were determined via video analysis, t = 0 s is defined as the time the water droplet first contacts the material surface. An adsorption rate was calculated by dividing the drop volume by the time it took for the drop to be fully adsorbed by the material.

Airborne particle sampling using filter-based standard methods

In order to present the comparable measurements of practical work practice, NMAM sampling method was applied following the same set up shown in Figure 1 for collecting resuspended ENPs using filter-based sampling for obtaining mass concentration and elemental carbon analysis. The NMAM method is typically for sampling of a work-shift; thus, the longer duration of the experiment (one hour contamination and six hours shaking) was conducted to provide a comparable amount of ENPs deposited onto the lab coat as practical working environment. It also resulted a higher level of resuspension sufficient for filter sampling with NMAM.

NMAM 5040 was used for elemental carbon analysis for MWCNT and carbon black. Particles were collected onto a quartz-filter in a 37 mm cassette at a sampling flow rate of 2 L/min [1]. NMAM 0500 was used to collect Al_2O_3 ENPs in a 37 mm closed face cassette with a poly vinyl chloride (PVC) filter at a sampling flowrate of 2 L/min [2]. Finally, NIOSH 7402 was used to collect MWCNT in a 25 mm open faced cassette with mixed cellulose ester (MCE) membrane filter [3] at a sampling flow rate of 2 L/min**.** The filters with particles collected following the NMAM 0500 and NMAM 7402 were weighed to obtain the mass change and the mass concentrations of collected particles were estimated. The fiber microscopic analysis of NMAM 7402 is not included in this paper. In addition, the deposited particles on the fabric swatches were examined by SEM.

Aerosolization of ENPs for protective clothing contamination

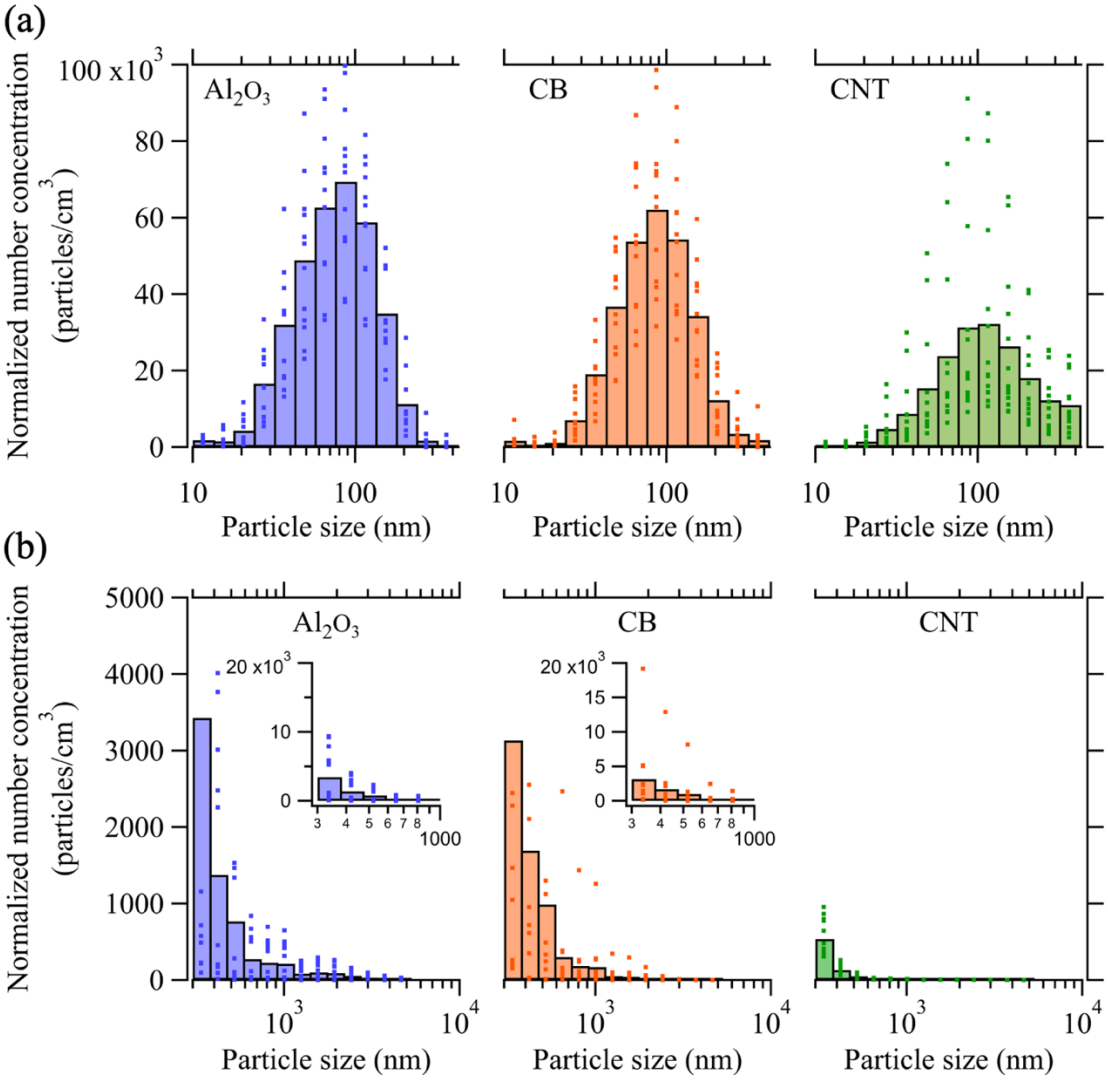

Figure S7. The aerosolized particle number concentration vs. the particle size (on a log scale) for the three ENPs used in this study. (a) Measured number concentration of 10–420 nm size range ENPs through NanoScan SMPS. (b) Measured number concentration of 0.3–10 µm size range ENPs through OPS. Data points represent 12 experiments for NanoScan SMPS and OPS, Histogram bars represent the averages of the 12 experiments for each ENP type. Dots are all individual data from 12 experiments.

The data show that the apparatus can produce ENPs in the concentration range of $10^4 – 10^5$ particles/cm^3. The Al_2O_3 was found to be the highest number concentration, followed by carbon black and CNTs. While the dispersed concentration of Al_2O_3 and carbon black were found to be comparable, they were about 2 times larger than the concentration of dispersed CNTs. Within the 10 and 420 nm size range, each contaminant showed well-defined maxima with Al_2O_3 and carbon black peaking at a size of ~90 nm (mode size) while CNTs showed a mode size nearer to ~115 nm.

A dominant result in Figure 2 is the difference in magnitude of the total number concentration between the three contaminants. The average concentration of aerosolized CNT

ENPs was about a factor of two less than the average concentrations of Al_2O_3 and carbon black. This result can be rationalized by considering the differing degrees of agglomeration for the three different ENPs. With the long fiber-tangling propensity typically observed for CNTs, many of the CNT ENPs were clearly observed to be agglomerates, forming considerably larger sized nanoparticles than the other ENPs. Indeed, some of the CNT ENPs would be beyond the sizes (10 nm – 10 μm) measured by our instruments.

The statistical analysis results as shown in Table S1 in supplementary material, the analysis of total number concentrations of aerosolized particles during contamination (Fig. 2) resulted in a strong correlation coefficient of 0.984 between Al_2O_3 and carbon black. The high correlation was also obtained between Al_2O_3 and CNT ENPs with the correlation coefficient of 0.784 and *p*-value of 0.001 meaning that there was a high level of similar size distributions between these ENPs.

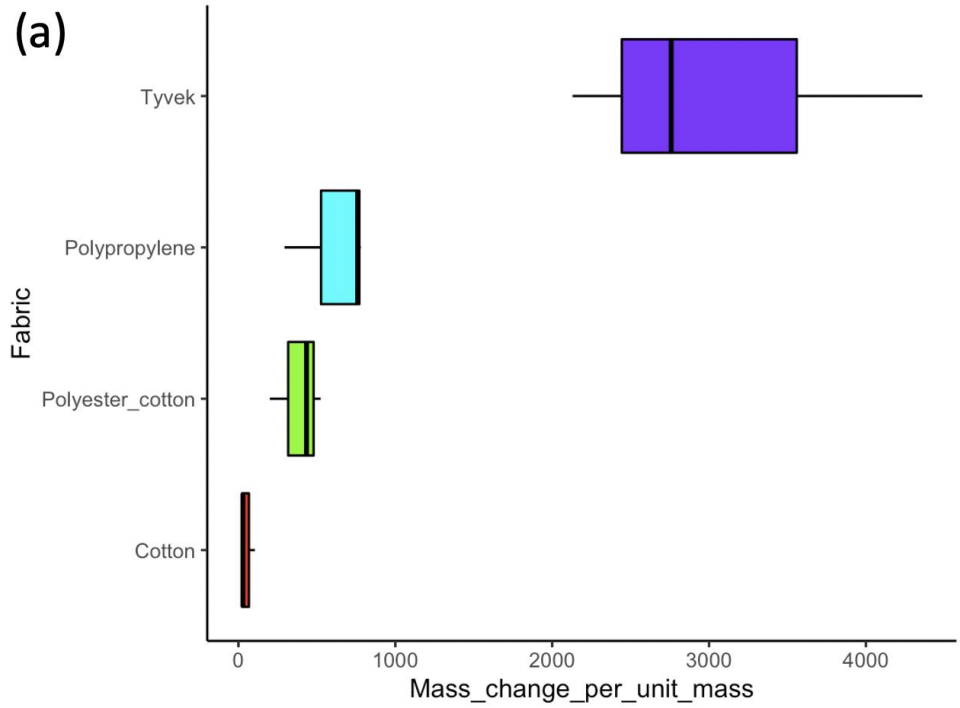

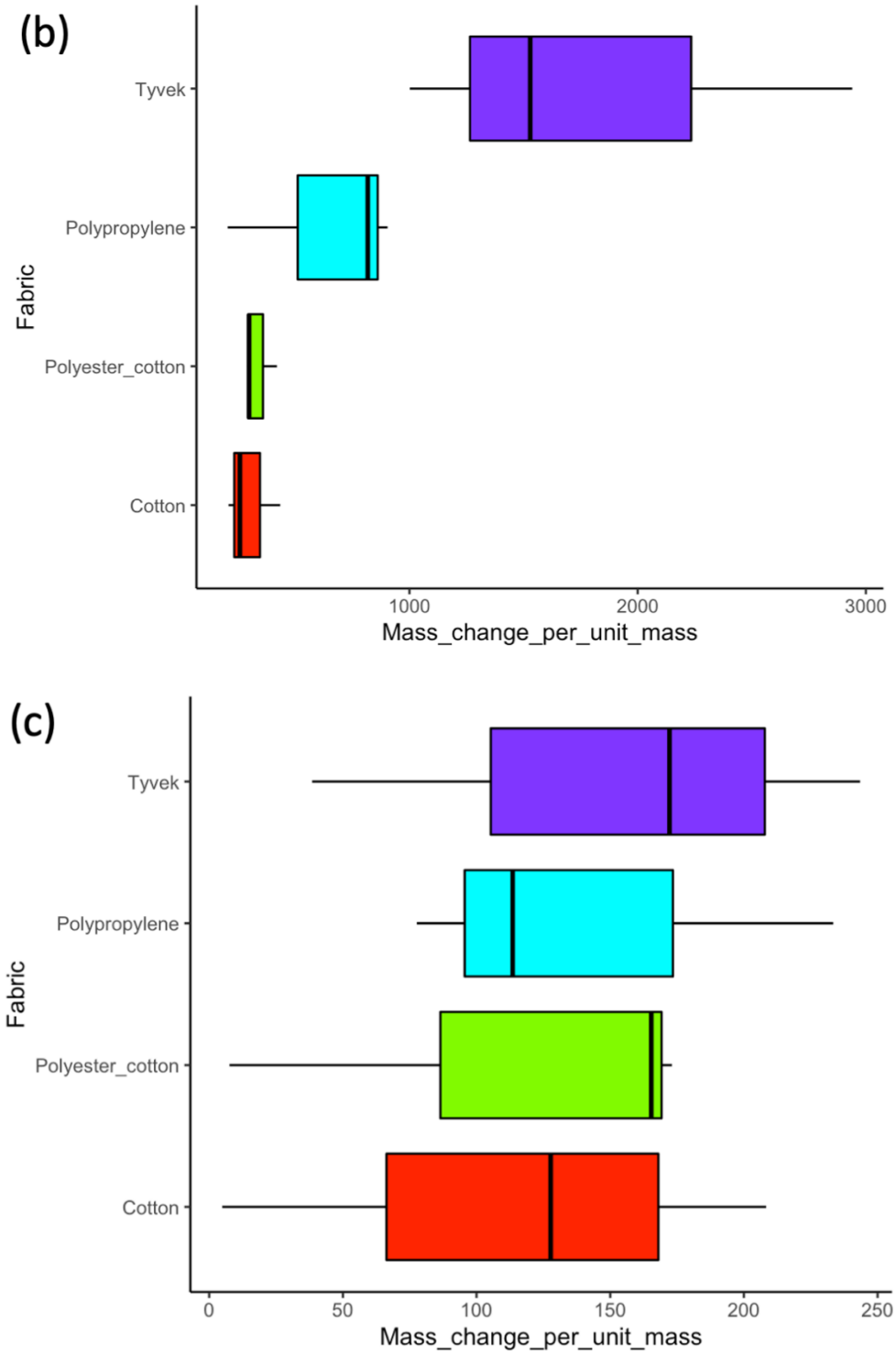

Figure S8. Statistical analysis of mass change per unit mass calculated through the measured mass before the aerosolization and release of ENPs: (a) Al_2O_3. (b) Carbon black. (c) CNT.

Theoretical forces related to particle-fabric adhesion

For the case of a perfectly round sphere of diameter D_s, comprised of material 1 (the ENP), resting on a cylindrical surface of diameter D_c, comprised of material 2 (a fiber of the fabric), the analytical form of the Hamaker adhesive force is complicated due to the geometry. However, progress can be made by realizing that 20 nm<D_s<200 nm while D_c is typically ~2000 nm. For a relatively large cylinder such that D_c/D_s<100, the interaction force between the ENP and the cylinder can be well approximated by a much simpler sphere-flat plane geometry. In this case, the adhesive force is given by the simple formula.

$$F_{ad} = \frac{H_{12} D_s}{12\, z_o^2} \qquad (1)$$

where H_{12} is the Hamaker constant describing the interaction between the ENP 1 and the planar surface 2. The parameter z_o is the separation distance between the sphere and the plane. For perfectly smooth surfaces, z_o is usually taken to equal an interatomic distance and is typically assigned a value of $z_o \approx 0.3$ nm. For a fixed ENP diameter D_s, it is clear from Eq. 1 that the Hamaker constant H_{12} controls the interaction strength of the adhesive force. In general, for micron size particles, the adhesion force given by Eq. 1 is expected to increase with the spherical particle diameter, implying that larger ENPs will be trapped by a greater adhesive force than smaller ones[4]. Thus one might expect smaller ENPs should be preferentially released upon shaking if the vdW adhesive force is dominant.

With the widespread use of the atomic force microscope (AFM), tabulated values of Hamaker constants for common engineering materials are becoming available, but reliable values for arbitrary combinations of materials are still not available. For this reason, H_{12} is often estimated using combination rules that rely on the values of the Hamaker constant inferred when identical materials interact with themselves. If H_{11} and H_{22} describe the interaction between a material 1 (or 2) with itself, then a commonly used approximation is that

$$H_{12} \approx \sqrt{H_{11} \times H_{22}}\ . \qquad (2)$$

Using Eq. 2 and literature values for H_{11} and H_{22} listed in Table 2(a), it is possible to construct estimates of H_{12} for the combination of materials relevant to this study (see Table 2(b)).

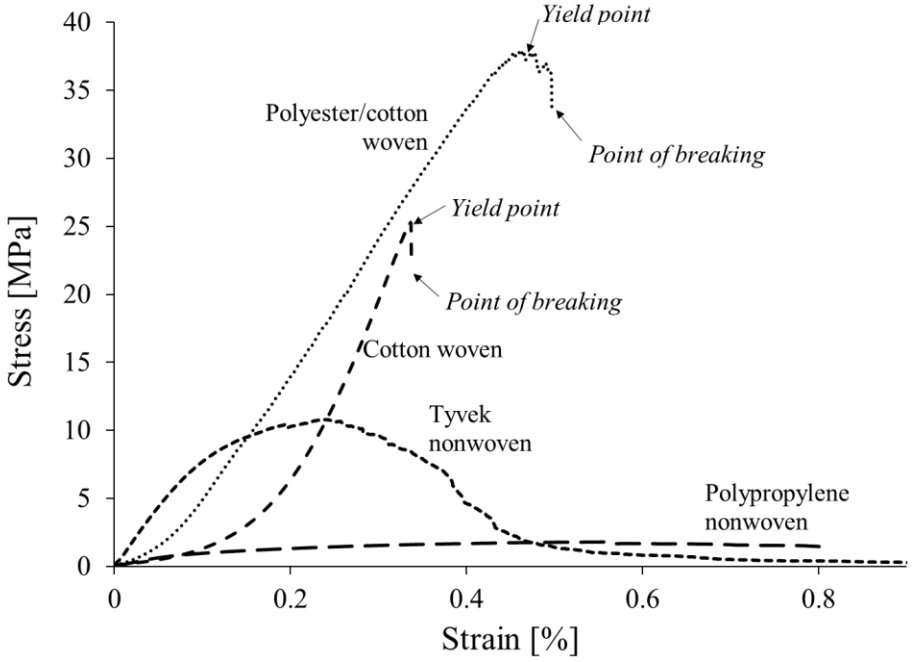

Figure S9. Representative strain-stress curves of four untreated fabrics including cotton woven, polyester cotton woven, Tyvek® nonwoven, and polypropylene nonwoven.

Table S3. Statistical analysis results with comparisons of total number concentrations of aerosolized ENPs during contamination of ENPs.

		Al_2O_3	**Carbon Black**	**CNT**
Al_2O_3	Pearson Correlation	1.000	0.984**	0.785
	Sig.		0.000	0.001
	N	13	13	13
Carbon black	Pearson Correlation	0.984**	1.000	0.864
	Sig.	0.000		0.000
	N	13	13	13
CNT	Pearson Correlation	0.785	0.864	1.000
	Sig.	0.001	0.000	
	N	13	13	13
**. Correlation is significant at the 0.01 level (1-tailed).				

Table S4. ANOVA One way test on release total number concentration of Al_2O_3, carbon black and CNT ENPs.

ENPs	Fabric	Mean difference	Lower Bound	Upper Bound	*p*-value
Al2O3	Polyester cotton - Cotton	-21.67	-98.28	54.95	0.80
	Polypropylene - Cotton	-114.82	-191.43	-38.20	0.01
	Tyvek - Cotton	-101.27	-177.88	-24.66	0.01
	Polypropylene - Polyester cotton	-93.15	-169.76	-16.54	0.02
	Tyvek - Polyester cotton	-79.60	-156.22	-2.99	0.04
	Tyvek - Polypropylene	13.55	-63.07	90.16	0.94
Carbon Black	Polyester cotton - Cotton	-21.31	-58.26	15.63	0.32
	Polypropylene - Cotton	-47.96	84.90	-11.01	0.01
	Tyvek - Cotton	-41.99	-78.93	-5.04	0.03
	Polypropylene - Polyester cotton	-26.64	-63.59	10.30	0.17
	Tyvek - Polyester cotton	-20.67	-57.62	16.27	0.34
	Tyvek - Polypropylene	5.97	-30.98	42.92	0.95
CNT	Polyester cotton - Cotton	-79.37	-153.82	-4.93	0.04
	Polypropylene - Cotton	-79.47	-153.92	-5.03	0.04
	Tyvek - Cotton	-81.46	-155.91	-7.01	0.03
	Polypropylene - Polyester cotton	-0.10	-74.55	74.35	0.99
	Tyvek - Polyester cotton	-2.09	-76.53	72.36	0.99
	Tyvek - Polypropylene	-1.99	-76.43	72.46	0.99
*. The mean difference is significant at the 0.05 level.					

Table S5. Statistical analysis results with comparisons of particle size distributions of resuspension Al_2O_3 ENPs.

		Cotton	**Polypropylene**	**Polyester cotton**	**Tyvek®**
Cotton	Pearson Correlation	1.000	0.660	0.694	0.697
	Sig.		0.014	0.0084	0.008
	N	13	13	13	13
Polypropylene	Pearson Correlation	0.660	1.000	0.857	0.845
	Sig.	0.014		0.000	0.000
	N	13	13	13	13
Polyester cotton	Pearson Correlation	0.694	0.857	1.000	0.863**
	Sig.	0.0084	0.000		0.000
	N	13	13	13	13
Tyvek®	Pearson Correlation	0.697	0.845	0.863**	1.000
	Sig.	0.008	0.000	0.000	
	N	13	13	13	13
**. Correlation is significant at the 0.01 level (1-tailed).					

Table S6. Statistical analysis results with comparisons of particle size distributions of released carbon black ENPs.

		Cotton	**Polypropylene**	**Polyester cotton**	**Tyvek®**
Cotton	Pearson Correlation	1.000	0.846	0.844	0.904
	Sig.		0.000	0.000	0.000
	N	13	13	13	13
Polypropylene	Pearson Correlation	0.846	1.000	0.956**	0.916
	Sig.	0.000		0.000	0.000
	N	13	13	13	13
Polyester cotton	Pearson Correlation	0.844	0.956**	1.000	0.851
	Sig.	0.000	0.000		0.000
	N	13	13	13	13
Tyvek®	Pearson Correlation	0.904	0.916	0.851	1.000
	Sig.	0.000	0.000	0.000	
	N	13	13	13	13
**. Correlation is significant at the 0.01 level (1-tailed).					

Table S7. Statistical analysis results with comparisons of particle size distributions of released CNT ENPs.

		Cotton	**Polypropylene**	**Polyester cotton**	**Tyvek®**
Cotton	Pearson Correlation	1.000	-0.019	-0.069	0.188
	Sig.		0.948	0.822	0.5364
	N	13	13	13	13
Polypropylene	Pearson Correlation	-0.019	1.000	0.742	0.814
	Sig.	0.948		0.003	0.000
	N	13	13	13	13
Polyester cotton	Pearson Correlation	-0.069	0.742	1.000	0.820
	Sig.	0.822	0.003		0.000
	N	13	13	13	13
Tyvek®	Pearson Correlation	0.188	0.814	0.820	1.000
	Sig.	0.5364	0.000	0.000	
	N	13	13	13	13
**. Correlation is significant at the 0.01 level (2-tailed).					

Table S8. Abrasion resistance measured by abrasion cycles before failure for four untreated fabrics.

Fabric	Fabric structure	Abrasion resistance*	Thickness (mm)
Cotton	Twill Woven	605 ± 48	0.660 ± 0.03
Polyester cotton	Plain woven	345 ± 17	0.406 ± 0.003
Tyvek®	Nonwoven	16 ± 1	0.152 ± 0.003
Polypropylene	Nonwoven	41 ± 3	0.254 ± 0.003

* Abrasion cycles before failure

Table S9. WCA for fabric samples[a].

Fabric	Static WCA (°)	Absorption Rate (μL s^{-1})
Tyvek®	125.9 ± 4.5	–
Polypropylene	121.7 ± 6.3	–
Polyester cotton	–	4.24 ± 0.75
Cotton	–	18.9 ± 3.5

a: All analyses were performed for n = 9; mean standard deviation are reported in parentheses.

REFERENCES

(1) NIOSH Manual of Analytical Methods (NMAM), Fourth Edition.
(2) CDC; Niosh. NMAM 0500: PARTICULATES NOT OTHERWISE REGULATED, TOTAL.
(3) ASBESTOS by TEM 7402. **1989**.
(4) Kumar, A.; Staedler, T.; Jiang, X. Role of Relative Size of Asperities and Adhering Particles on the Adhesion Force. *Journal of colloid and interface science* **2013**, *409*, 211–218. https://doi.org/10.1016/J.JCIS.2013.07.039.

Chapter 4 supplementary materials

XPS characterization of UT and FC plasma treated fabrics

Atomic compositions of the untreated (UT) and plasma treated fabrics are included in Table 1. The surface chemistry of the UT PP and Tyvek® materials is mostly carbon, 89.2% and 82.8% respectively, which supports the hydrocarbon chemical structure for both compounds. The 100% cotton (cotton) and blend samples showed an increased amount of O on the surface. Also note that the blend fabric contained small amounts of Si (4.8%). This is likely from the manufacturing process of these materials, as a silicon-based softener is commonly used in a fabric softening step during the production of garments made of rougher materials (e.g. polyester). High-resolution C_{1s} XPS spectra are depicted in Figure S1 for all the UT fabrics studied herein, suggesting the surface of these materials consists of carbon in environments corresponding to C-C/C-H, C-O, and C=O at binding energies 284.6, 286, and 288.5 eV, respectively. As expected for the nonwoven fabrics (Fig. S1a and d), no C=O functionality was measured, and these samples contained the smallest amount of C-O functionality. Cotton-containing materials (Fig. S1b and c) show elevated amounts of oxygen bound to carbon functionality, again supported by the chemical structure of cotton, inset in Figure S1b.

Compared to the UT fabrics, the FC coated fabrics gained ~10% F (with corresponding decreases in percent O and C). The FC samples (Fig. S2) still retain a C-C/C-H peak centered at ~284.7 eV, arising from the underlying fabric. Although typical carbon-fluorine peaks (CF_3 at 293.5 eV and CF_2 at 292.0 eV) were not present, the high-resolution F_{1s} spectra have a prominent peak at ~689.0 eV, signifying that the samples contain some F-C binding. As the C-CF (286.9 eV) and CF (289.9 eV) peaks slightly overlap with the C-O and C=O peaks, it was challenging to fit these spectra with these binding environments separately. Therefore, the peaks at ~286.5 eV and ~288.1 eV were attributed to both the carbon-oxygen and carbon-fluorine peaks and labeled C-O/C-CF and C=O/CF, respectively. Because of the absence of some carbon-fluorine peaks and the low percent of F in all FC samples, a glass slide was treated with a FC plasma (p = 30 mTorr, P = 50 W, sample distance of 10 cm) to ensure film deposition was occurring in the reactor and that these unexpected results were a consequence of analyzing these morphologically complex fabrics. The high-resolution C_{1s} spectrum of this treated glass slide can be seen in Figure S3, and the atomic composition data are included in Table 1. Based on an O:Si ratio of ~2, both the O and Si contributions can be assigned to the glass substrate. In addition, these samples contain ~30% F (almost three times that of the fabric samples), indicating good film deposition under these parameters. Notably, the high-resolution C_{1s} spectrum contains all the expected carbon-fluorine peaks. Thus, the prominent contribution from the underlying fabric and low F concentration of the FC treated samples are likely sampling anomalies arising from the complex morphology.

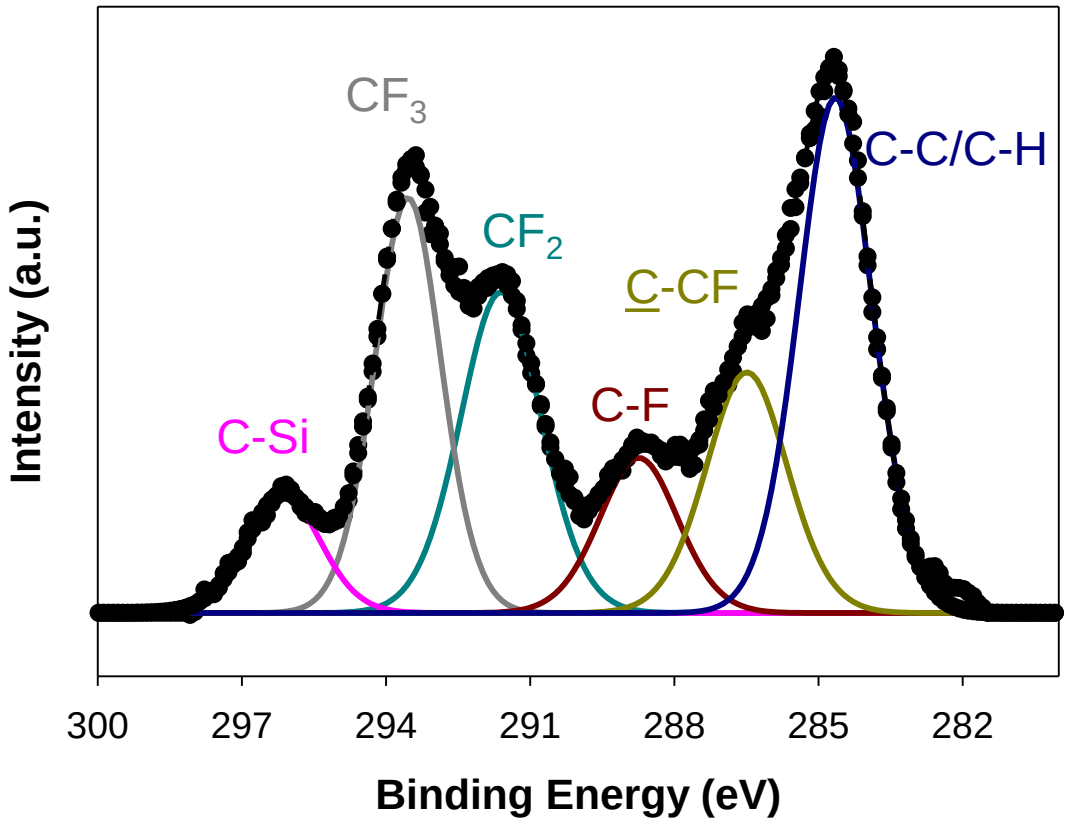

Figure S1. High-resolution C_{1s} XPS spectrum of a glass slide after FC treatment (P = 50 W, p = 30 mTorr). Labels correspond to assigned peak binding environments.

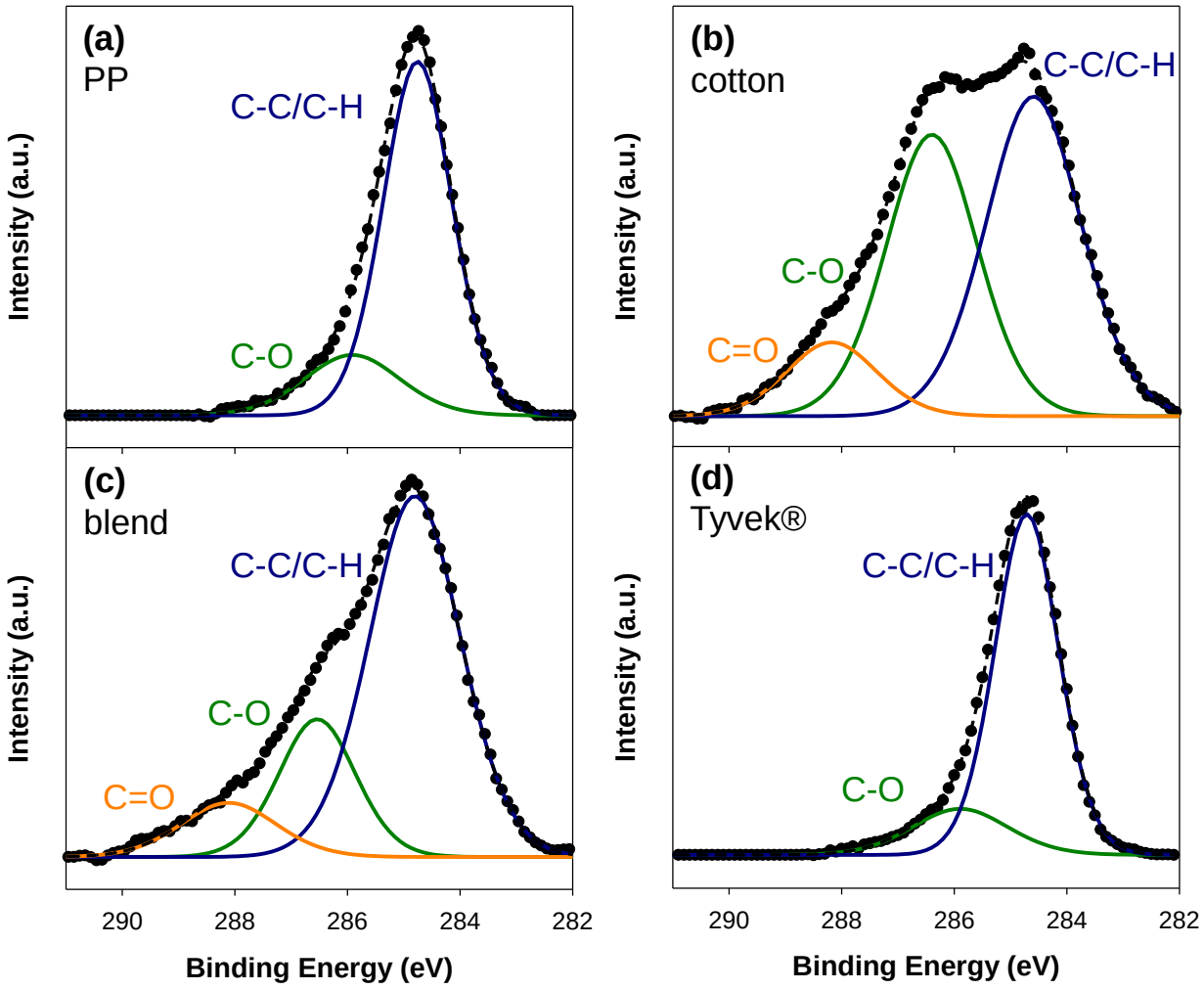

Figure S2. High-resolution C_{1s} XPS spectra of the UT (a) PP, (b) cotton, (c) blend, and (d) Tyvek®. Inset in (b) shows the chemical structure of cotton and peak labels correspond to assigned binding environments.

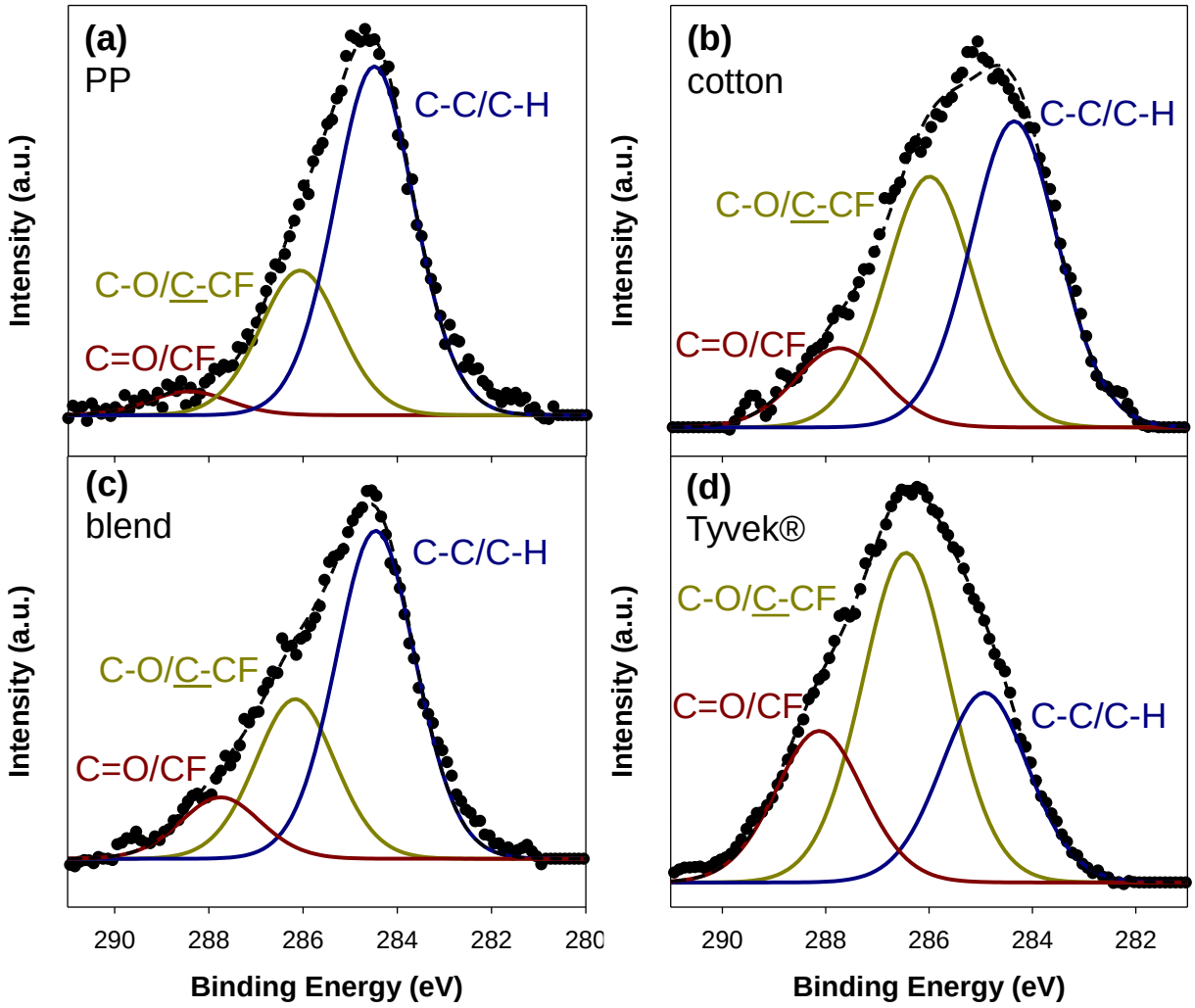

Figure S3. High-resolution C_{1s} XPS spectra for (a) PP, (b) cotton, (c) blend, and (d) Tyvek®, after FC plasma treatment (P = 50 W, p = 30 mTorr).

Table S1. WCA for UT and FC plasma treated fabrics.[a]

	Fabric	Static WCA (°)	Absorption Rate (μL s^{-1})
UT	PP	121.7 (2.1)	--
	Tyvek®	125.9 (1.5)	--
	blend	--	4.24 (0.25)
	cotton	--	18.9 (1.2)
FC	PP	123.7 (1.0)	--
	Tyvek®	125.0 (2.6)	--
	blend	--	0.101 (0.006)
	cotton	139.4 (0.9)	--

[a]All analyses were performed for n = 9; errors are reported in parentheses.

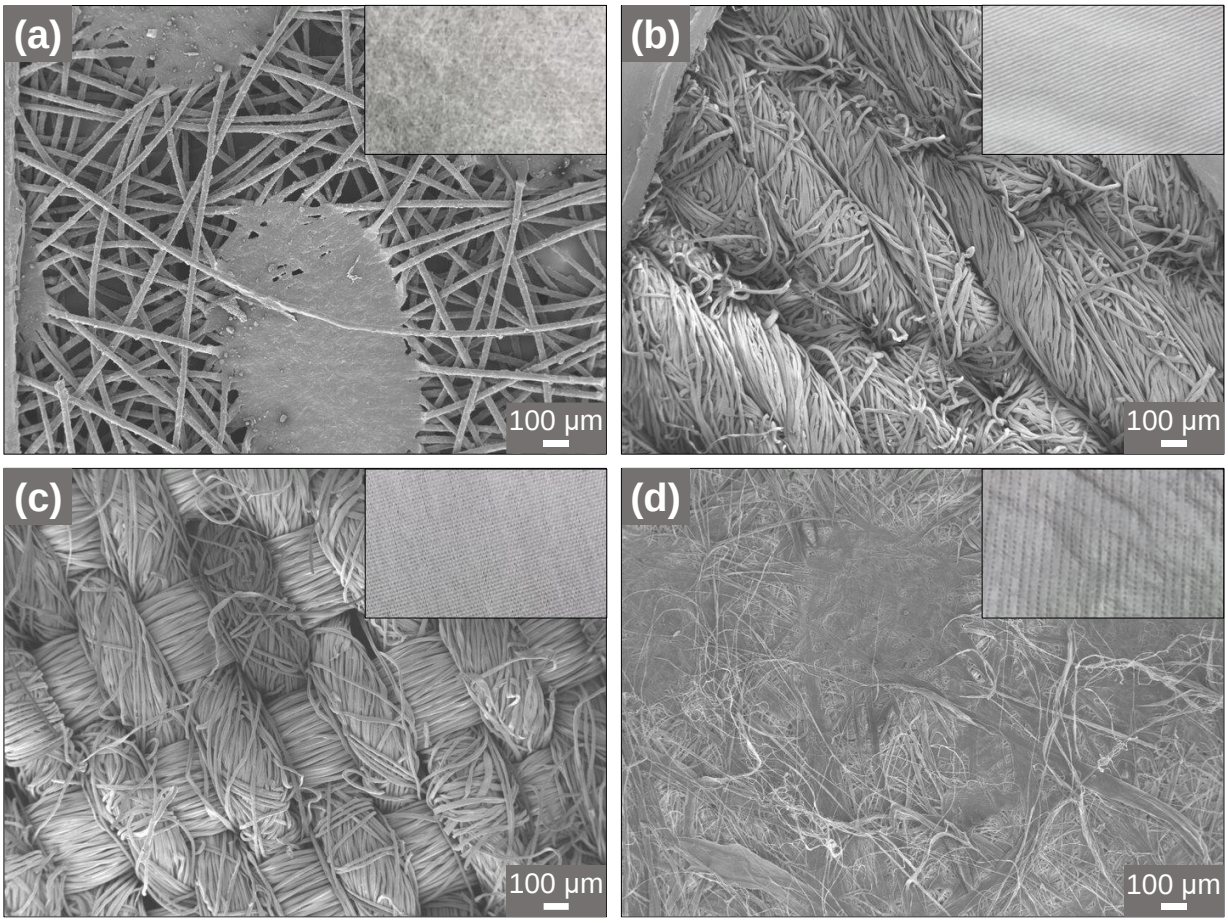

Figure S4. SEM images of UT (a) PP, (b) cotton, (c) blend, and (d) Tyvek®. All images taken at ×50 magnification. All scale bars represent 100 µm and insets are photos of the fabric.

Table S2. Mass change of UT and plasma treated fabrics after ENPs contamination.

			Tyvek®		Cotton		PP		Blend	
		Sample	**Δ_{mass} (mg)**	**error**	**Δ_{mass} (mg)**	**error**	**Δ_{mass} (mg)**	**error**	**Δ_{mass} (mg)**	**error**
Al_2O_3	**UT**	contaminated	1.810	0.130	1.305	1.085	1.260	0.130	0.825	0.285
		shaken	0.665	0.405	0.395	0.125	0.320	0.150	-	-
	FC	contaminated	1.360	0.090	0.170	1.260	1.380	0.530	1.510	0.450
		shaken	0.385	0.225	-	-	0.045	0.005	-	-
	H_2O	contaminated	0.685	0.055	0.880	0.210	0.995	0.195	0.665	0.315
		shaken	0.040	0.040	-	-	0.085	0.075	0.135	0.035
CB	**UT**	contaminated	0.410	0.090	0.418	0.342	0.880	0.100	1.645	0.015
		shaken	0.210	0.040	-	-	0.300	0.015	0.010	0.010
	FC	contaminated	0.350	0.140	0.550	0.230	0.833	0.278	0.405	0.415
		shaken	0.245	0.045	0.055	0.005	0.105	0.025	0.107	0.017
	H_2O	contaminated	0.080	0.040	0.393	0.158	0.777	0.147	0.460	0.100
		shaken	0.045	0.015	-	-	0.098	0.053	-	-
CNT	**UT**	contaminated	0.127	0.017	-	-	-	-	-	-
		shaken	-	-	-	-	-	-	-	-
	FC	contaminated	-	-	-	-	0.045	0.025	-	-
		shaken	-	-	0.508	0.043	0.605	0.005	1.780	2.090
	H_2O	contaminated	-	-	-	-	-	-	-	-
		shaken	-	-	-	-	-	-	0.035	0.590

"-" indicate samples where the $\Delta_{mass} \leq 0$.

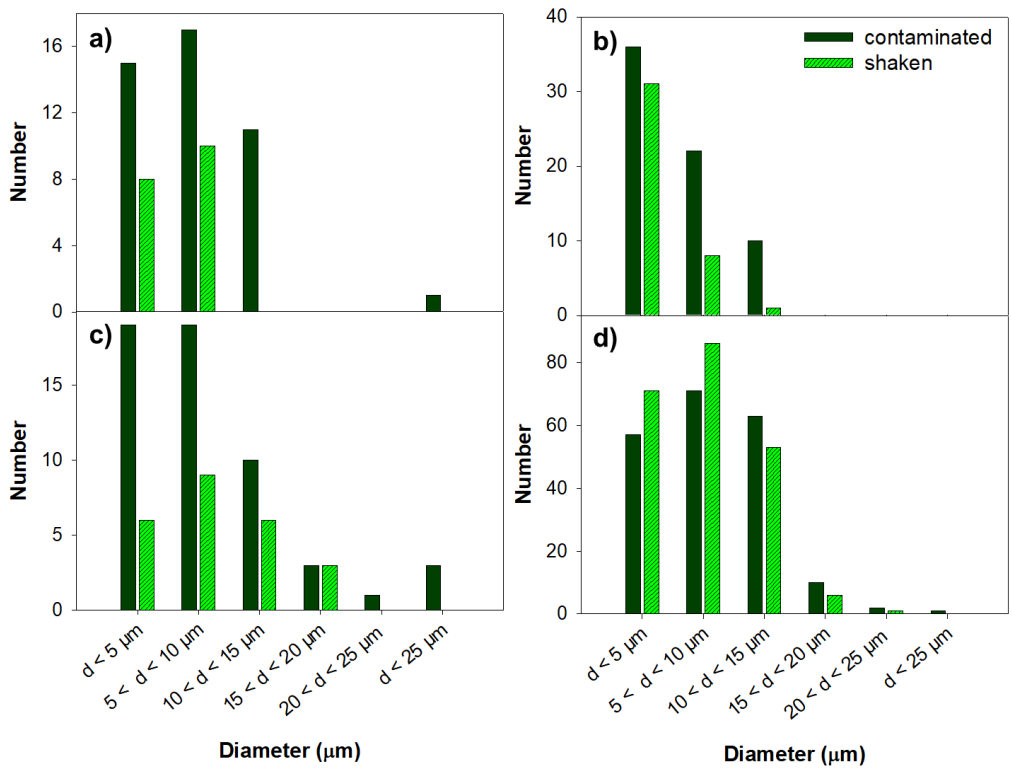

Figure S5. Number of (a-b) CB and (c-d) CNT agglomerates on (a, c) UT and (b, d) FC PP from same spot analysis. Dark green bars represent counts from contaminated samples and light stripped green bars represent counts after shaking the same sample.

Table S3. Raw counts of CB agglomerates on UT and plasma treated fabrics after contamination and shaking.[a]

	Tyvek®						**cotton**						**PP**						**blend**					
	Contaminated			After Shaking			Contaminated			After Shaking			Contaminated			After Shaking			Contaminated			After Shaking		
Size Range	UT	FC	$H_2O_{(v)}$	UT	FC	$H_2O_{(v)}$	UT	FC	$H_2O_{(v)}$	UT	FC	$H_2O_{(v)}$	UT	FC	$H_2O_{(v)}$	UT	FC	$H_2O_{(v)}$	UT	FC	$H_2O_{(v)}$	UT	FC	$H_2O_{(v)}$
1-100nm	5	2	0	1	0	0	0	0	0	1	0	0	0	0	0	0	0	0	11	0	0	1	0	0
101-200nm	45	22	11	45	8	1	11	18	2	17	8	1	2	1	0	2	1	0	43	4	0	14	6	0
201-300nm	62	26	13	65	17	14	22	33	4	26	15	0	17	5	11	14	4	0	43	7	7	26	6	5
301-400nm	51	24	7	46	16	14	12	37	6	20	12	1	6	7	17	31	6	0	32	9	9	12	10	14
401-600nm	76	30	6	35	30	17	21	36	7	18	7	2	21	12	12	43	17	2	36	23	8	34	9	22
600-800nm	37	18	4	16	13	6	13	19	1	8	2	0	9	17	14	23	8	1	19	8	10	11	17	19
800nm-1um	19	10	6	2	10	9	4	16	3	12	4	0	5	11	6	16	6	3	9	6	0	7	6	10
1um-5um	129	96	42	103	84	22	46	99	14	29	23	2	30	88	30	60	31	27	57	41	25	24	25	27
5um-10um	35	42	6	55	48	2	26	28	19	11	9	1	59	63	25	22	9	13	14	36	46	12	19	9
11um-15um	6	8	0	4	9	1	10	8	5	5	0	1	43	12	12	6	2	5	5	10	23	1	7	2
16-20um	1	4	0	0	1	0	4	1	3	1	0	0	12	8	3	2	2	1	1	5	10	2	3	1
21-25um	0	0	0	0	0	0	1	0	1	0	0	0	4	1	8	1	0	1	0	2	4	1	1	0
26-30um	0	0	0	0	0	0	1	0	0	0	0	0	3	1	0	1	0	0	0	1	0	0	0	0
31-40um	0	0	0	0	0	0	4	1	0	0	0	0	3	3	2	2	0	0	1	1	0	0	0	0
41-50um	0	0	0	0	0	0	0	0	0	0	0	0	1	0	0	0	0	0	0	0	0	0	0	0
51-60um	0	0	0	0	0	0	1	0	0	0	0	0	0	0	0	0	0	0	0	0	0	0	0	0
Total #	**466**	**282**	**95**	**372**	**236**	**86**	**176**	**296**	**65**	**148**	**80**	**8**	**215**	**229**	**140**	**223**	**86**	**53**	**271**	**153**	**142**	**145**	**109**	**109**

[a]All measurements made from 3 – 7 images per sample.

Table S4. Raw counts of Al_2O_3 agglomerates on UT and plasma treated fabrics after contamination and shaking.[a]

	Tyvek®						cotton						PP						blend					
	Contaminated			After Shaking			Contaminated			After Shaking			Contaminated			After Shaking			Contaminated			After Shaking		
Size Range	UT	FC	$H_2O_{(v)}$	UT	FC	$H_2O_{(v)}$	UT	FC	$H_2O_{(v)}$	UT	FC	$H_2O_{(v)}$	UT	FC	$H_2O_{(v)}$	UT	FC	$H_2O_{(v)}$	UT	FC	$H_2O_{(v)}$	UT	FC	$H_2O_{(v)}$
1-100nm	2	0	1	3	0	0	5	3	5	5	0	1	5	1	0	1	1	1	0	0	0	0	1	0
101-200nm	1	4	7	21	3	20	25	6	60	3	9	7	18	24	17	9	13	13	20	6	5	11	22	11
201-300nm	1	5	17	17	2	28	19	10	25	2	6	8	27	28	15	10	20	15	42	12	15	15	22	32
301-400nm	1	7	15	16	3	20	16	1	10	1	1	10	3	25	10	5	12	7	25	11	7	18	10	10
401-600nm	12	15	21	12	8	24	15	4	9	0	5	7	16	31	27	6	14	13	33	20	15	18	13	12
600-800nm	6	19	9	4	9	10	15	1	7	1	1	4	16	11	7	4	2	3	10	11	6	2	8	8
800nm-1um	11	15	4	2	12	2	4	0	2	0	1	0	5	4	6	0	1	2	1	5	2	3	5	2
1um-5um	26	61	26	19	54	0	22	1	9	1	5	2	7	15	10	8	4	5	8	8	4	13	5	6
5um-10um	14	6	8	1	18	0	16	3	0	0	4	0	3	2	3	3	3	0	3	8	3	3	0	4
11um-15um	4	1	4	0	4	0	10	1	1	0	2	0	1	1	1	0	0	0	0	7	2	2	0	0
16-20um	1	0	0	0	0	0	2	0	0	0	0	0	0	2	2	2	1	0	1	2	1	0	0	0
21-25um	0	0	1	0	0	0	2	0	0	0	0	0	0	0	0	0	0	0	1	0	0	0	0	1
26-30um	2	0	1	0	1	0	0	0	0	0	0	0	0	0	0	0	0	0	0	0	0	0	0	2
31-40um	0	0	0	0	1	0	1	0	0	0	0	0	0	0	0	0	0	0	0	0	0	0	0	0
41-50um	0	0	0	0	0	0	0	0	0	0	0	0	0	0	0	0	0	0	0	0	0	0	0	0
51-60um	0	0	0	0	0	0	0	0	0	0	0	0	0	0	0	0	0	0	0	0	0	0	0	0
Total #	**81**	**133**	**114**	**95**	**115**	**104**	**152**	**30**	**128**	**13**	**34**	**39**	**101**	**144**	**98**	**48**	**71**	**59**	**144**	**90**	**60**	**85**	**86**	**88**

[a]All measurements made from 3 – 7 images per sample.

Table S5. Total number of CNT after release.[a]

Plasma Precursor Gas	Fabric	# CNT Bundles	# Individual CNT
UT	PP	61	25
	Tyvek®	156	248
	blend	160	45
	cotton	103	11
FC	PP	86	24
	Tyvek®	214	174
	blend	281	39
	cotton	151	59
$H_2O_{(v)}$	PP	35	28
	Tyvek®	131	53
	blend	145	7
	cotton	63	0

[a]All measurements made from 3 – 7 images per sample.

C. PRODUCTS

C.1 PUBLICATIONS

Are there publications or manuscripts accepted for publication in a journal or other publication (e.g., book, one-time publication, monograph) during the reporting period resulting directly from this award?

Yes

Publications Reported for this Reporting Period

Public Access Compliance	Citation
N/A: Not NIH Funded	Maksot A, Sorna SM, Blevens M, Reifenberger RG, Hiyoto K, Fisher ER, Vindell T, Li YV, Kipper MJ, Tsai CS. Engineered Nanoparticle Release from Personal Protective Clothing: Implications for Inhalation Exposure. ACS Applied Nano Materials. 2022 February 11;5(2):2558.
N/A: Not NIH Funded	Hiyoto K, Sorna SM, Maksot A, Reifenberger RG, Tsai CS, Fisher ER. Effects of Surface Hydrophobicity of Lab Coat Fabrics on Nanoparticle Attachment and Resuspension: Implications for Fabrics Used for Making Protective Clothing or Work Uniform. ACS Applied Nano Materials. 2023 April 21;6(9):7384.

C.2 WEBSITE(S) OR OTHER INTERNET SITE(S)

NOTHING TO REPORT

C.3 TECHNOLOGIES OR TECHNIQUES

NOTHING TO REPORT

C.4 INVENTIONS, PATENT APPLICATIONS, AND/OR LICENSES

Have inventions, patent applications and/or licenses resulted from the award during the reporting period? No

If yes, has this information been previously provided to the PHS or to the official responsible for patent matters at the grantee organization? No

C.5 OTHER PRODUCTS AND RESOURCE SHARING

NOTHING TO REPORT

D. PARTICIPANTS

D.1 WHAT INDIVIDUALS HAVE WORKED ON THE PROJECT?

Commons ID	S/K	Name	Degree(s)	Role	Cal	Aca	Sum	Foreign Org	Country	SS
CANDACETSAI	Y	Tsai, Candace SuJung	BS,MS,MS,DSC	PD/PI	2.7	0.0	0.0			NA
MKIPPER7	Y	Kipper, Matthew	BS,PHD	Co-Investigator	0.2	0.0	0.0			NA
REIFENBR	Y	Reifenberger, Ronald		Co-Investigator	0.5	0.0	0.0			NA
ARVINDRAMAN	Y	Raman, Arvind		Co-Investigator	0.0	0.2	0.0			NA
MBLEVENS	N	Blevens, Melissa Sue	BS,MS,PHD	Graduate Student (research assistant)	0.6	0.0	0.0			NA
	N	Chen, Yi-Hsuan		Graduate Student (research assistant)	0.0	0.0	2.0			NA
	N	Maksot, Aigerim		Graduate Student (research assistant)	3.9	0.0	0.0			NA
	N	Huang, Jingwen		Graduate Student (research assistant)	0.0	0.0	0.6			NA

Glossary of acronyms:
S/K - Senior/Key
Cal - Person Months (Calendar)
Aca - Person Months (Academic)
Sum - Person Months (Summer)
Foreign Org - Foreign Organization Affiliation
SS - Supplement Support
RS - Reentry Supplement
DS - Diversity Supplement
OT - Other
NA - Not Applicable

D.2 PERSONNEL UPDATES

D.2.a Level of Effort

Not Applicable

D.2.b New Senior/Key Personnel

Not Applicable

D.2.c Changes in Other Support

Not Applicable

D.2.d New Other Significant Contributors Not Applicable
D.2.e Multi-PI (MPI) Leadership Plan Not Applicable

E. IMPACT

E.1 WHAT IS THE IMPACT ON THE DEVELOPMENT OF HUMAN RESOURCES? Not Applicable
E.2 WHAT IS THE IMPACT ON PHYSICAL, INSTITUTIONAL, OR INFORMATION RESOURCES THAT FORM INFRASTRUCTURE? NOTHING TO REPORT
E.3 WHAT IS THE IMPACT ON TECHNOLOGY TRANSFER? Not Applicable
E.4 WHAT DOLLAR AMOUNT OF THE AWARD'S BUDGET IS BEING SPENT IN FOREIGN COUNTRY(IES)? NOTHING TO REPORT

G. SPECIAL REPORTING REQUIREMENTS SPECIAL REPORTING REQUIREMENTS

G.1 SPECIAL NOTICE OF AWARD TERMS AND FUNDING OPPORTUNITIES ANNOUNCEMENT REPORTING REQUIREMENTS

NOTHING TO REPORT

G.2 RESPONSIBLE CONDUCT OF RESEARCH

Not Applicable

G.3 MENTOR'S REPORT OR SPONSOR COMMENTS

Not Applicable

G.4 HUMAN SUBJECTS

G.4.a Does the project involve human subjects?

Not Applicable

G.4.b Inclusion Enrollment Data

NOTHING TO REPORT

G.4.c ClinicalTrials.gov

Does this project include one or more applicable clinical trials that must be registered in ClinicalTrials.gov under FDAAA?

G.5 HUMAN SUBJECTS EDUCATION REQUIREMENT

NOT APPLICABLE

G.6 HUMAN EMBRYONIC STEM CELLS (HESCS)

Does this project involve human embryonic stem cells (only hESC lines listed as approved in the NIH Registry may be used in NIH funded research)?

No

G.7 VERTEBRATE ANIMALS

Not Applicable

G.8 PROJECT/PERFORMANCE SITES

Not Applicable

G.9 FOREIGN COMPONENT
No foreign component
G.10 ESTIMATED UNOBLIGATED BALANCE
Not Applicable
G.11 PROGRAM INCOME
Not Applicable
G.12 F&A COSTS
Not Applicable

I. OUTCOMES

I.1 What were the outcomes of the award?

This study showed substantial particle release results for all types of tested fabrics. The release inhalable particle concentration for cotton and polyester cotton fabric were determined to be the highest from the aerosolization of Al2O3 and carbon black (CB) engineered nanoparticles (ENPs), while Tyvek® and polypropylene showed the lowest amount of release concentration. From the exposure of carbon nanotube (CNT) ENPs, the cotton fabric showed the highest release concentration compared with other tested fabrics. The release concentration of cotton and polyester cotton were significantly different from Tyvek® and polypropylene for Al2O3 and CB ENPs, while for CNT ENPs cotton fabric turned out to be significantly different from all other fabrics. Moreover, for all types of tested fabrics the total number concentrations of resuspended ENPs at the breathing zone are higher than particles released from the back side of the worker wearing the contaminated protective clothing. The total number concentration from one hour contamination and six-hour release processes could represent the exposure of full-shift work presenting risk of human exposure.

Regarding dermal route of exposure from penetration of contaminated ENPs, we found that Tyvek fabric was shown to be the most protective. Tyvek consistently showed the lowest penetration percentages when challenged with all three different types of ENPs, and some results showed that Tyvek had statistically significantly lower penetration than all three other fabrics. Polypropylene fabric had the highest penetration percentages when challenged with Al2O3 and CB ENPs in the 100 nm-1 μm size range.

The primary technical tool employed in this study to elucidate ENP interacting force with fabric fiber is the Atomic Force Microscope (AFM). The AFM measures the interaction of a sharp tip integrally attached to a flexible microcantilever as the tip is made to approach, contact, indent and then withdraw from the surface of a fabric of interest. Using an AFM, systematic F(z) data were acquired from each fiber under ambient and reduced humidity conditions using the AFM tip as a surrogate for an oxide ENP. Analysis of the results offered useful conclusions that characterize the physical interaction of an oxide ENP in the ~15 nm diam. size range with the individual fibers.

The surface chemistry and wettability of these fabrics was tuned using either a C3F8 or H2O(v) plasma and monitored with X-ray photoelectron spectroscopy (XPS) and water contact angle (WCA) analysis. Contamination and release of ENPs were quantified by monitoring the change in mass after contamination and shaking of the fabrics and using scanning electron microscopy (SEM) image analysis. The C3F8 plasma deposited a FC coating, increasing the material hydrophobicity, whereas the H2O(v) plasma implanted O-functionality and etched the surface, nominally increasing the hydrophilicity and roughness of the surfaces. Notably, the latter treatment ultimately resulted in a relatively permanent increase in hydrophilicity of the cotton and Tyvek®, whereas the other two materials exhibited hydrophobic recovery after a month of aging post treatment. Overall, the lowest contamination levels arise from exposure to CNT. Plasma treatment results in differential contamination, with the H2O(v) plasma treated fabrics demonstrating the lowest CB contamination, whereas the lowest Al2O3 contamination and resuspension occurs with the C3F8 plasma treated cotton.

Notably, different surface treatments resulting in materials repellent to airborne particles could be used in treating fabrics used for making protective clothing or work uniforms to minimize the contamination and spread of unwanted particles. With the concern of the potential carcinogenicity of CNT, the C3F8 plasma deposited FC coating, named FC surface treatment, may support the treated fabric traps CNT, thereby minimizing subsequent exposure.

Ultimately, the differences of the ENP behavior on the untreated (UT) and plasma modified fabrics indicate that both fabric weave pattern and surface chemistry impact nanomaterial attachment and resuspension. These efforts toward understanding the role of material properties on the attachment of ENP may lead to strategies for determining what types of fabric are best for protecting the wearer from adverse health effects from exposure to nanomaterials.